High Speed Videograpic Quick Stop Device for Orthogonal Machining

by

Chase Allan Wortman

A thesis submitted to the Graduate Faculty of
Auburn University
in partial fulfillment of the
requirements for the Degree of
Master of Science

Auburn, Alabama
December 14, 2013

Keywords: orthogonal machining, metal cutting mechanics, quick stop device, high speed videography

Approved by

Lewis N. Payton, Chair, Associate Research Professor, Mechanical Engineering
Robert L. Jackson, Associate Professor, Mechanical Engineering
Dan Marghitu, Professor, Mechanical Engineering

Abstract

Advances in digital high speed video acquisition make it possible to create a fully integrated virtual quick stop device to observe the orthogonal metal cutting process in real time. This research aims to provide additional information and updated imagery to aid in the development of a predictive theory of the metal cutting process. Existing shear zone models are applied to force data paired with high speed video footage to see if these models accurately predict the way in which metal is deformed during orthogonal machining.

A high speed videographic quick stop device was developed to observe the metal cutting process. This system allows force data from a dynamometer to be paired frame by frame with the imagery from a high speed camera. Frame rates as high as 1,000 frames per second were used to obtain a high resolution data set for analysis. The images of highly polished and etched metal surfaces allow the researcher to see how the grain structure of the metal deforms in front of the tool edge as it moves through the material. The angle at which the grain structure deforms can then be measured.

Analysis of the data indicates that the plane in which a metal undergoes plastic deformation is affected by the material properties of the metal samples and the cutting factors (tool angle, feed, etc.) used. The hardness value of a metal undergoing the metal cutting process has been shown to have a significant effect

on the resulting angle at which it will plastically deform. Copper 101, Aluminum 1100, and 1018 Steel were the materials used for this study. The hardness of these metals was increased by cold rolling. Tensile samples were cut from each unique metal sample and tested for precise material property values. Customized high speed steel (HSS) tools at three different rake angles were used for the orthogonal machining of the metal samples.

The utilization of a fully integrated, computer controlled cutting environment in conjunction with the high speed virtual quick stop device permits the collection of a highly synchronized data set for all parameters being studied. A statistical analysis of this data provides the additional information on the shear process under orthogonal metal cutting conditions. The better understanding of the metal cutting process can aid in improvements to the control of metal machining processes.

Acknowledgments

I would like to dedicate this thesis to my family and friends who have supported me throughout this entire process. Foremost, I would like to thank my beautiful wife-to-be Jessica Geddes for all of her love and support throughout my entire graduate school career. I cannot imagine a better experience at Auburn than I have had with you.

I have to thank my parents, Darryl and Cindy, for always keeping me on the right track and fully supporting me in all the decisions I have made in my life. To my brother and best friend, Grant, I have enjoyed being able to live with you during our time at Auburn and experience the best years of our lives together. To my little sister Sarah I would like to say that I am amazed by the woman that you have become and thank you for being the greatest sister in the world.

Next, I have to acknowledge my life-long friends, Hans Driessnack, Zack Moore, and David Brown, who have been a source of encouragement as they also work their way through their respective post-college studies.

Finally, I would like to thank Dr. Payton for giving me the opportunity to work in the DML and providing guidance and support throughout my graduate school career. I would also like to thank my colleagues Justin Evans, Vishnu Chandrasekaran, Drew Sherer, Wesley Hunko, and Michael Carter for all of your help in completing this thesis. War Eagle.

Table of Contents

List of Tables

List of Figures

List of Symbols

α	Tool Rake Angle
φ	Onset of Shear Plane Angle
ψ	Shear Front Angle
β	Mean Friction Angle Tool Face
μ	Friction Coefficient
t_{ord}	Ordered Depth of Cut
t_o	Uncut Chip Thickness
t_c	Cut Chip Thickness
w	Width of the Cut Chip
r_c	Ratio of Chip to Un-cut Chip thickness
F_c	Horizontal Cutting Force
F_t	Vertical Cutting Force
F	Frictional Force upon Chip
N	Normal Force upon Chip
R	Resultant Force upon Chip
F_s	Shear Force on the Plane
F_n	Normal Force on the Plane
A_s	Area of the Shear Plane
τ_s	Shear Stress on the Shear Plane

γ	Shear Strain (also ε in some works)
V	Cutting Velocity
V_c	Chip Velocity
V_s	Shear Velocity
HP	Horsepower
HP_s	Specific Horsepower
P	Power Required to Cut
MRR	Metal Removal Rate
U	Specific Total Cutting Energy
U_f	Specific Friction Energy
U_s	Specific Shear Energy
σ_s	Normal Stress
L	chip contact length on tool face

Introduction

The machining of metals is the most widely used process in the production of mechanical products by the manufacturing industry in the United States as well as many other countries world-wide. It was estimated that metal cutting was used to create approximately fifteen percent of all products produced by the manufacturing industry in the U.S. in 1989. This percentage has remained virtually unchanged over the years making the economic impact today close to $300 billion. This huge economic impact compels the continuing research into developing improvements in machining processes and practices.

Machining can be defined as "a machine-performed process suitable for utilization to produce products on an industrialized basis". Humans have been machining products since the invention of a boring machine capable of boring a cy1inder true "within the thickness of a worn shilling" in 1775 (Merchant). Yet, machining is still an art. Ask any machinist and they will tell you the same. Three different machine shops can be given the same stock and asked to make the same part; three different sets of machining parameters will be used to create the part. This is because there is currently no accepted formula that can take the material properties of a piece of stock and output the ideal machining parameters for that material.

Fred W. Taylor made it his life's work to answer three questions necessary for any machining operation:

1. What tool shall I use?

2. What cutting speed shall I use?

3. What feed shall I use? (Taylor)

He understood that to answer these three questions many variables must be investigated. Over 26 years he studied twelve variables that he determined were the most influential to the machining process. Of those twelve variables, he believed the most important was "the quality of the metal which is to be cut" (Taylor). This variable can be understood as the material properties of the metal. At the time of Taylors investigations there were very few methods to analytically define these material properties. Therefore, he focused on the other variables that he could control and developed advances in metal cutting that would propel the manufacturing industry into what it is today.

In the 107 years since Taylor published his findings in "On the Art of Cutting Metals" many engineering advances have been made in the area of material testing. Today, there are standardized tests to define almost every property of a piece of metal stock. Using this information the "quality of the metal which is to be cut" can be defined more precisely than ever before. Experiments relating these material properties to their effects on the cutting force required to machine them provides information necessary to better answer Taylor's three great questions.

If a universal metal cutting formula is to be developed, a mathematical model must be developed that can accurately represent was happens as a tool removes metal from the stock. Many theories have been developed over the years to try and do this. In an effort to simplify this complex problem a form of machining called orthogonal metal cutting has been the subject of much study. Orthogonal metal cutting is a two-dimensional planar cutting process. The orthogonal machining approach allows the application of geometrical relationships between the tool and material to calculate the force and direction of the shear strain during metal cutting in conjunction with other metal cutting properties.

This research will address the geometrical relationships and attempt to relate the material properties obtained through standardized material testing to predict the cutting forces observed during orthogonal machining. The metal specimens will be optically observed at high magnification using a high speed camera while undergoing the orthogonal machining process. Cutting forces will be recorded simultaneously and synchronized with the high speed imagery. This synchronized data will be used to study the relationship of cutting tool geometry, depth of cut, feed, and material properties with the recorded cutting forces.

The work pieces in this experiment were cold rolled, causing a change in the grain structure of the metals. Cold rolling causes an increase in the hardness or strength of the metal, decreases ductility, and increases the dislocation density ( ). These known metallurgical effects, of which Taylor was unaware of at the time of his publication, now allow a detailed study of the “metal quality” or hardness

and it’s previously unstudied effect on the shear plane models proposed by orthogonal machining experiments to date.

Scope and Objectives

The goal of this thesis is to conduct orthogonal machining experiments to study the effects of machining parameters on the resulting cutting forces and shear angles in Copper 101, Aluminum 1100, and 1018 Steel. A detailed observation of the orthogonal metal cutting process was made possible using an all-digital high speed videographic quick stop device. The high speed videographic quick stop device consists of a high speed digital camera synchronized to force measurements from a dynamometer. Precise feed control is also made possible by utilizing a variable frequency drive (VFD) electric motor to move the workpiece underneath the cutting tool. National Instrument's LabVIEW software was used to create a virtual instrument for automatic data collection and organization. These updates to previous virtual quick stop devices permit more precise control over the orthogonal machining process than ever before.

The objectives of the experiment included:

1) Develop a better understanding of the metal cutting process
2) Develop a technique that allowed the observation of the chip formation process using a digital high speed camera at high magnification
3) Measure the Shear Plane Angle (ϕ), Shear Front Angle (ψ), and other geometries of interest directly from the images obtained

4) Capture high resolution still images of the metal cutting process during cutting that clearly show the geometries of interest for future publication
5) Investigate the propped Shear Front Angle (ψ) of Black and Huang in a new material not previously investigated; 1018 steel.
6) Investigate how the crystal structure of the metal to be machined affects the resulting geometries of interest and cutting forces
7) Perform tensile tests of the specimens to be machined for precise non-theoretical data of each specimen undergoing study
8) Publish the data set in a format (as appendices) which other researchers may use as a quality resource in their studies

Literature Review

Historical Survey

There have been various attempts to study, measure and quantify the variables in metal cutting since the beginning of the industrial revolution. A number of machine tools (e.g. lathes) were developed in their present form in the 1840's and 1850's during the emergence of the steam engine and its attendant uses. It was at about this same time that the first scientific papers on metal cutting appeared.

Economics, which F.W. Taylor cited as the prime mover behind his own studies, and metal cutting, have been closely linked since the earliest attempts to study the metal removal process. For example, in the earliest reference which could be found relating to scientific studies of the cutting process, Cocquilhat (23) in 1851, centered his studies upon the cutting with a drill of a rotating work piece. From these fundamental studies, he was able to extend his basic observations of the metal cutting process to more worldly interests. With the knowledge of work required per unit volume of material removed and assumptions of wages and working days, he then made some calculations on the costs of digging tunnels, cutting marble and trench digging.

The first experiments in which the influence of tool geometry was studied were reported by Joessel (47) in 1864. Forces were obtained in lathe cutting and drilling by measuring the torque required to turn the machine while cutting, care being taken to subtract the torque required to overcome the friction of the machine. The effects of depth of cut, speed, and rake angle were studied. References to "cutting fluids" are also found in his work (linseed oil, quicklime and nitric acid to name a few), although no explanation of their benefit was attempted.

The first attempts to study chip formation are those of Time (75) in 1870 and Tresca (76) in 1873. Time was the first to correctly model the process ahead of the tool as one of shear, although he may be criticized for his viewpoint that the chip formation took place by fracturing of the metal on successive shear planes rather than by plastic deformation. This is understandable though since the plastic deformation of metals in operations other than cutting was only beginning to be investigated at the time.

Mallock (55) produced a set of drawings of polished and etched chips in 1881 which rival modern photomicrographs in quality. He deduced that the cutting process was one of shear along a sharply defined shear plane with friction occurring along the tool face. With Time, he thought of fracture as occurring on the successive shear planes and described the chip as a "metallic slate." Mallock observed that the friction between the chip and the tool decreased when a "cutting fluid" was applied. His drawings clearly show that when cutting copper, the use of soap and water as a cutting fluid increased the shear plane angle, which is most

easily described as a line from the tip of the tool to the back of the undeformed chip, Figure 1. He was also the first to attempt to categorize the bluntness of the leading edge of the tool (the cutting edge) as a factor.

In 1892, Haussner (35) was successful in building the first instrument which could directly measure the forces involved in metal cutting. In this planning dynamometer, the work was restrained by a stiff spring. Deflections of the spring were magnified and a record was drawn by the dynamometer of the force against the distance of the cut. Although he was successful only in measuring the force horizontally along the cut, this was a major advance. He also noted the earliest comments on what appears to be the built up edge in stating that "with ductile materials, after cutting starts, chips welded to the tool and were very hard to separate". He may also have been the first to deduce the presence of a normal stress along the shear plane, concluding that the elements were not "freely sheared but is under a normal pressure".

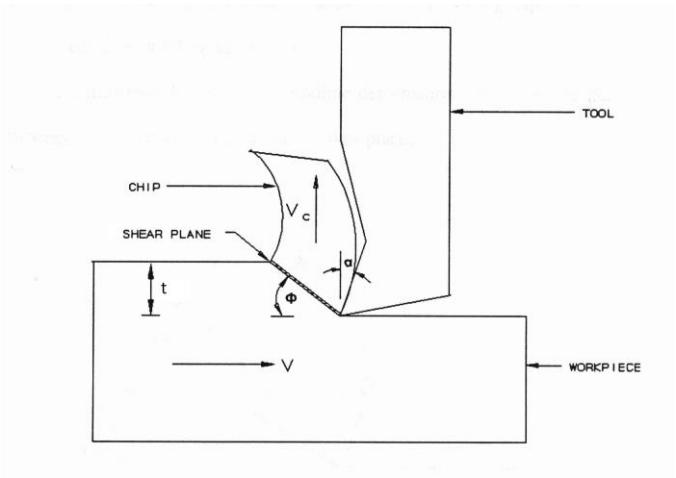

Figure 1: Shear Plane Angle and Tool Rake Angle

Zvorykin (95) published an extensive review of planing in 1893 using his new hydraulic dynamometer. He concurred with Haussner that the resultant force was not necessarily in the cutting direction. Assuming that the force in the direction of the cutting velocity would be a minimum led him to conclude the first attempt to predict the shear plane angle of Figure 1 in terms of the tool rake angle α and friction angle β.

$$\psi = 45 + \frac{\alpha}{2} - \frac{\beta}{2} - \frac{\beta'}{2} \tag{1}$$

Φ corresponds to the shear plane angle, β is the friction angle on the chip and β' is a friction angle for the shear plane itself. This is the first of many formulations of the functional relationship amongst the various angles detailed shortly in an attempt to formulate a predictive relationship based upon the observed geometries at the tool interface. This equation will appear again in the literature review of modern theory, with β' equal to zero:

$$\phi = 45 + \frac{\alpha}{2} - \frac{\beta}{2} \tag{2}$$

Equation (2) was derived independently in 1896, in the German engineering handbook "Ingenieur und Maschininenmechanick" (91). The basis of derivation in that case was that the shear plane would be the plane of maximum shear stress. The German handbook marks the beginning of the ongoing search for a predictive approach to the shear plane angle which eludes engineers to the current day. It carefully compared equations (1) and (2) at great length, offering reasons for the disagreement. Those equations continued in the literature after the turn of the

20th century. Linder (53) in 1907 and Ernst and Merchant (31) in 1941 obtained equation (1). Piispanen (64) in 1937 and Merchant (56) in 1945 obtained equation (2). The development of the many versions of this predictive equation will be detailed at great length in the Shear Zone Section of the literature review since one of the goals of the experiment is to compare the various models through a statistical analysis of the results.

Force analysis would continue to improve to the current day dynamometers and began to be joined with photographic studies in the "Roaring Twenties" when Coker and Chakko (19) carried out experiments in 1922, and Coker (20) in 1925 carried out a series of photo elastic experiments on the action of cutting tools. They were able to show in their photographs that there were zones of approximately radial compression and tension ahead of and behind a line going forward from the tool point, which corresponds to the plane defined by the angle φ in Figure 1. His photographs were not taken during cutting however, but during a stoppage of the tool. Ishii (44) in 1929 and Schwerd (71) were the first to study the cutting process while cutting was actually in progress. Photographs were also taken through a microscope by Boston (14) which presented detailed appearance of the metal cutting process. Their photographs were instrumental in the thought processes of the metal cutting investigators of the 1940's and continue to be highly regarded today by photographic experts in the metal cutting field.

It was also at this time that one of the first experiments examining hardness was conducted by in 1926 by Herbert (36). He showed that the chip material was harder than the work material and demonstrated that metal cutting

involved intense strain hardening which could only come about through the mechanisms of plastic flow.

Cutting Geometry with a Single Edge

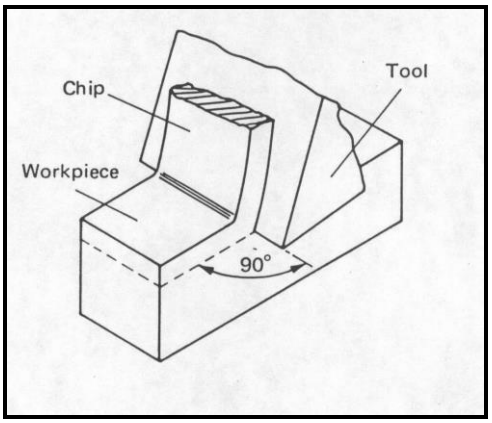

Figure 2: Orthogonal Machining Cut (12)

Orthogonal cutting such as depicted in Figure 2 is seldom used in practice, although it remains the simplest model for scientific analysis. Nearly all practical cutting processes are oblique, where the leading tool edge is inclined to the relative velocity vector between the tool and work. Even in today's computer age, modeling such a difficult geometry remains a daunting task. Thus, it is necessary to consider how the mechanics of the orthogonal cutting can be extended and altered to describe oblique cutting. Beginning in the 1940s, the Orthogonal Machining Process (OMP) of Figure 2 became the basis upon which subsequent models and discussions were based. The commonly used phraseology is provided in the List of Symbols. Most of the derived equations are summarized

in Appendix 1. A complete discussion of the model and the formulas derived from it are beyond the scope of this experiment, but excellent reviews may be found in Degarmo, Black and Kohser's text (27) or the work of Shaw (68), Trent (77) or Wright (78). A short discussion is however necessary to set up the shear zone review and discussion.

There are three basic chip types formed during the orthogonal machining process as first denoted by Ernst (30). Type 1 is a discontinuous or segmented chip type; Type 2 is continuous and smooth; Type 3 is continuous with a buildup of chip material between the tool and chip which is commonly referred to in the literature as "built-up edge" or BUE. All of the models discussed hereafter assume a Type 2 chip.

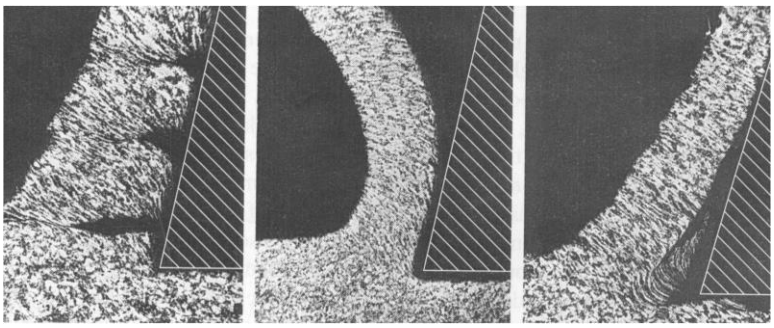

Figure 3: Type 1, 2, and 3 Chips Respectively (68)

The modern era of metal cutting research began with the nearly simultaneous work of M.E. Merchant and V. Piispanen during the years leading up to and during World War II. These two men independently proposed the classic force relationships that are used to describe the OMP model.

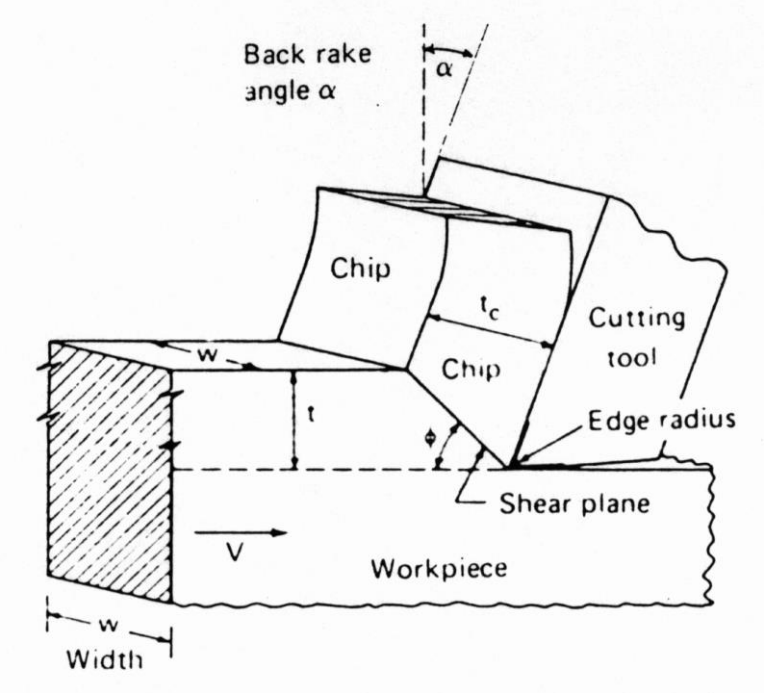

Figure 4: Orthogonal Cutting Process (27)

Figure 4 depicts the commonly accepted symbology of the Merchant and Piispanen model, detailed in the List of Symbols. Basically, the shearing process occurs on a single plane extending from the edge of the cutting tool to the free surface of the workpiece. This plane is commonly referred to as the "shear plane". The shear angle φ is measured from the horizontal to the plane as depicted in Figure 4 and varies depending upon the particular cutting conditions. The shape of the zone on or around this plane has been the topic of intense academic interest since publication of the models in the 1940s occurred. Before beginning the review of the many "shear zone" models, a basic review of the process which led to the development of the geometric force relationships of Appendix 1 will be made using the nomenclature of the List of Symbols.

Both Merchant and Piispanen independently developed similar concepts for a force diagram which illustrates the geometrical relationship between the cutting force components during orthogonal machining. This has become the fundamental basis allowing the formulation of the relationships detailed in Appendix 1. Both researchers viewed the chip as an independent body held in mechanical equilibrium by the two equal and opposing resultant forces R and R'. The force R is due to the force exerted by the workpiece on the chip. The force R is composed of two components; the shearing force along the shear plane (Fs) and a force normal to the shear plane (Fn). The force R may also be resolved into two other components, the cutting force (Fc) and the thrust force (Ft). Figure 5 shows these relationships in what is now commonly referred to as the Merchant force diagram.

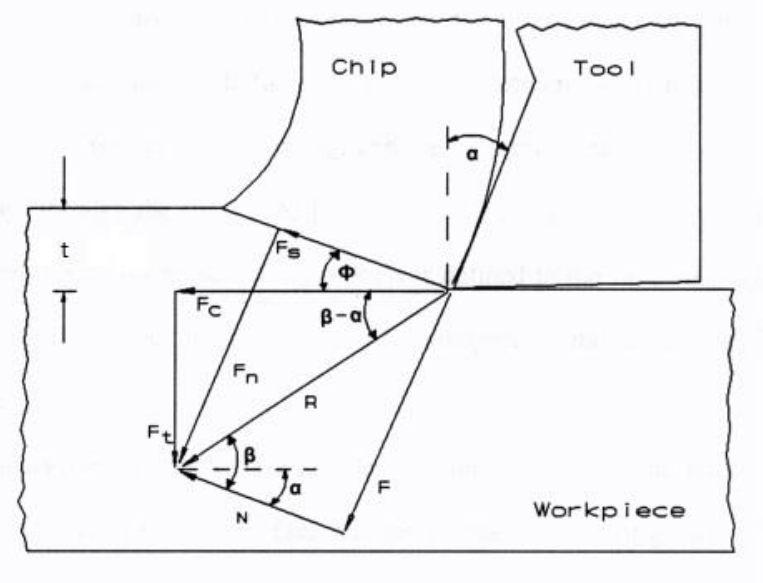

Figure 5: Merchant Force Diagram (68)

The Merchant force diagram applies the opposing force concept of the free body diagram of the chip to the orthogonal cutting process shown in Figures 2, 4 and 6. The force R' is the force that is exerted upon the chip by the cutting tool. It may be resolved into two components, F and N, where F is the friction force between the chip and the cutting tool and N is the force normal to the chip and the cutting tool. The forces Fc and Ft are easily measured during the orthogonal cutting experiments by the use of a force dynamometer. The force due to friction F can then be calculated from the measurement of the cutting and thrust forces as shown in the following equation:

$$F = F_c \times \sin\alpha + F_t \times \cos\alpha \tag{3}$$

The coefficient of friction μ that acts between the cutting edge of the tool and the chip is defined by the following equation:

$$\mu = \frac{F}{N} = \tan\beta \tag{4}$$

The angle β is between friction force F and the normal force N as shown in Figure 5. Merchant's orthogonal model permitted the calculation of values such as equations (3), (4), (5) and the others in Appendix 1 using forces readily measurable with modern dynamometers. The angle β is particularly important in the various predictive shear strain models as shall be demonstrated and investigated.

The resultant R, which is equal, opposite and collinear with R' may be resolved into Fn and Fs using the measurement of the cutting and thrust forces as with the following equation:

$$F_s = F_c \times \cos\phi - F_t \times \sin\phi \quad (5)$$

Merchant's and Piispanen's work have permitted the quantification of forces at and along the tool-chip interface (Appendix 1). This has formed the basis for modern attempts to develop a predictive mechanism for the shear front plane by establishing their own version of equations (1) and (2) using the geometry of Figure 5. This marks the beginning of the modern "shear zone" investigation.

The Shear Strain Models

The Merchant model of orthogonal cutting permitted the development of expressions for flow stress, shear energy, temperature and chip morphology such as those listed in Appendix 1. Shear strain, as well as shear stress, was described in his model but has not been as successful in predicting results. Various models for the shear process have been proposed in the machining literature. These models may be divided into two broad categories, the thin-zone and thick-zone models. Neither model is completely successful but each has its proponents. The thin-zone model appears to be most successful in describing cutting at a high speed, whereas the thick-zone model is most often used to describe the machining process at very low cutting speeds.

Merchant's model represented the shear zone as a single plane, or thin-zone model. The angle of inclination of the shear plane to the cutting direction was defined by the angle φ. Merchant observed that the crystal structure of the

material was elongated by the shear process and gave the direction of crystal elongation the direction ψ.

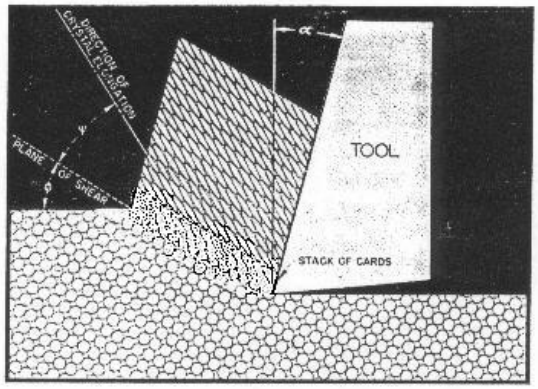

Figure 6: Merchant's Observation of Chip Formation (56)

Merchant did not develop the plastic deformation aspect of his observations. Both Merchant and Piispanen used a "deck of cards" concept to visualize the shear zone process, where the shear mechanism during chip formation can be illustrated by the incremental displacement of cards in a stack (Figure 7). Each card moves forward a small amount in respect to the next card in the stack as the cutting process occurs. Merchant (57) proposed that the crystalline structure of the metal was elongated by the shear process, and that the direction of elongation was in a different direction than the shear plane.

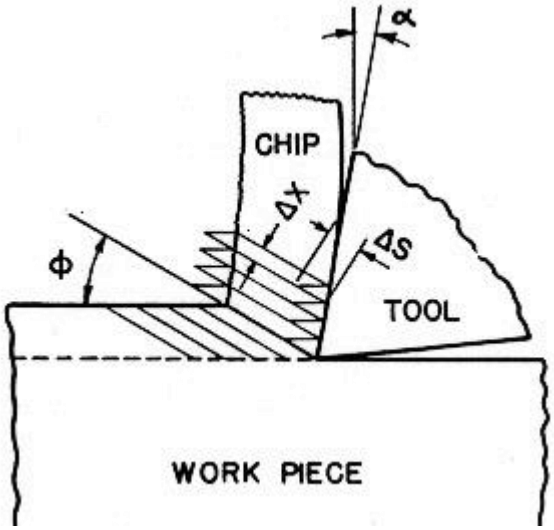

Figure 7: Merchant's Stack of Cards Model (56)

The thickness of each card element was ΔX, and each element in the model was displaced through distance ΔS with respect to its adjacent neighbor. Therefore, the shear strain, γ, could be expressed as $\gamma = \Delta S / \Delta X$. From the geometry of his stack of cards, Merchant thus developed the following equation:

$$\gamma = \frac{\cos \alpha}{\sin \phi \times \cos(\phi - \alpha)} \tag{6}$$

Ernst and Merchant would eventually observe (31) that the angle between the resultant force R and the shear plane was thus given by:

$$\phi = 45 + \frac{\alpha}{2} - \frac{\beta}{2} \tag{7}$$

Equation (7) was the first of many modern attempts to derive a functional angle relationship f (α, β) of some type. It has come to be referred to as the Ernst and

Merchant solution (29). Although independently derived, this is again the result Zvorykin published in 1893 as equation 2 in this review.

Lee and Shaffer (52), in their 1951 paper, examined the geometry by considering that a part of the chip would behave as an ideal plastic solid. Using Mohr diagrams they developed the following relationship amongst the angles of the Merchant model:

$$\phi = 45 + \alpha - \beta \tag{8}$$

Thus both equation (7) and (8) suggest a strong interaction between the frictional angle and the tool rake angle in determining the shear plane angle. This has not proven to be a very satisfactory observation. Eggleston et al (29) noted in his detailed review of the observations of the angle relationships that neither the Ernst and Merchant formulation, based upon the minimum energy criterion, nor the ideal plastic-solid solution of Lee and Shaffer, nor the mathematical derivations of Hill are in agreement with all the experimental observations.

Merchant's model has been extensively examined, published and cited as the first thin-zone model. It has been seriously criticized by some academics because of its inability to describe the actual deformation process in machining. For example, a particle moving along the cutting direction into the shear plane must abruptly change direction at the plane and then flow in the direction of the chip. This represents a discontinuity in the tangential component of velocity on the shear plane, requiring an infinite acceleration across the shear plane. An examination of the actual shape of the deformation zone is one of the goals of this

experiment and a further review of the many shear zone models is continued below.

Okushima and Hitomi (60) developed a simplified thick-zone model in 1961 which is depicted as Figure 8. The suggested a very large transitional zone AOB.

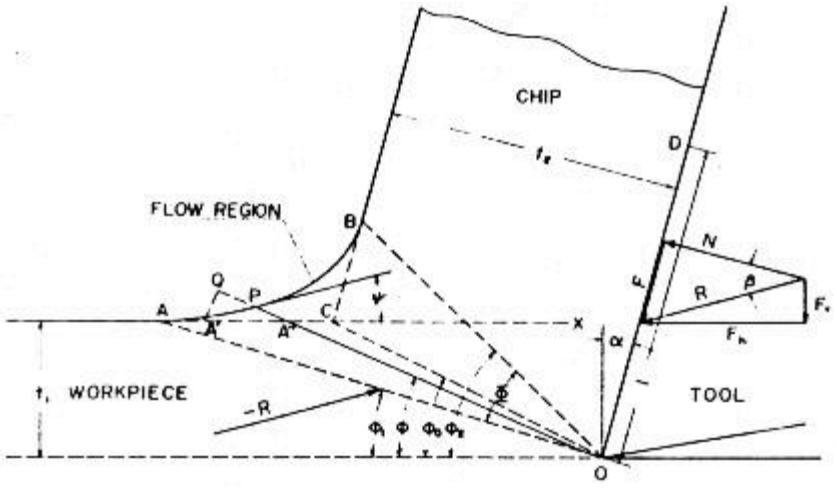

Figure 8: Okushima and Hitomi's Model (60)

The AOB zone existed for plastic deformation of metal between the rigid region of the workpiece and the plastic region of the steady chip as it moved away up the tool face. Plastic deformation began to occur at the starting boundary line of the shear zone, OA, and the plastic strain gradually increased as the cut progressed. Shear strain inside the shear zone AOB was expressed as follows:

$$\gamma = \cot\phi - \cot(\phi - \Psi) \tag{9}$$

Here ϕ is the inclination angle of the arbitrary radial plane, and ψ is the tangent to the free surface (curve between A and B in Figure 8) with the machined surface.

This model predicted that the shear strain was zero at the lower boundary of the shear zone and obtained the maximum at the upper boundary of the shear zone.

In 1966, Zorev (94) proposed the thick zone model detailed in Figure 9. Line OL defined the initial boundary of the zone and OM the final boundary of the shear zone. Inside the shear zone LOM, there was a family of shear lines along which shear deformations were formed. Work material passed through the shear zone and was subjected to increasing shear strain:

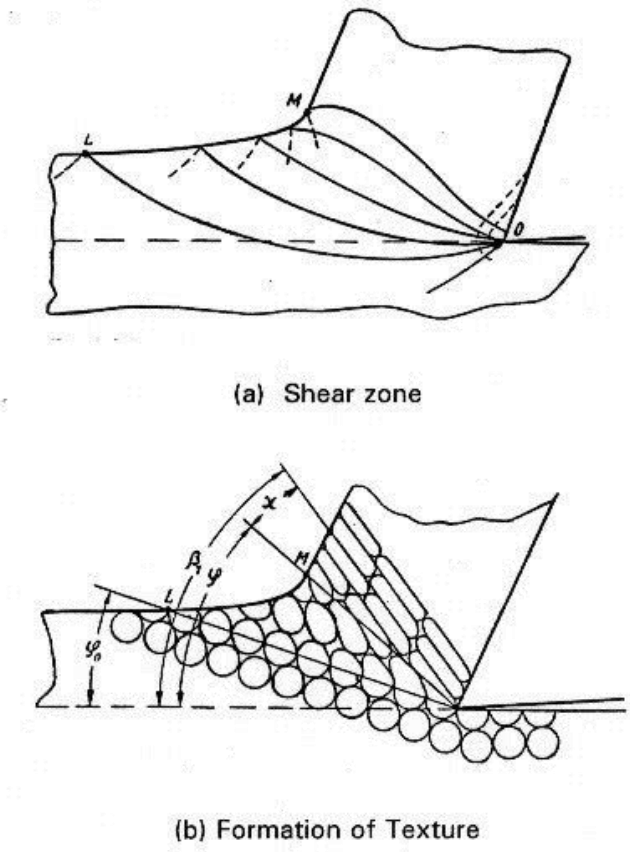

Figure 9: Zorev's Model of a Thick Zone

The initial boundary of shear zone is similar to the onset shear plane proposed by Black in a later paper. The direction of shear deformation was tangent to each

line. The shear direction was approximately parallel to the initial boundary of the shear zone.

Zorev's expression of the shear strain is the same as equation (9) above. The texture of the chip formation, due to shear deformation, changed from an equiaxial structure into a non-equiaxial structure, as shown in the lower (b) section of Figure 9. The angle ψ in his formulation, between the direction of the texture and the direction of the plastic shear, was a function of the degree of plastic deformation and was determined by the following relationship:

$$\cot \Psi = \frac{\gamma}{2} + \sqrt[2]{1 + \frac{\gamma^2}{4}} \tag{10}$$

Oxley (63) proposed a parallel-sided shear zone model in 1989 as depicted in Figure 10. The total maximum shear strain in the shear zone was found by multiplying the average maximum shear strain-rate in the zone by the time a particle took to flow through the zone.

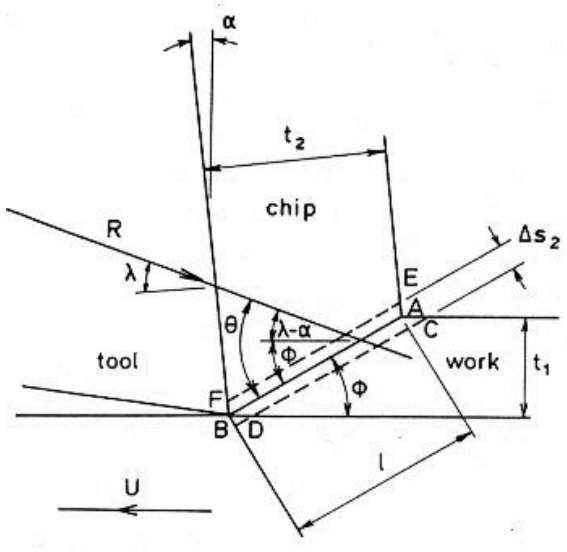

Figure 10: Oxley's Parallel-Sided Shear Zone Model (63)

Maximum shear strain was expressed as

$$\gamma_{ef} = \frac{\cos\alpha}{\sin\phi \times \cos(\phi - \alpha)} \tag{11}$$

It was assumed that one half of the total strain in the shear zone occurred at the centerline, AB. The shear strain in the plane defined by AB was taken as

$$\gamma_{ab} = \frac{\cos\alpha}{2 \times \sin\phi \times \cos(\phi - \alpha)} \tag{12}$$

A "stationary" shear zone model was presented by Van Luttervelt (83) in 1977 as depicted in Figure 11. This model is similar to Oxley's parallel sided shear zone model.

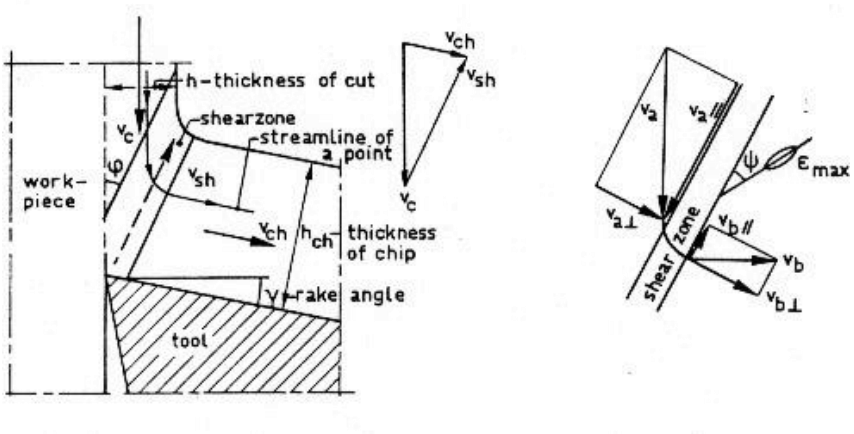

Figure 11: Van Luttervelt's Stationary Shear Zone Model (83)

The material entered the shear zone with velocity Va, which might be resolved into two components, one parallel to the shear zone and the other perpendicular to the shear zone. The material left the zone with a velocity Vb, which could also be

decomposed into its parallel and perpendicular components. The shear strain within the zone was derived from these components as:

$$\gamma = \frac{\cos(2\times\phi-\alpha)}{\sin\phi\times\cos(\phi-\alpha)} \tag{13}$$

The direction of maximum elongation described in Van Luttervelt's model is the same as in Oxley's model.

Another shear zone model was suggested in 1996 by Huang (39), working as a graduate student for J.T. Black. During a review of Brigg's (13) experiment using high speed magnification to observe the cutting of aluminum, Huang developed a new "stack of cards" model and a new shear strain equation of orthogonal machining. In reviewing the tapes made by Briggs, he observed that the material deformed in a totally different fashion than that which had been described in the machining literature. The plastic deformation of material as observed by Huang and Black is depicted in Figure 12.

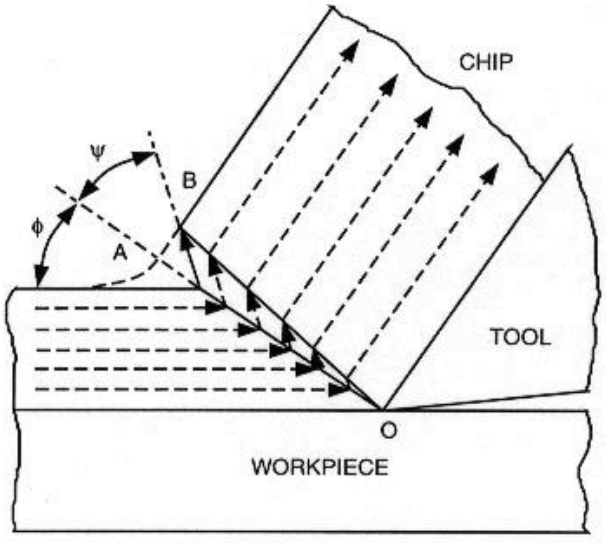

Figure 12: Huang's Observation of Flow in Shear Zone (39)

As the material in the workpiece moves from left to right, toward the cutting tool along the cutting direction, it approaches the shear zone, designated by the triangle AOB. When the material encounters the onset shear plane AO, it changes direction and appears to move at an inclination angle, ψ, to the plane. This is the shearing of the metal caused by the massive movement of many dislocations. Upon reaching the plane BO, the shearing process stops, and the material changes direction a final time and moves in a direction parallel to the tool face. The shape of AOB is triangular and the onset shear plane is flat. The material encounters plane AO simultaneously and shear is in mass all along the boundary. This onset of shear fronts creates the shear plane and defines the lower boundary of the shear zone. Thus φ has been more properly termed by Black the Onset of Shear Plane angle (6). The termination of the shear fronts forms the upper boundary of the shear zone as noted by Black and Briggs (9). The shear fronts are inclined at an angle, ψ, originating from the plane connecting the tool tip to the free surface. His reasoning behind this movement was the presence of dislocations in the material. Figure 13 details the angular relationships as derived by Huang.

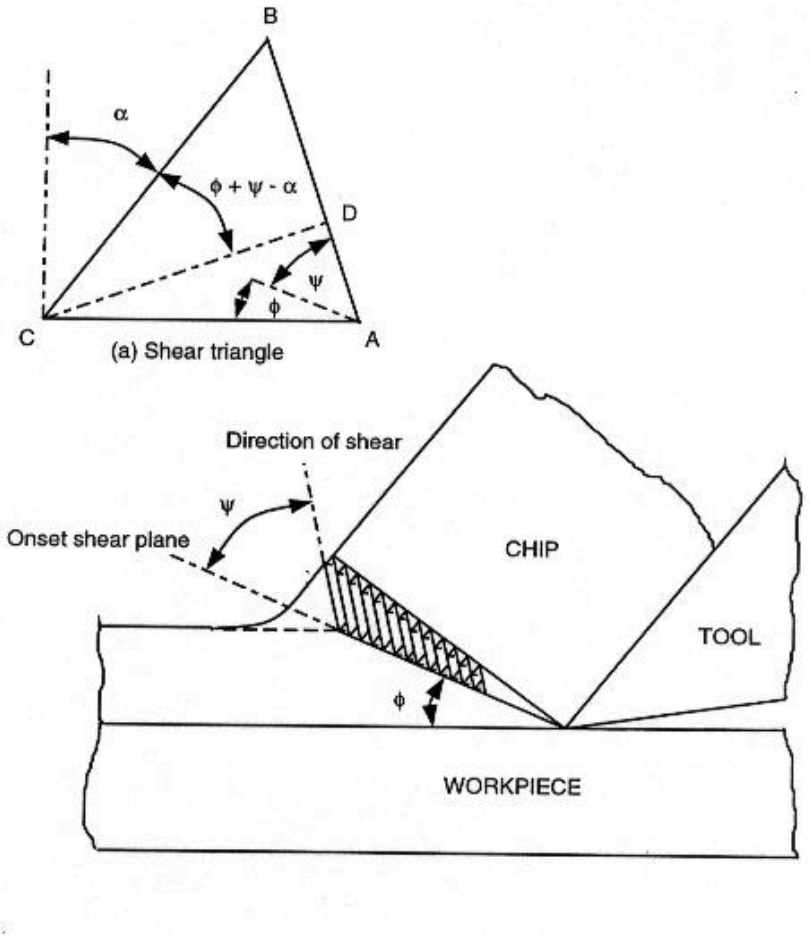

Figure 13: Huang's "New" Stack of Cards Model

Huang's model is significantly different than Merchant's model. In the new card model, an element shears at the direction ψ relative to the onset shear plane. (In Merchant's model, an element shears in the direction of the shear plane φ. In Zorev's model the work material shears tangentially to a shear line that is approximately parallel to the initial shear plane.) Using minimum energy criteria Huang developed the following relationships for ψ and γ:

$$\varphi = 45 - \phi + \frac{\alpha}{2} \tag{14}$$

$$\gamma = \frac{2 \times \cos \alpha}{1 + \sin \alpha} \tag{15}$$

Reference (39) details all the mathematical derivations of Huang's work as does a later appendix. He explains the movement at the shear plane in terms of dislocation theory.

Dislocations and Metal Cutting

Dislocations have been a major field of study in material engineering and applied physics for over seventy years now, but metal cutting researchers have not typically addressed hardness, dislocation density or dislocation movement in their work with a few noted exceptions. Dieter (28) gives an excellent overview of dislocation theory in general as it applies to material. His integrated overview of the effects of cold rolling in his discussion of metallurgical structure will prove useful later in discussing the conclusions of this experiment.

Research on the effects of material hardness in metal cutting since the efforts of Taylor at the turn of the century and Herbert in the 1920's has been sparse. P.K. Wright (92) made a great contribution to this area in 1982 when he suggested that the work hardening characteristics of the material are the most dominating influence on shear angle in machining. The friction angle and the tool/chip contact interface are important, but not governing factors in his review of available data sets. He was not able to develop a predictive theory from his analysis, but he believed that it would be possible to predict a "ϕ range" for a

material. He ignored the effects of the frictional constraints at the chip-tool interface in his analysis.

Von Turkovich (84) discussed dislocation theory as it applied to shear stress in his 1967 paper. Although he was primarily concerned with high speed machining in this paper, he believed that shear stress computation in a Type 2 Chip was possible using the materials elastic constant G(T), the materials characteristic Burger's vector (b) and the dislocation density.

Ramalingham and Black (66) showed that the important variables involving dislocations are the "number and orientation of slip systems, certain characteristic dislocation parameters as the stacking fault energy, the interaction of dislocations with vacancies and solute atoms" in the scanning and transmitting electron microscopy studies of α brass. In their microscopic studies, they cut the material with diamond blades and studied the recrystallization at a molecular level.

Black (6) proposed a model in 1979 for the plastic deformation that occurs in metal cutting. He demonstrated that the magnitude of the flow stress and the onset of shear angle φ correlated to the stacking fault energy of the material being cut. His resultant flow stress model predicts a catastrophic shear front, or shear plane, ahead of the tool, created by the annihilation and subsequent heat generation as the metastable cells in his model rearrange themselves. The model observes that dislocations sources originate near the tool tip, driving dislocations into the cell networks. There is a rapid buildup of applied stress levels as the

number of dislocations increase, causing a forest hardening effect at the tip of the tool (24)

Black's paper notes that more than one shear front would be crossing the material from the tool tip to the free surface at any one point in time, comparing this effect to waves at the seashore. Waves from the ocean will intersect a jetty on the beach at many different points along the length of the jetty, but always at the same angle. This is a good analogy to the deformation observed by Black Huang in aluminum as they developed the "new stack of cards" model. Note that there are many cards sitting on the "onset of shear plane at angle ψ. The onset angle ϕ is dictated by other material properties. Black's theory predicted that as work-hardening increased; the resistance to the onset of shear will increase. This delay in the initiation of shear would translate into an increase in the onset shear plane angle ϕ. If measuring techniques existed for the angle ψ, one could examine the relationships stated in equations (7), (8) and (14) as well as the shape of the shear zone.

Black and Krishnamurthy (11) conducted a small experiment where they examined the relationships between hardness and shear stress in 6061-T6 aluminum. They noted that shear stress varied with the material hardness over the four samples. They were widely spaced, with varying hardness produced by annealing the as received aluminum. There results suggested that dislocations could possibly explain the differences which they had observed. In particular, when the aluminum was softened by heat treating, the dislocation density was reduced as predicted by Cottrell and others. This reduces the amount of pinning

in the material, allowing more mobility which translates into a lower yield stress. This is also discussed in Dieter (28). Cold rolling has a similar, although opposite effect which will be discussed later.

High Magnification Photography

The observation of the shear zone and the geometries associated with it is a difficult task. The deformation process is a complicated one occurring under very high rates of strain in a small area, making it extremely difficult to measure the shear strain expressions experimentally.

Photography and optics have advance dramatically since Coker's photo elastic attempts in the 1930's. With the advent of scanning electron microscopy techniques, the fundamental structure of various chips that developed during micromachining has been observed at very high levels of magnification by Black (5), Ueda and Iwata (79), and others. This coupled with advances in high speed film and digital imaging such as the Briggs experiment (13) permits a detailed study of the deformation zone ahead of the tool.

Cook and Shaw (21) used magnified cinematography as early as 1951 to analyze the shear process. They observed a thick shear zone and at various times two shear zones. One zone (the primary zone) extended from the tip of the tool along the shear plane while the secondary zone at times appeared adjacent to the tool face. They noted that the frequency of the two zones was "perhaps" more

pronounced when cutting materials that strain harden easily and produce thick chips.

Agrawal and Amstead (1) examined the cutting of mild steels with a FASTEX high speed motion camera in the 1960s. They detected the presence of Built Up Edges (BUE), crack formations, and deformation ahead of and below the tool. Their study would also indicate that the shear zone region was not a simple, narrow zone problem. Agrawal and Amstead recognized that their system had technique problems common to all photographers: control of lighting, vibration, movement of the target, focal length, depth of field and magnification.

Oxley (61) conducted experiments with cinematography through a microscope up to 50X to directly observe the cutting zone. These were instrumental in his formulations of the Oxley shear zone model.

Komanduri and Brown (51) recorded at rates up to 3000 frames per second to study chip formation at high (180 sfpm) rates of speed. They encountered the standard problems that Agrawal, Amstead and others encountered when trying to trade off magnification for depth of field. Lighting was a significant problem in their experiment.

Black and James (7) were more successful using high speed motion pictures to record at up to 4000 frames per second as they analyzed the results of their Quick Stop Device (QSD) experiments for orthogonal machining. They were instrumental in studying the disengagement process of the chip from the tool.

J.H.L. The (74) attempted to study the commencement of cutting (the incipient stage) using a high speed camera and a stroboscope. The qualities of the films produced were not consistent and set-up was very difficult and time consuming.

Warnecke (89) used a microscope and a high speed 16 mm camera to study the chip formation process and the initialization of the BUE. He produced a very good video of the overall process that has good classroom value, but the quartz plate technique used to provide optical contrast and limit lateral deformation of the chip limited the ability to observe the microscopic deformation of the chip. Still, this was an excellent advancement in the use of lighting, with a wide range of cutting speeds being observed.

Briggs (13) used a high quality Kodak Ektapro Imaging System (using the EM Model 1012 Processor) and an Infinity K2 Lens with and intensified Imager to conduct an experiment examining some of the classical factors (α, depth of cut, V, tool contact length, and temperature) in an experiment whose primary video objective was to produce a classroom video for metal cutting. The tapes produced of the shear zone were without doubt the best produced to date and formed the basis without further experimentation of Black and Huang's "new" deck of cards model. The existence of a definitive, easily viewed zone of plastic deformation was strongly supported by his studies of aluminum. The primary drawback with the system being used was the cost and availability. The unit was borrowed and it usage was limited to a very small amount of time. Since then, simpler video

cameras at a fraction of the cost have emerged on the top end of the consumer market that may be useful in a continued study of the shear zone.

Scanning Electron Microscope (SEM) technology has been invaluable in establishing the role of dislocations in the cutting process. Black (4) studied single and polycrystals using the SME and published the work (5). Von Turkovich and Black (86) used SME in studies of chip and workpiece deformation. Ramalingham and Black (66) developed the first in-situ machining technique (machining microscopically within the SEM itself on a stage they developed) and observed the formation of shear fronts and heterogeneous plastic flow during chip formation. It also established the validity of post cut (static) examination of chip morphology to explain the mechanics of chip formation. Black and Cohen (18) would later extend in-situ techniques to measure, for the first time, shear velocity directly, along with chip velocity, shear strain and the strain rate. Their measured velocities were comparable to the calculated velocities of standard orthogonal mechanics from the equations listed in Appendix 1. Scanning electron microscopy is important also because it permits the before and after analysis of dislocation generation during work hardening by the tool face.

Summary

In the time since F.W. Taylor's generation, great advances have been made in modeling the metal cutting process. Brinell invented a means to reliably

measure and compare the hardness of materials that escaped Taylor. Dynamometers have been developed with great accuracy to measure the forces involved in cutting as modeled by Merchant and others. Photography now allows for a detailed study of the shear zone ahead of the tool, both macroscopically and microscopically. Remarkably, no one has conducted a detailed study of the effects of hardness. Predictive models for the metal cutting process are still inconsistent and incomplete.

Materials, Instruments, and Machines

Many different materials, instruments, machines, electrical hardware, and software were used during this experiment. The following lists and figures describe in great detail what was used to obtain the results presented in this thesis. All figures will include a detailed description of the particular piece of equipment and how it was used.

The materials chosen for this experiment are listed below along with the source from which they were obtained. The initial hardness temper or level of hardness is also listed for each material as they were specifically chosen prior to ordering.

Copper 10100 OFE (oxygen free electronic)
- Farmers Copper
- Temper H01

Aluminum 1100
- McMaster-Carr
- Temper H14

1018 Steel
- McMaster-Carr
- Hardness: Medium (Rockwell B70)

The equipment and instruments listed below were used together to create the virtual quick stop device in its entirety. The equipment listed includes everything from the base machine, upgrades to the machines, fixturing of the

workpiece specimens, cutting tools, recording equipment for forces and feeds, lighting, video recording hardware, and software used data acquisition.

CINCINNATI No. 2 HM Horizontal Milling Machine

BALDOR 1/8 Horsepower Three Phase Induction Electric Motor

WOOD'S E-Trac AC Inverter

Quick-Stop Workpiece Holder

HSS Stick Tools, (0.75 x 0.75 inches) at Various Rake Angles

YUMO Rotary Encoder

KISTLER Dual Mode Amplifier

KISTLER Dynamometer

NATIONAL INSTRUMENTS USB-6008

DOLAN JENNER Fiber-Lite A-200

STOCKER AND YALE Imagelite Lite Mite Model 20

Fiber Optic Ring Light

Modified Load Lift Camera Stand

Cross Slide Vice

DRS TECHNOLOGIES Lightning RDT Camera

INFINITY InfiniVar Lens

NATIONAL INSTRUMENTS LabVIEW

XCITEX Midas 2.0 Video Capture Software

The following equipment was used to prepare the various copper, aluminum, and steel specimens to the appropriate dimensions and properties before undergoing the orthogonal machining process. This list also includes any machinery used to create any custom fixtures or tooling required as well as the material testing equipment used to obtain the material properties of the final specimens. Software used for design and post processing of data also listed.

CINCINNATI Arrow VMC-750 CNC Mill

BRIDGEPORT Vertical Milling Machine

SOUTHBEND Lathe

DO ALL Vertical Band Saw

WILTON Belt Sander

STANAT Rolling Mill

ROCKWELL Hardness Tester

BRINELL Hardness Tester

MTS Q Test 100 Tensile Tester

DASSAULT SYSTEMS Solidworks Modeling Software

AUTODESK HSMWorks CAM Software

MATHWORKS MATLAB

MINITAB 15 Statistical Analysis Software

MICROSOFT Excel 2010

GIMP Image Manipulation Software

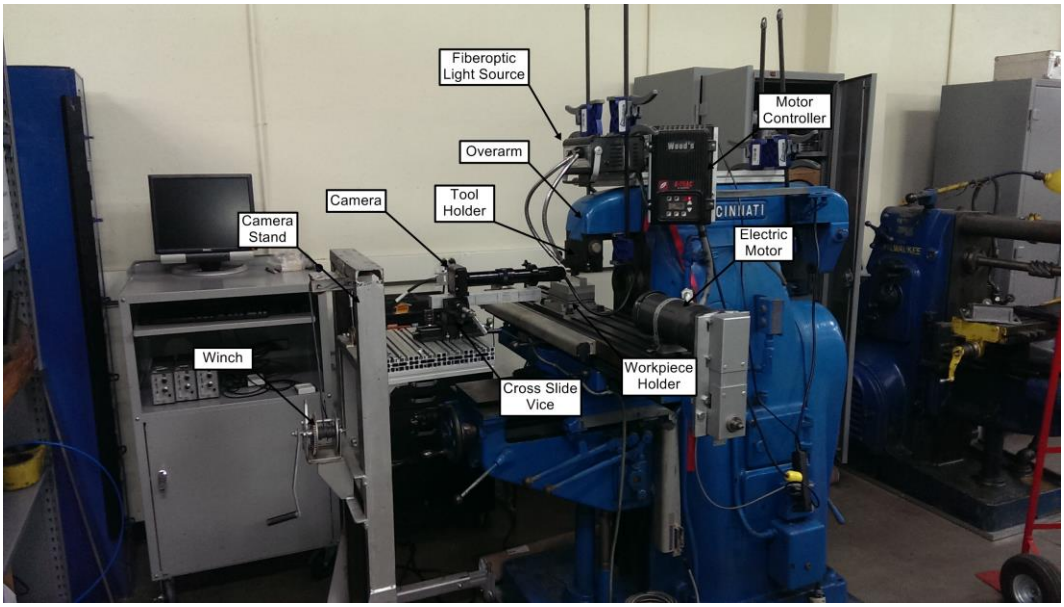

Figure 14: Elevated View of Equipment Setup

An elevated view of the testing area is shown in Figure 14 above. The major components are notated. A computer cart containing the data acquisition PC is seen in the left hand corner. The cart also holds the NI USB modules as well as the amplifiers for the dynamometer. The user must first start the data acquisition programs and start the camera recording before moving to the near side making sure not to hit the camera stand in the process to start the motor controller. This location was necessary due to cable lengths and proximity to the power bus located on the wall.

Figure 15 shows the workpiece holder with the camera moved out of the way. The workpiece holder was made out of aluminum and covers the entire dynamometer face and attaches to it with socket head cap screws. The socket head cap screws are recessed into the block so as to allow more room for the

camera lens to get close to the specimen. The slot cut into the top of the workpiece holder is just over 4 inches long to hold a 4 inch long specimen.

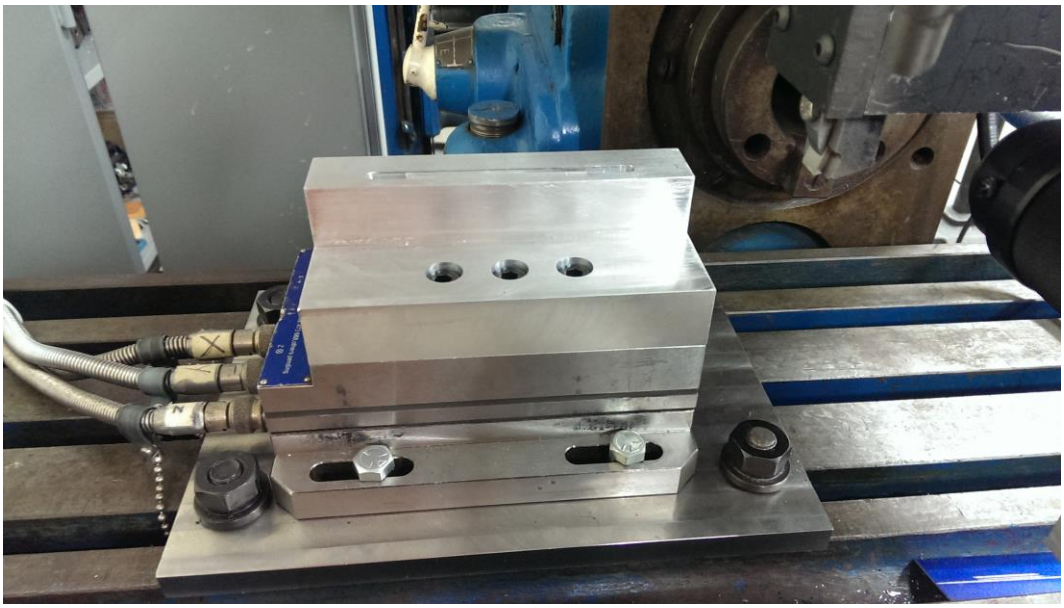

Figure 15: Quick Stop Workpiece Holder

The back side of the holder has ten threaded holes for set screws that apply a clamping force onto the specimen undergoing testing. A finite element analysis was performed on the workpiece holder to ensure that the front wall of the slot would not yield when the set screws were all tightened. The dynamometer itself is attached to a steel plate that is then attached to the horizontal milling table using T-nuts and bolts.

The tool holder can also be seen in Figure 15 in greater detail. The tool in the figure is an older version of the tools used. The tools used were ¾ by ¾ high speed steel tools ground to the correct angles.

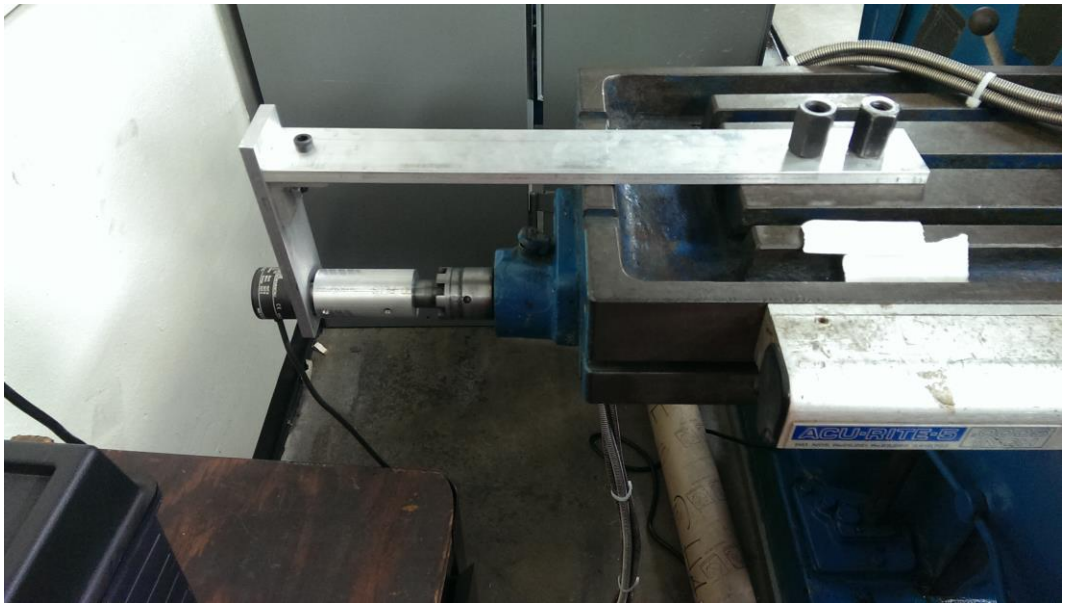

Figure 16: Rotary Encoder

In the figure above the rotary encoder can be seen attached to the lead screw of the horizontal milling machine. A coupler was machined on the lathe that would couple the lead screw to the rotary encoder shaft. The supporting bars going from the table to the encoder are there to make sure that the encoder does not rotate with the shaft. The supports were attached to the horizontal milling table with T-nuts and bolts.

Figure 17: Kistler Dual Mode Amplifiers

The Kistler dual mode amplifiers can be seen in Figure 17 above. Each axis of the dynamometer has its own amplifier. All of the functions for the amplifiers are located on the front as shown for easy operation.

Figure 18: National Instruments USB-6008

The National Instruments USB-6008 can be seen on the above. Two of these data acquisition device was used for many different purposes. The rotary encoder connected to one and the other one took in the amplifier signals for data logging. The device that took in the data from the amplifiers also output a signal to the high speed camera letting it know when to start recording. This allowed software triggers to be defined for to aid in the capture of images for processing.

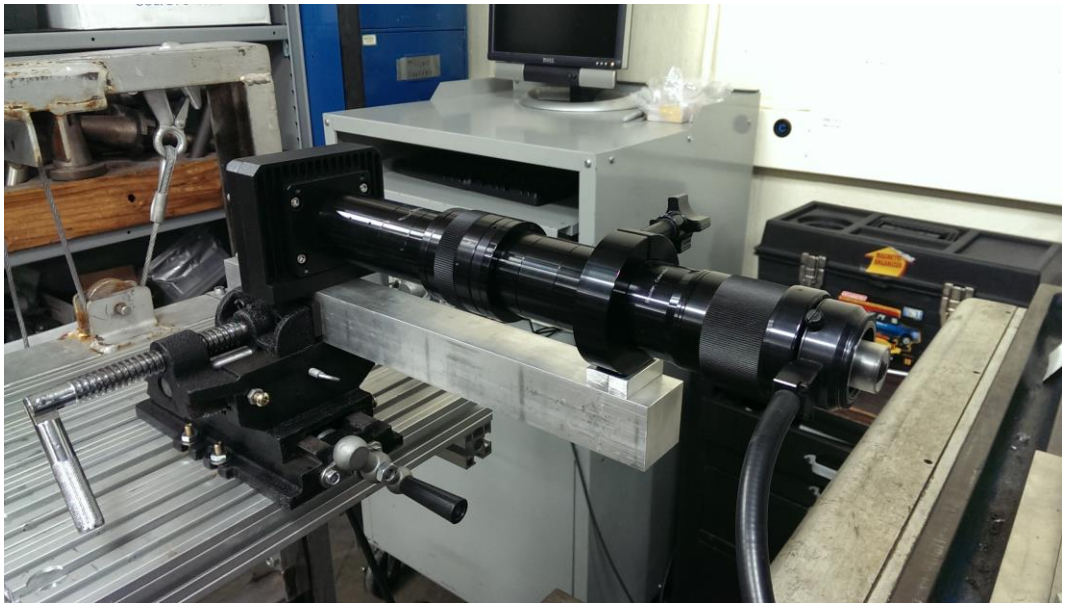

Figure 19: Modified Load Lift Camera Stand

The camera stand can be seen in full in Figure 14. Figure 19 shows a close up view of the camera and how it is attached to the custom made camera stand. Notice how the stand has a modular table that allows many different attachments. The cross slide vise is mounted to the camera stand table with bolts and nuts that slide into the T-slot grooves in the table. The camera is attached to a rectangular piece of aluminum which is clamped in the cross slide vice. The piece of aluminum extends out to support the weight of the camera lens as well. The cross slide vice made adjusting the camera position on a very fine scale a much easier task.

Figure 20: DRS Technologies Lightning RDT Camera

The DRS high speed camera can be seen above with some of the hardware specifications marked.

Figure 21: Cincinnati Arrow VMC 750 CNC Mill

The Cincinnati CNC milling machine can be seen on the previous page. This machine was used to cut out the tensile samples from each specimen as well as size the samples to the correct thicknesses before cold rolling. G-code was generated on a separate PC and then loaded via USB stick onto the CNC machine.

Figure 22: Bridgeport Vertical Milling Machine

The Bridgeport milling machine shown above was used to get the specimens to the correct size to fit into the workpiece holder after cold rolling.

Figure 23: Do All Vertical Band Saw

The vertical band saw seen in Figure 23 was used to initially rough cut out the specimens from the raw metal stock.

Figure 24: Wilton Belt Sander

The belt sander was used to remove burrs from specimens while undergoing the machining down to thickness to make sure that they sat flat in the vice resulting in perfectly flat pieces. The belt sander was also used for initial sanding of the samples after coming out of the rolling mill.

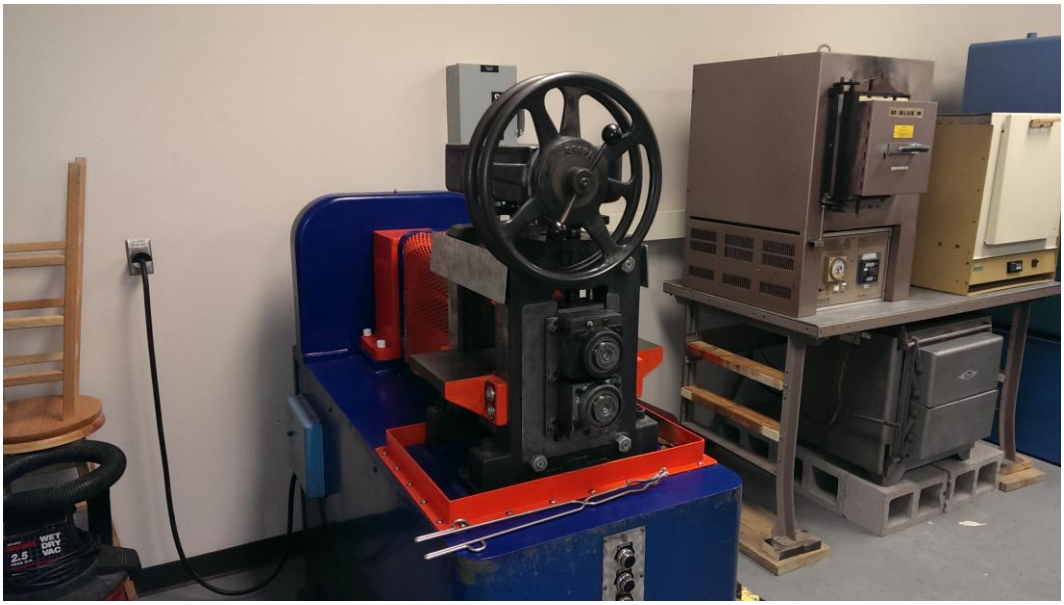

Figure 25: STANAT Rolling Mill

The Stanat rolling mill was used to reduce the thickness of the specimen needing a percent reduction to increase the hardness. Calibration of the rolling mill was performed before use to make sure that the thickness was being reduced evenly across the samples undergoing the cold working. A powerful motor turns the rollers and the thickness gap is controlled by the large wheels seen in Figure 25. The wheels turn worm gears which turn spur gears connected to lead screws that adjust the roller gap. Each side of the roller can be adjusted separately but the two wheels can be locked together also so that both sides of the roller move at the same time. The thickness gap was reduced by just a couple mils at a time to slowly reduce the thickness of the specimen. This was especially necessary for the steel samples which put a lot of load on the rolling mill motor.

Figure 26: Rockwell Hardness Tester

Figure 26 shows the Rockwell hardness tester used to test the aluminum and steel samples. The appropriate tip was placed in the tester for a Rockwell B test. The screw handle was turned to raise the sample to be tested into the testing tip. The lever on the side is then pulled which releases the load required for the test. Once the load has been fully applied another lever is pulled which removes the force and the deflection is shown on the dial on the front of the machine. This dial has values that correspond directly to the Rockwell B scale.

Figure 27: Brinell Hardness Tester

The Brinell tester used was located in the Materials Engineering building. The Brinell hardness tester is different than the Rockwell hardness tester in that the indentation is made and then measured optically. An appropriate test load is selected and counter weights are hung from the back of the machine for that particular load. The indentation ball is much larger than the Rockwell B test ball. The load is applied to the samples after being raised underneath the testing ball.

The testing ball makes an indentation in the workpiece that can be measured optically later.

Figure 28: Brinell Hardness Testing Scope

The testing scope shown above in Figure 28 was used to measure the indentation from the Brinell hardness tester. The scope had an attached light to illuminate the indentation and inscribed lines on the lens that can be seen when focusing on the piece indentation. The lines are aligned to the indentation and an optical measurement is taken. This measurement is then looked up on an

empirical chart of Brinell hardness calculations for the testing load used. This value in the chart is you Brinell hardness value.

Figure 29: MTS Q Test 100 Tensile Tester

The tensile testing machine used can be seen in Figure 29. It is an MTS Q Test 100. The 100 stands for 100kN force that it is rated to apply. A load cell is attached to the upper section of the tester which is attached to ball screws on both sides that move it up and down. Various jaws or fixtures can be attached to the

upper section. The tensile testing machine moves at a constant displacement rate and records the forces applied to the load cell.

Figure 30: Tensile Testing Jaws with Specimen Inserted

The jaws used for the tensile testing of the metal samples were of the screw clamping type. A screw collar is tightened which clamps down on the piece. The jaws are designed so that as the pulling force increases the clamping force does as well. Figure 30 shows the jaws clamping a sub-size specimen.

Construction and Methodology of the Experiment

Sample Preparation

Three different workpiece materials were studied in this experiment: Copper 10100, Aluminum 1100, and 1018 Steel. Each material arrived in a different initial state. The copper 10100 arrived as pre-cut ¼ inch by 3 inch by 4 inch pieces. The copper was manufactured to meet ASTM B152/2009 standards and included the appropriate documentation to verify its purity. The aluminum 1100 arrived as a $^{3}/_{8}$ inch by 3 inch by 72 inch piece of rectangular stock. The 1018 steel arrived as a 3/16 inch by 3 inch by 72 inch piece of rectangular stock. The final size of all specimens to be tested needed to be $^{1}/_{8}$ inch by 3 inch by 4 inches. The aluminum and steel stock was cut on a horizontal band saw to just over size in length. All samples were then ready to be reduced in thickness to the appropriate thickness values before rolling.

The thickness values were calculated so that the appropriate percent reduction would be administered to each sample during rolling to the final thickness of $^{1}/_{8}$ inch. The initial hardness of each metal had to be taken into account when calculating the percent reduction desired. Aluminum and steel hardness tempers are defined by the ultimate tensile strength of the produced material and are controlled by various industry standards. Empirical charts have

been derived that specify the increase in tensile strength that must be achieved from the annealed state to result in a full hard temper of H18 in the case of the aluminum samples. The designation of H14 for the aluminum indicates that the tensile strength is approximately midway between that of the annealed temper and the H18 temper. The medium hardness designation of the 1018 steel indicates the same approximate half hard temper as the aluminum. Percent reductions were chosen for the aluminum and steel to achieve an additional 29% reduction for the hardest specimens. Resulting hardnesses were compared against industry data to verify that a full hard temper was achieved.

Copper temper designations are more simply defined as a percent reduction from the annealed state. A graph from the ASM handbook defines the percent reduction required to achieve the desired hardness tempers. Values were chosen from this graph for a wide temper gradient after the copper samples were rolled. A table of the thicknesses and percent reduction required for each sample before rolling is shown on the next page

Material	Thickness (in)	Percent Reduction (%)
Copper 10100	0.125	0
Copper 10100	0.139	10
Copper 10100	0.169	26
Copper 10100	0.205	39
Copper 10100	0.245	49
Aluminum 1100	0.125	0
Aluminum 1100	0.149	16
Aluminum 1100	0.176	29
1018 Steel	0.125	0
1018 Steel	0.149	16
1018 Steel	0.176	29

Table 1: Specimen Percent Reduction Values

The samples were reduced to these calculated thicknesses using the Cincinnati CNC vertical mill. A g-code program was written to remove material from the entire face of each sample at a prescribed depth per pass using a fly cutter. Material was removed from both sides of each sample so that the two sides would be perfectly parallel to each other. Allowing the CNC machine to reduce the thickness of each sample to its desired thickness allowed the researcher to prepare the next sample for insertion into the machine as soon as it had finished with the previous one. Measurements for the thickness were taken off of the parallels that the samples were resting on resulting in very repeatable results.

Once all of the samples were to the correct pre-rolled thickness, each one was cold rolled to $^1/_8$ inch using the Stanat rolling mill. Duplicates of each metal and thickness were produced as well for redundancy. Hardness tests were performed on all specimens. A Rockwell hardness tester was used to test the steel and copper samples. A Rockwell B hardness test has the most appropriate range for these two metals. The aluminum samples were too soft to be tested with a Rockwell hardness tester so a Brinell tester was used. All hardness values were converted to the Brinell hardness scale as its range covers all hardnesses of all samples. A table below lists the hardness values of all samples and their duplicates. Names include the metal and initial thickness before reduction.

Name	Brinell	Name	Brinell	Name	Brinell
Aluminum 0.125 (1)	31.2	Copper 0.125 (2)	66	Copper 0.245 (1)	84
Aluminum 0.125 (2)	32.3	Copper 0.139 (1)	77	Steel 0.125 (1)	135
Aluminum 0.149 (1)	34.4	Copper 0.139 (2)	77	Steel 0.125 (2)	135
Aluminum 0.149 (2)	34.1	Copper 0.169 (1)	81	Steel 0.149 (1)	154
Aluminum 0.176 (1)	39.8	Copper 0.169 (2)	82	Steel 0.149 (2)	157
Aluminum 0.176 (2)	40.2	Copper 0.205 (1)	83	Steel 0.176 (1)	171
Copper 0.125 (1)	67	Copper 0.205 (2)	83	Steel 0.176 (2)	171

Table 2: Hardness Values

At this stage the samples were all the same thickness of $^{1}/_{8}$ inch, however they were now all different lengths due to the cold rolling deformation. A Bridgeport vertical milling machine was used to resize all of the samples to 3 inches by 4 inches in preparation for tensile test removal and polishing. The Cincinnati CNC machine was utilized again to mill out the tensile test specimens for each specimen. The tensile test design conformed to the ASTM E8 sub-size specimen standard. Figure 31 illustrates the dimensions of the ASTM E8 sub-size specimen.

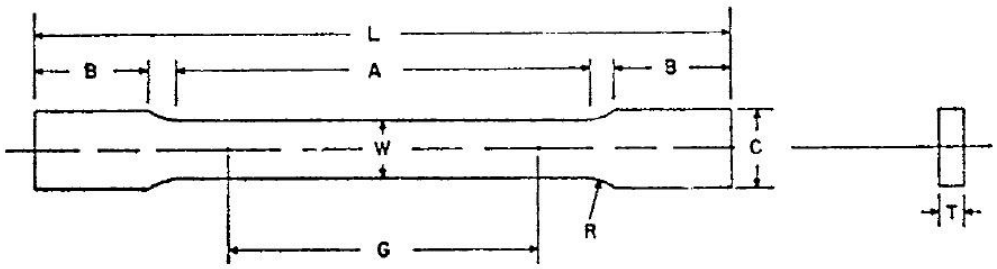

	Subsize Specimen
	6 mm [0.250 in.] Wide
	mm [in.]
G—Gage length (Note 1 and Note 2)	25.0 ± 0.1 [1.000 ± 0.003]
W—Width (Note 3 and Note 4)	6.0 ± 0.1 [0.250 ± 0.005]
T—Thickness (Note 5)	
R—Radius of fillet, min (Note 6)	6 [0.250]
L—Overall length, min (Note 2, Note 7, and Note 8)	100 [4]
A—Length of reduced section, min	32 [1.25]
B—Length of grip section, min (Note 9)	30 [1.25]
C—Width of grip section, approximate (Note 4 and Note 9)	10 [0.375]

Figure 31: ASTM E8 Sub-size Specimen Dimensions

The specimens were remachined to a rectangle shape after tensile test removal and were ready for sanding and polishing.

The sanding process began by putting the samples back in the CNC milling machine and making a light pass with the fly cutter. This reduced the sanding required significantly. After the fly cutting operation the samples were sanded using various grit sandpapers. The samples were sanded first with 180 grit paper, followed by 240, 320, 400, 500, 600, 1000, and finally 2000 grit. Samples were then polished using a polishing compound designed for each metal. At this point the samples had reached an almost mirror finish and were ready for etching.

All copper and steel workpieces were etched to provide optimum reflective characteristics and definition to the material microstructure. Chemical etchants were prepared for the copper and steel samples according to Table 3 and Table 4.

Water	**Nitric Acid**	**Silver Nitrate**
H_2O	HNO_3	$AgNO_3$
250 ml	250 ml	2.5 grams

Table 3: Copper Etchant

Nitric Acid	**Ethanol**
HNO_3	CH_3CH_2OH (95%)
10 ml	500 ml

Table 4: Nital Etchant for Steel

The aluminum samples were not etched due to the extremely dangerous nature of the chemicals required for aluminum etching. The optical quality of the aluminum samples was sufficient without etching.

Cutting Setup

The now prepared samples were ready to undergo the orthogonal machining process. The workpiece to be cut was placed in the workpiece holder that was attached to the dynamometer and held in place with up to ten set screws.

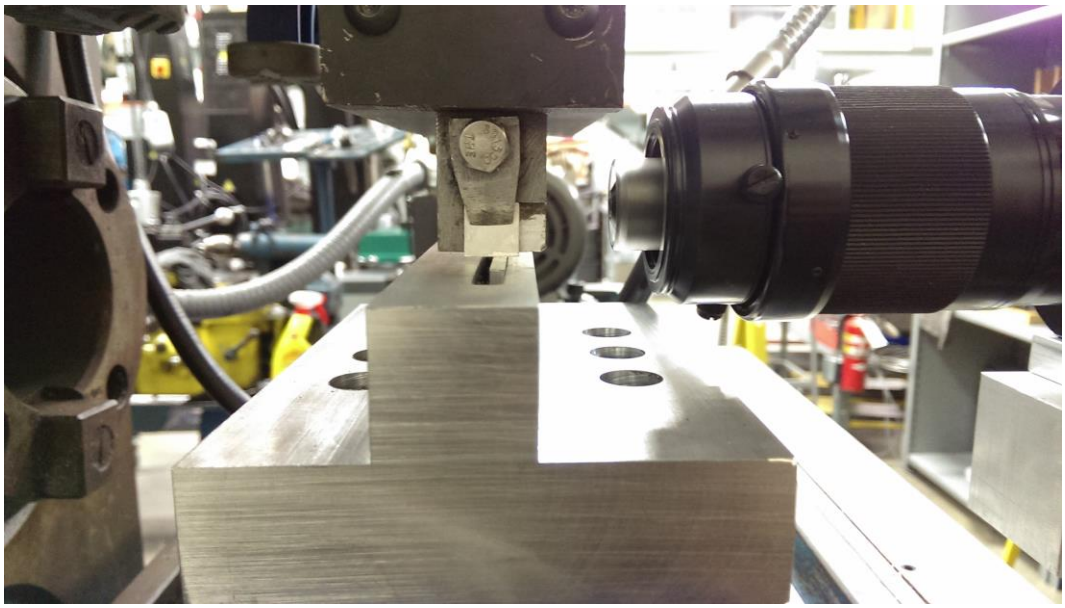

Figure 32: Workpiece in Position

Figure 32 shows a workpiece in the workpiece holder looking down the y axis. The position of the sample underneath the cutting tool is near the front edge of the tool and the camera is in position to record the run. The camera is shown with the fiber optic lights off as they are so bright that it is hard to take a picture of it.

During the experiment, the table fed the workpiece directly into the tool. The dynamometer measured the cutting force (F_c) and the thrust force (F_t), passing its output signal to the charge amplifier. Output from the charge amplifier was then directed to the NI USB-6008 data acquisition modules and recorded using a LabVIEW program. During the experiment, the camera was at all times focused slightly to the left of the tool tip so as to magnify and record the shear plane region ahead of the tool. Detailed information about the machine setup and instrument validation is included in the next section.

Experiment Sequence

Before runs were made on a given day the machine was calibrated. This calibration included checking the camera focus and scale against the micrometer slide as well as a couple test runs in a scrap sample to check for proper machine movement. After calibration a workpiece was selected according to the run number and mounted in the workpiece holder. The cutting tool corresponding to the run number was loaded into the tool holder and tightened down. The cutting tool was then used to remove a small amount of material from the workpiece (less than .005 inches). This topping cut also corrected for any non-parallelism between the cutting tool and the workpiece thus reducing the possibility of a non-uniform feed. The effectiveness of the topping cut was monitored using the Midas software. Once uniform cuts were established, the forces would stabilize

across the entire topping cut. This was clearly evident in the LabVIEW graph display.

After the first cut the z-axis was zeroed so that the following cut would be the correct depth from the now perfectly parallel face. The tool was returned to the starting side of the workpiece and readied for a data run. It was now time to turn on the signal amplifiers for the dynamometer. They were switched on and then flipped into recording mode. This starts the transmission of force data to LabVIEW. The LabVIEW data acquisition program was started which takes in the force data and tells the camera when to start recording. The camera was put into recording mode and awaiting the signal from LabVIEW. The z axis of the horizontal milling machine was adjusted to the desired depth of cut for the run. The feed on the motor controller was then adjusted as well. With everything now in the correct state for the start of a run, the forward feed button is pressed on the motor controller. This started moving the tool into the workpiece generating a force signal which in turn started the data recording.

As soon as the run completed the camera video was saved and the tool moved back to the starting position. The force data was saved automatically with an auto-incrementing file name format. All force data and images are time stamped from the system clock to the nearest millisecond. This time stamp from the same clock is critical to synchronizing the force data with the images of the material undergoing shear.

The process continued through all of the required data runs. If there was any error in the recording process the run would be repeated until the desired number of replicated was achieved for each set of parameters.

Post Processing

The post processing of all the data was done using various programs selected for their performance in their respective areas of data processing. LabVIEW was utilized to convert the data generated by the data collection program into an Excel format that is readable by MATLAB for force data analysis. MATLAB used the Excel files generated by the LabVIEW program to extract the force data and output the average force for each run during a period of steady state forces. This data was exported to another Excel file for use to calculate the resultant forces, strains, and stress according to Merchant's model. GIMP is an image analysis program that was used to measure the angles of interest as well as the tool angle and uncut chip thicknesses. Pixel paths were drawn at the appropriate points and these pixel paths were exported to a text file that was then analyzed using another MATLAB program to calculate the angles from the pixel coordinates. How each program accepted and generated data will be detailed here. All programs mentioned have the full code published in Appendix 5.

LabVIEW produced data files of the force measurements from the dynamometer in a proprietary .TDM file format. A LabVIEW program

incremented though all the .TDM force data files and generated a formatted Excel file.

MATLAB incremented through all Excel files generated by the previous LabVIEW file and displays a graph of the cutting force data. The figure below shows a plot that is displayed to select the appropriate range of data for average force calculation.

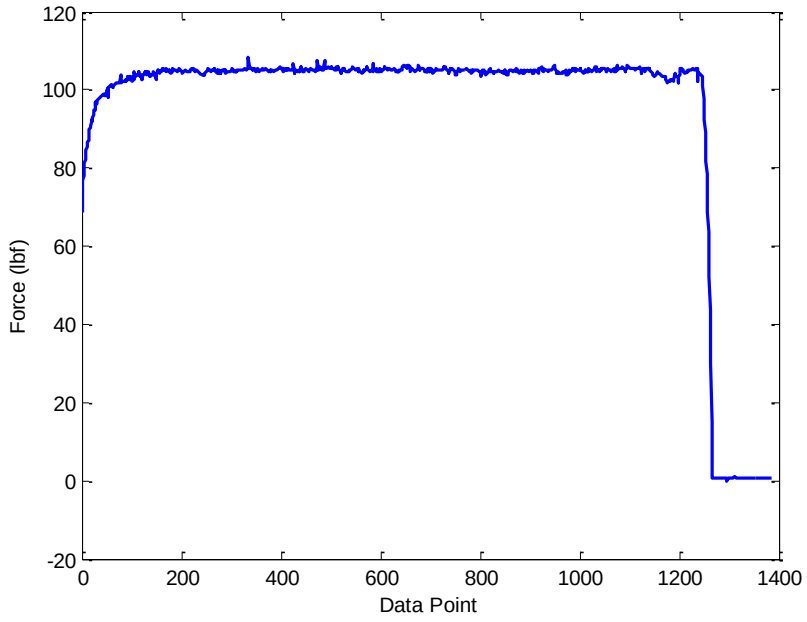

Figure 33: Average Force Selection Plot

The figure on the next page is a snapshot of the command window which asks for the data range. Once a range is specified it outputs the average forces.

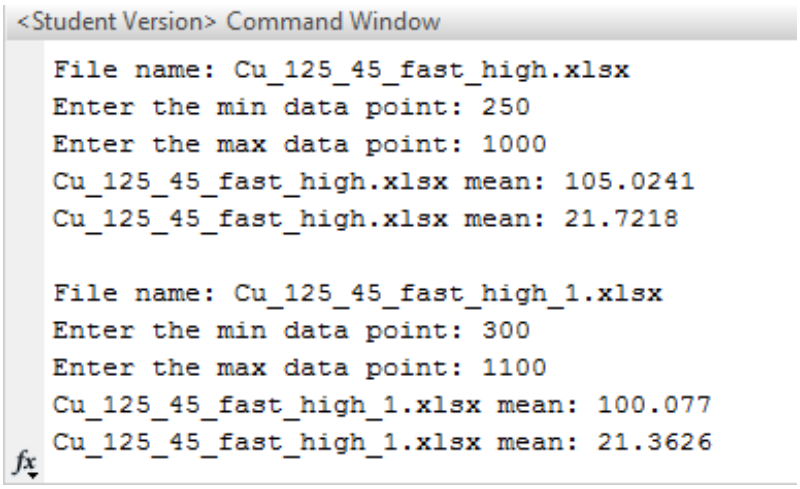

Figure 34: Average Force Input

The MATLAB program also writes all of the force data to an Excel file for further study.

The figure on the next page shows the GIMP screen and the paths drawn for angle measurement. Make note of each lines purpose. There is a line defining the surface of the uncut specimen. There is a line defining the tool face. There is a line defining the angle of onset shear and another defining the angle of shear motion. Drawing these lines often required watching the movie of the footage to get accurate lines for the shear lines.

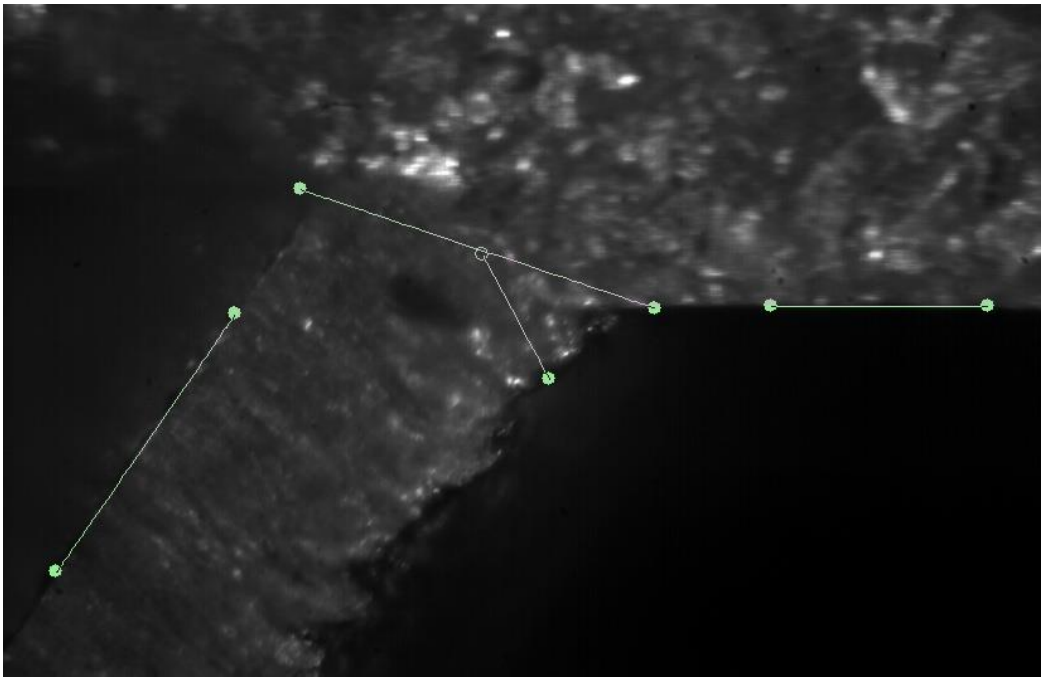

Figure 35: GIMP Path Selection

The figure below shows the outputs of GIMP in the form of a text file. Notice the data points in the file.

```
<?xml version="1.0" encoding="UTF-8" standalone="no"?>
<!DOCTYPE svg PUBLIC "-//W3C//DTD SVG 20010904//EN"
              "http://www.w3.org/TR/2001/REC-SVG-20010904/DTD/svg10.dtd">

<svg xmlns="http://www.w3.org/2000/svg"
     width="17.7778in" height="14.2222in"
     viewBox="0 0 1280 1024">
  <path id="Unnamed"
        fill="none" stroke="black" stroke-width="1"
        d="M 918.00,507.00
           C 918.00,507.00 1176.00,507.00 1176.00,507.00M 68.00,823.50
           C 68.00,823.50 280.00,516.67 280.00,516.67M 359.00,368.00
           C 359.00,368.00 780.67,509.33 780.67,509.33M 654.67,594.00
           C 654.67,594.00 574.67,445.33 574.67,445.33" />
</svg>
```

Figure 36: GIMP Path Output File

The points are listed in the order of the lines being drawn. This made it necessary to draw the lines in the same order every time. Once this was done the text file would be in a set format that could be post processed later.

Another MATLAB program took these pixel coordinates and used basic trigonometry equations to calculate the angles of interest and other optical values. The full code for these calculations can be viewed in Appendix 5.

Instrument Validation and Statistical Design of Experiments

Machine Setup

The goal of instrument validation is to verify that the High Speed Videographic Quick Stop Device for Orthogonal Machining is a valid instrument for making orthogonal cuts at predetermined parameters and its ability to record the resulting information. This study is valid for the quick stop device as it exists in its current form in 2013. Any modifications to the system will require a reevaluation of the machine and its capabilities. The foundation of the virtual quick stop device is a Cincinnati Milacron horizontal milling machine. The horizontal milling machine is used as a rigid base for making the orthogonal cuts. The machine itself is never powered up as none of the powered functions of the machine are utilized.

A 1/8 horsepower Baldor three-phase induction electric motor is used to move the milling table in the x direction underneath the stationary tool holder. The Baldor electric motor is connected to a Wood's E-Trac motor controller. This motor controller permits precise speed control of the motor using a variable frequency drive (VFD). The frequency at which this motor controller sends power to the motor directly controls the motor RPM. The formula for calculating the RPM of an electric motor using VFD is calculated as

$$n = 120 \times \frac{f}{P} \tag{16}$$

where n is the RPM, f is the frequency of the power, and P is the number of pole pairs in the electric motor. A 20/1 gear reducer is installed on the motor to increase the torque provided by the motor. The speed of the motor is monitored in real time using a rotary encoder.

The tool holder is attached to the overarm dovetail of the horizontal milling machine. If the horizontal milling machine was being used for traditional milling, an arbor support would attach to the overarm dovetail. The overarm is designed to incur very high loads during normal horizontal milling operations and is extremely rigid and perfectly parallel to the milling table making it an ideal platform to attach the tool holder to. The overarm is adjustable in the y direction to reduce the distance of the tool holder from the main base. This distance was minimized to increase rigidity even further. The tool holder is designed to hold a high speed steel (HSS) tool that has been ground to a specified angle to the milling table below. The tool is also held perfectly perpendicular to the table motion so that it is a true orthogonal cut with all force being exerted into the piece in a single plane.

A workpiece holder was designed to attach to the Kistler dynamometer and also provide maximum clamping force on the sample being cut. The dynamometer is attached to the milling table via a steel adapter plate that fixes into the milling tables T-slots. This fixture ensures that the workpiece will be perfectly parallel to the x direction of the table.

The camera for recording the deformation of the workpiece during cutting is attached to a custom made stand. The stand is a load lift modified to allow the fixture of various attachments. A cross slide vice has been attached to the load lift table which allows the camera to be precisely moved in the x and y directions for easy camera positioning. A winch on the back of the lift moves the camera in the z direction.

Run Setup

The correct initial setup of the machine is necessary for repeatable measurements to be made on any given day. The setup begins be positioning the camera and calibrating the focus and scale. This is accomplished by moving the camera stand into position in front of the tool holder. The cross slide vice and be used for fine adjustments in the x direction and the height should be adjusted using the winch. Insert a tool into the tool holder and tighten the screws that hold the tool in place. It is important to make sure that the tool is inserted all the way up into the tool holder for repeatable tool rigidity. Insert a workpiece into the workpiece holder and tighten it down with the set screws. It is important to make sure that the sample is firmly contacting the bottom of the workpiece slot during tightening of the set screws.

Place the calibration slide against the workpiece with the etched side against the material. This places the scale on the same plane as the workpiece. Move the workpiece holder underneath the tool and raise it until the top of the

calibration slide is just touching the tool. This will keep the slide from falling. Be sure not to crush the slide while raising the workpiece holder.

Start the Midas software on the computer connected to the camera and make sure you can see a live feed. Turn on the fiber optic ring light to provide enough light for the camera at the high magnification. The camera lens has two adjustment knobs. One is for the zoom level and the other for focusing. Adjust the camera lens zoom to the maximum level and the focus to the closest setting. When the object is in focus at these settings the camera is achieving the maximum zoom possible by the lens. Move the camera in the y direction until the micrometer scale comes into focus. The y-direction of the horizontal mill table can be adjusted as well to bring the scale into focus as long as the workpiece remains underneath the tool. Once the scale is clearly visible do not move the camera or adjust the zoom or focus of the camera lens until all runs are completed for the session. Record the scale for a couple seconds. This video will be used for a pixel to inch ratio. This ratio can be calculated in the Midas software or later in an external program. Carefully remove the micrometer scale from against the workpiece.

Raise the workpiece underneath the tool so that both can be observed by the camera. Run the motor in reverse until the tool is just to the side of the workpiece. Adjust the workpiece holder to remove 0.002” of material. The adjustment of the workpiece can be measured using a dial indicator attached to the milling machine base and then contacting the milling table. Check the depth of cut for the first cut with the video from the camera. This provides a check for

the dial indicator. Set the motor controller to the desired run speed and make a pass with the tool. This will establish a perfectly parallel plane between the workpiece and tool for the rest of the runs. Once the cut in completed lower the workpiece just enough so that when it is run in reverse to start the next run the tool does not slide back over the workpiece. If necessary the workpiece can be refocused by moving the milling table to bring the piece into better focus. As long as the camera has not been adjusted, when the sample is in focus it will be at the same scale as when it started.

Data Results

The experimental data was collected, during which time the process was carefully monitored for any irregularities or obvious discrepancies. The following types of data were collected through direct measurement (electronically for the forces and stresses, and optically for the angles).

Data	Symbol	Units
Tool Rake Angle	α	degrees
Uncut Chip Thickness	t_o	inches
Cut Chip Thickness	t_c	inches
Horizontal Cutting Force	F_c	pounds force (lbf)
Vertical Cutting Force	F_t	pounds force (lbf)
Shear Plane Angle	ϕ	degrees
Shear Front Angle	ψ	degrees
Ultimate Stress	F_u	pounds force (ksi)

Table 5: Observed Data Results

During initial selection of the parameters to be used it appeared that the three tool angles selected would produce nice type 2 chips for all materials at all hardnesses. It was discovered during testing that this was not the case. The 25 degree tool would not reliably produce type 2 chips in the aluminum, steel, and softer copper specimens. The 25 degree tool would produce nice type 2 chips every now and

then but often it would plow into the material making it unsuitable for subsequent runs. This caused significant time delays and made it practically impossible to collect a reliable data set for analysis. During the course of the experiment it was also noted that during some runs the tool underwent minor deflections in some materials. The tool angle was verified using the optical data and is noted in the data set in Appendix 3.

Using the collected data collected during the experiment it was possible to calculate the values of primary interest in metal cutting using the relationships derived by Merchant, Payton, and others. The table below details the values that were calculated.

Data	**Symbol**	**Units**
Chip Thickness Ratio	r_c	none
Friction Force Upon Chip	F	newtons
Normal Force Upon Chip	N	newtons
Shear Force on Plane	F_s	newtons
Normal Force on Plane	F_n	newtons
Mean Friction Angle at Tool	β	degrees
Area of Shear Plane	A_s	in^2
Shear Stress on Shear Plane	τ_s	MPa
Friction Coefficient	μ	none
Shear Strain	γ	none
Resultant Force	R	newtons
Resultant Shear Stress	R_τ	MPa

Table 6: Calculated Data Results

Below is a sample data set of all measured and calculated results. Values with the light grey background are set values as specified by the design of experiments. Values with the dark grey background are measured values and values with the white background are calculated values.

Run	Material	Initial Thickness (in)	Material Hardness (BHN)	Rake Angle (degrees)	Feed Rate (in/min)	Depth of Cut (in)	Replicate	Measured Rake Angle (degrees)	Measured Depth of Cut (mil)	Fz Thrust Force (lbf)	Fy Cutting Force (lbf)
98	Cu	0.139	77	35	7.5	0.008	2	34.7	7.8	19.25	127.89
99	Cu	0.139	77	35	7.5	0.008	3	34.4	8.2	19.20	132.08
100	Cu	0.139	77	35	7.5	0.004	1	34.9	4.1	9.46	66.89
101	Cu	0.139	77	35	7.5	0.004	2	35.5	3.5	10.09	75.91

Table 7: Run Parameters and Measured Force Data

Run	Cut Chip Thickness (in)	Chip thickness ratio	Phi (degrees)	Measured Phi (degrees)	Measured Psi (degrees)	Psi (degrees)	Friction Force, F (newtons)	Normal Force, N (newtons)	Fs Merchant (newtons)	Fn Merchant (newtons)	Fs Payton (newtons)	Fn Payton (newtons)
98	0.027	0.30	16.3	20.8	19.4	46.2	396.44	416.91	522.01	241.84	186.75	544.15
99	0.0265	0.30	16.7	22.0	22.5	45.8	406.96	432.28	538.42	250.19	195.52	560.59
100	0.012	0.33	18.7	19.2	20.8	43.8	205.15	219.60	268.46	135.06	100.06	283.37
101	0.0125	0.32	17.8	17.3	26.1	44.7	230.44	250.86	307.78	145.95	116.11	320.24

Table 8: Measured Optical Data and Calculated Forces

Run	Beta (degrees)	Shear Area, As Merchant (in^2)	Shear Area, As Payton (in^2)	Shear Area, As Adjusted (in^2)	Shear Stress, Ts Merchant (MPa)	Shear Stress, Ts Payton (MPa)	Shear Stress, Ts Adjusted (MPa)	Friction Co-efficient
98	43.6	0.0034	0.0034	0.0037	236.54	84.62	79.25	0.76
99	43.3	0.0034	0.0034	0.0036	249.09	90.46	84.53	0.76
100	43.1	0.0015	0.0015	0.0016	277.29	103.35	95.53	0.75
101	42.6	0.0016	0.0016	0.0017	303.82	114.61	106.42	0.74

Table 9: Calculated Areas and Stresses

Run	Shear Strain ϒ Merchant	Shear Strain ϒ Payton	Shear Strain ϒ Adjusted	Resultant Force (newtons)	Resultant Shear Stress Merchant (MPa)	Resultant Shear Stress Payton (MPa)	Resultant Shear Stress Adjusted (MPa)	Measured Ultimate Stress (MPa)
98	3.08	1.04	0.39	575.30	260.69	260.69	244.13	279.93
99	3.01	1.04	0.40	593.70	274.67	274.67	256.69	279.93
100	2.67	1.04	0.46	300.52	310.40	310.40	286.93	279.93
101	2.81	1.04	0.43	340.63	336.25	336.25	312.22	279.93

Table 10: Calculated Forces and Resultant Stresses

Results of the Videographic Study

The virtual quick stop videographic analysis proved very capable of doing the analysis intended. Video of each run was captured in real time resulting in a massive amount of data for each run. The video of each run had its share of useful and unusable images. As the tool progressed through the material the material would often move in and out of focus during the duration of the cut. This was due to the material specimens either not being perfectly flat or being bent slightly out of flat when it was being secured in the workpiece holder.

After each run completed a portion of the video from the run was saved for further analysis. The selection was determined by the focus of the image and a clear view of the shear plane. As force data was recorded during the entire cut, there was sufficient force data for any range of image selection. The figure on the next page illustrates a sample of the force data collected during a run sequence.

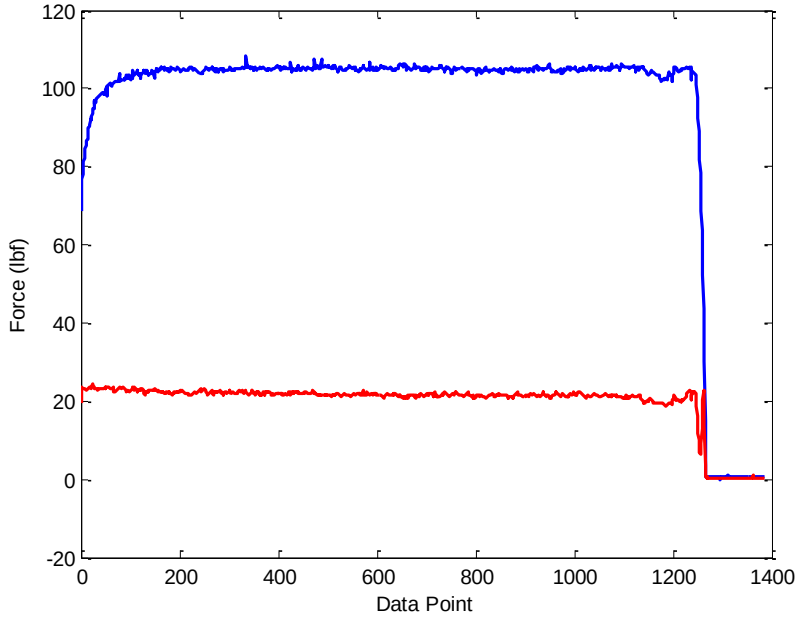

Figure 37: Measured Force Plot

The range of images was exported as a video file which would be analyzed with software during post processing.

During post processing individual images were selected from the video file which best represented the shear plane during the cut and when forces has stabilized. This individual image was used to measure the angles of interest as well as the tool angle and depth of cut. Measured shear angles were compared with the calculated values of Merchant's model with extremely good effect. This system of measurement greatly reduced the time required and decreased the margin of error typically associated with measuring the angles of interest using traditional methods. The depth was cut was observed to vary up to +-0.0005 inches and is attributed to slight slack in the lead screw controlling the z axis of the horizontal milling machine.

The figure below illustrates the observed geometry of the shear zone in all materials.

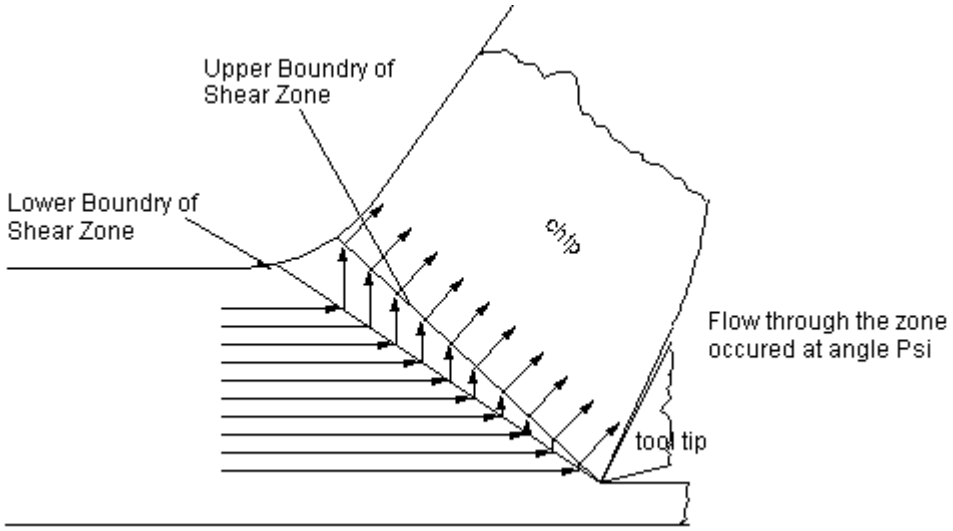

Figure 38: Observed Geometry of Shear Zone

This geometry is consistent with the observations of Briggs (13), Huang and Black (40), and Payton (96). The movement of the crystals into and through the shear zone definitely follows the Huang model of movement. The large amount of data collected was prepared for statistical analysis to be detailed in the next section.

Statistical Analysis

Statistical analysis was performed on the data collected from the dynamometer and optical methods. Statistics have proven useful in verifying models developed by others as well as suggesting new models. It is an integral part of the modern engineering solution; however it requires sufficient amounts of data to make it truly useful. This experiment produced a sufficient amount of data on the forces predicted by Merchant's model and it modified models. In addition, the angle measurements α, β, ϕ, and ψ tied to these forces were available for analysis. The statistical software package Minitab was used to examine the data collected and to compare the predictive models for the angles of interest. More importantly, the effects of material hardness induced by cold working the materials upon the cutting process were examined.

The statistical technique of analysis of variance (ANOVA) is used to determine the effect of various factors on a particular response. This technique measures the degree of variation among factors and determines which factors have a statistically significant effect on the response. ANOVA was performed for a variety of responses and for individual materials as well as the entire data set as a whole.

The first interactions examined were the effects of the run selection parameters on the cutting forces. The figures below detail how each factor influenced the cutting forces seen by the cutting tool.

Analysis of Variance for Fy Cutting Force (lbf), using Adjusted SS for Tests

Source	DF	Seq SS	Adj SS	Adj MS	F	P
Work Piece Material	2	797751	867584	433792	750.56	0.000
Feed Rate (in/min)	1	683	683	683	1.18	0.278
Rake Angle (degrees)	2	196115	196115	98057	169.66	0.000
Depth of Cut (in)	1	251987	251987	251987	435.99	0.000
Replicate	2	73	73	36	0.06	0.939
Error	279	161251	161251	578		
Total	287	1407859				

S = 24.0408 R-Sq = 88.55% R-Sq(adj) = 88.22%

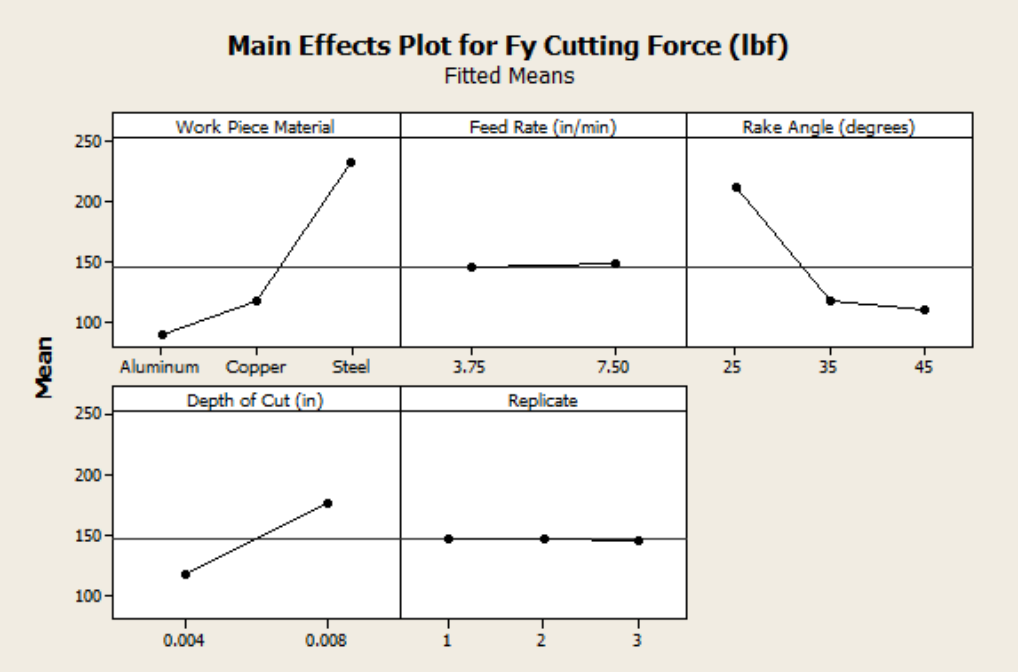

Figure 39: Cutting Force ANOVA

The results show that the work piece material had the largest influence on the cutting forces. The second most influential factor was the depth of cut

followed by the tool rake angle. These results also show that the feed rate at which the material was cut had no statistical influence on the resulting cutting forces. The replicate also had no influence which is a good indicator of a well-designed experiment.

Workpiece material hardness was one of the main areas of interest in this thesis. Additionally, the comparison of calculated stress values to the real world tensile pull data was to be examined. The following figures illustrates the data obtained when observing the material hardness vs. the calculated resolved stress in the material as well as the material hardness vs. the measured ultimate stress data obtained from the tensile testing.

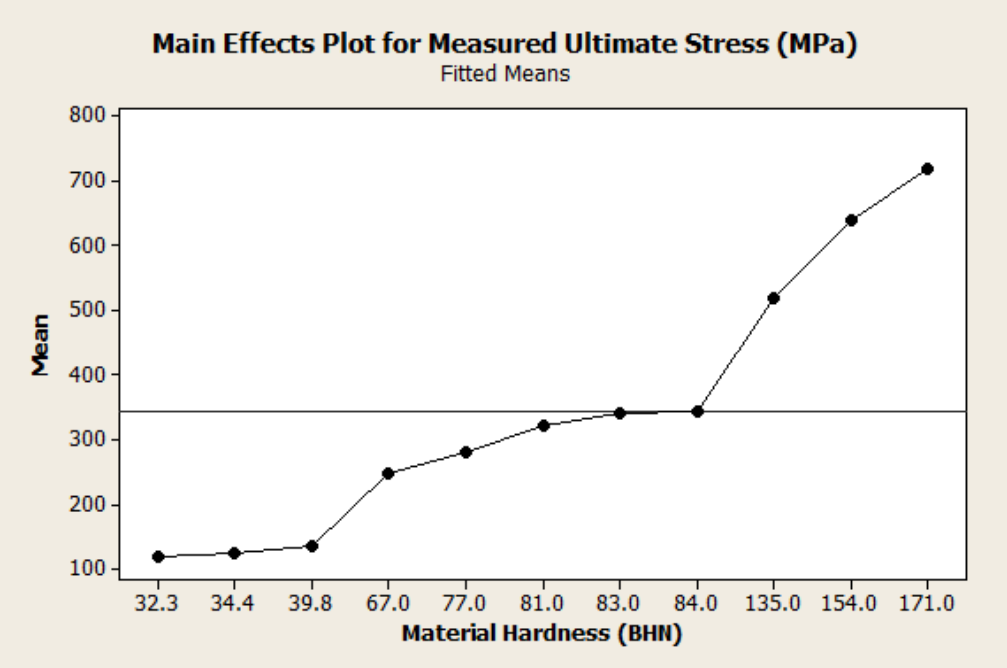

Figure 40: Hardness vs. Measured Stress

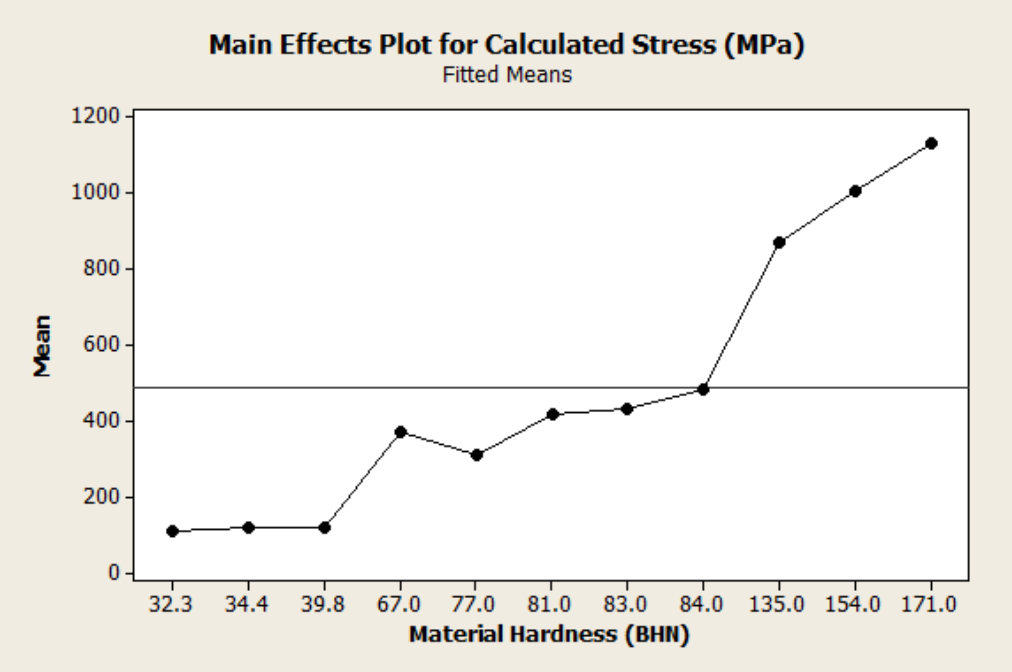

Figure 41: Hardness vs. Calculated Stress

These figures show that the caluculated values for the resultant stress follow almost the exact same trend as those from the measured stress values. This data gives hard evidence in favor of the Black and Huang shear zone model. It must be pointed out however that even though the trend is almost identical, the calculated values were often higher than those measured. The reason for this is beyond the scope of this thesis but is listed as a topic for future work.

Since the values for the calculated stress were very close to the measured values for copper, a paired t-test was performed. The results of this test are shown in the figures below.

```
Paired T for Resultant Shear Stress - Measured Ultimate Stress (MPa)

                            N   Mean  StDev  SE Mean
Resultant Shear Stress    144  450.6  224.7     18.7
Measured Ultimate Stress  144  312.7   36.5      3.0
Difference                144  137.8  225.1     18.8


95% CI for mean difference: (100.7, 174.9)
T-Test of mean difference = 0 (vs not = 0): T-Value = 7.35  P-Value = 0.000
```

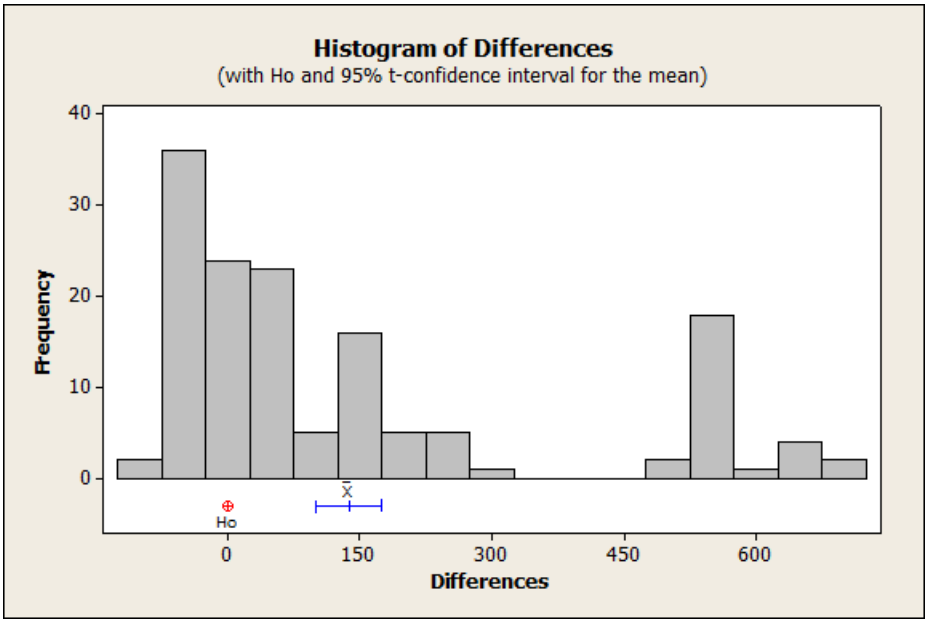

Figure 42: Paired T-Test of All Copper Samples

In the histogram of differences generated by the paired t-test it can be seen that a cluster of values are apart from the rest. Investigating this reveals that the values are associated with the 45 degree tool. Another paired t-test was performed without the 45 degree tool and the following results were obtained.

```
Paired T for Resultant Shear Stress - Measured Ultimate Stress (MPa)

                            N    Mean  StDev  SE Mean
Resultant Shear Stress     84  307.97  44.87     4.90
Measured Ultimate Stress   84  316.96  35.45     3.87
Difference                 84   -8.99  44.95     4.90

95% CI for mean difference: (-18.75, 0.76)
T-Test of mean difference = 0 (vs not = 0): T-Value = -1.83  P-Value = 0.070
```

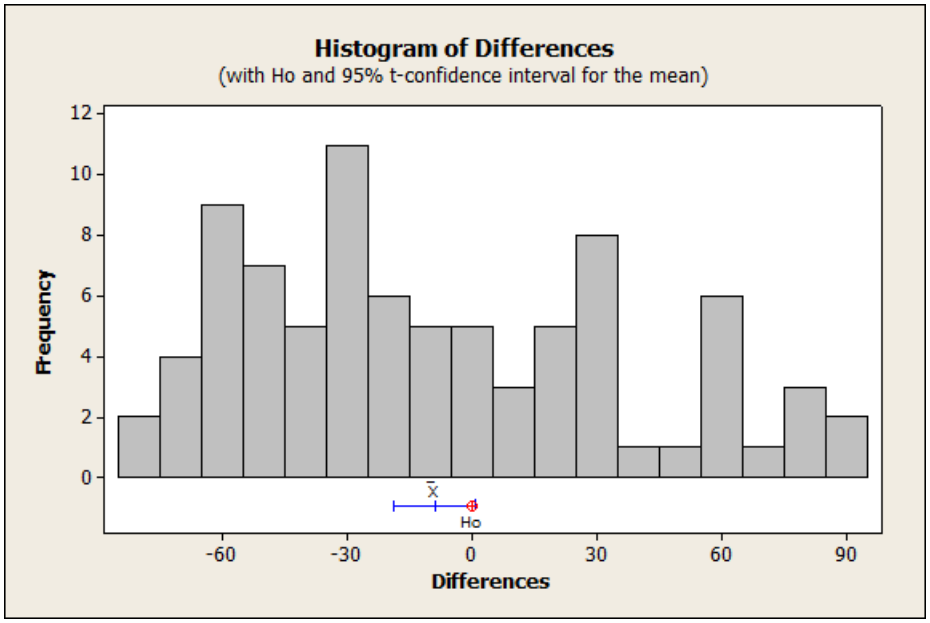

Figure 43: Paired T-Test of Low Tool Angle Copper Samples

The results of this t-test show that the difference between the calculated stress values and those of the measured samples are statistically the same. This is further evidence in favor of the Black and Huang model. Investigation into why the 45 degree tool was producing values that do not agree with the current model is listed as another area of future research. Initial thoughts into this matter are centered on the idea that as the tool angle increases the friction force of the chip moving across the tool for an extended length start to play a much larger role in

their contribution to the cutting force. This same topic has been discussed by P.K. Wright (92) as well as more recently by Payton (96).

Conclusions and Future Work

The results generated by the high speed videographic quick stop device led to the following conclusions:

(1) The videographic technique for acquiring data on the angles of interest in synchronization with the direct measurement of the cutting forces reduces the time required for data collection by an order of magnitude from traditional methods

(2) Software was developed that streamlines the optical measurement of the angles of interest as well as other data points to define the cutting parameters as well as the resulting cutting action during orthogonal machining

(3) It has been shown that shear plane angles can be accurately measured using frames acquired using a high speed digital camera during the orthogonal machining process

(4) Hardness values of various materials have been shown to have a significant effect on shear angles as well as the stress required to shear the metal under orthogonal machining

(5) For specific materials at low tool angles, the ultimate stress of a material can be calculated from the cutting forces and shear angles

(6) High resolution still images of the metal cutting process showing the geometries of interest can be acquired using the high speed videographic quick stop device

(7) Additional experimental data was acquired for a new material not previously investigated: 1018 Steel

Recommendations for Future Work

The high speed videographic quick stop device for orthogonal machining is a significant improvement over prior dynamometer techniques used to study the orthogonal machining process. The costs of the high speed camera and electronic drive were small compared to the time savings permitted. However, there were still some shortcomings with the system. Lighting of the workpiece was very difficult due to the very small area of interest. Fiber optic lights had to be used to provide very localized light for any images to be obtained. Providing additional light is difficult since the distance between the camera lens and the workpiece is very short. Additionally, the field of view of the camera lens was very small and this resulted in the workpiece moving in and out of focus during the length of the cut. The following recommendations would greatly enhance th4e capabilities and usefulness of the high speed virtual quick stop device.

(1) A new lens which provides a higher depth of field and possibly higher magnification would help with the focusing of the workpiece during the duration of the cut

(2) Acquire an additional fiber optic light source or a higher wattage light source to prove more light to the workpiece during cutting

(3) Develop image analysis software that can automatically define the angles of interest to remove the manual definition currently required

(4) Develop a method for printing or etching a pattern onto the workpiece to better observe the material as it moves through the shear zone

(5) Acquire a faster computer with more memory that would permit a longer recording time as well as making high frame rates possible for the duration of the run

(6) Develop a process for measuring the chip contact distance along the tool face to help investigate the effects of chip friction along the tool face for higher tool angles

(7) Borrow or acquire a laser interferometry system that is capable of measuring the strain rates and strain directly from the optical qualities of the material

(8) Coordinate studies with the use of a scanning electron microscope to measure dislocation density in the materials to be studied

(9) Acquire additional materials for study to provide additional data for the orthogonal machining process

The high speed videographic quick stop device can be easily modified or upgraded for a variety of additional research areas. The high speed at which data can be acquired and analyzed using specially designed

software permit the development of more complete models for the complex system of metal cutting. Ideally the future world of metal machining may no longer be an art form but a well understood area of engineering. Fully understanding all of the interactions between the tool and workpiece will give way to the optimization of machining practices to level currently unobtainable. This optimization will lower the cost of high precision goods and increase the overall quality of products worldwide.

References

1. Agrawal, S.N., Amstead, B.H., "Study Reveals Mechanics of Chip Formation," *Machinery*, pp. 114-119 March 1961.

2. Armarego, E. J. A. and Brown, R. H., The Machining of Metals, Prentice-Hall, Englewood Cliffs, NJ, 1969.

3. Bell, Adam C., Ramalingham, S., Black, J.T., "Dynamic Metal Cutting Studies as Performed in the SEM," *Proceedings of the North American Metal Working Research Conference*, Vol. 2, pp. 99-110 May 14 and 15, 1973.

4. Black, J T., "On the Fundamental Mechanism of Large Strain Plastic Deformation—Electron Microscopy of Metal Cutting Chips," *ASME Journal of Engineering for Industry*, Vol. 93, pp. 507-526, 1971.

5. Black, J T., "On the Fundamental Mechanism of Large Strain Plastic Deformation—Electron Microscopy of Metal Cutting Chips," *ASME Journal of Engineering for Industry*, Vol. 93, pp. 507-526, 1971.

6. Black, J T., "Flow Stress Model in Metal Cutting," *ASME Journal of Engineering for Industry*, Vol. 101, pp. 403-415, 1979.

7. Black, J T. and James, C. R., "The Hammer QSD-Quick Stop Device for High Speed Machining and Rubbing," *Journal of Engineering for Industry*, Vol. 103, pp. 13-21, 1981.

8. Black, J T., Breneiser, D., and Mitchell, H.B., "Dynamic Shear Stress Constancy with Respect to Deformation Textures in 6061-T6 Aluminum and Alpha Brass," *3rd NAMRC*, 1975.

9. Black, J T. and Briggs, N. D., High Speed Videographs of the Orthogonal Machining of Aluminum," *Tribology Symposium, ASME*, PD-Vol. 61, 1994, pp. 41-54, 1994.

10. Black, J T. and Huang, J. M., "Shear Strain Model in Machining," *Manufacturing Science and Engineering*, MED-Vol. 2-1, MH-Vol. 3-1, ASME International Mechanical Engineering Congress & Exposition, pp. 283-302, 1995.

11. Black, J.T. and Krishnamurthy, R., "Effect of Hardness on Flow Stress of Aluminum," unpublished, Auburn University.

12. Boothrody, G. and Knight, W. A., Fundamentals of Machining and Machine Tools, Maecel Dekker, Inc., New York, 1989.

13. Briggs, N. D., "Observation of the Orthogonal Machining Process Using High Speed Videography," *Master's Thesis*, Auburn University, 1993.

14. Boston, O.W., "What Happens when Metal is Cut," *Transactions ASME*, Vol. 52, p. 119, 1930.

15. Campbell, J.D., "Dynamic Plasticity: Macroscopic and Microscopic Aspects," *Materials Science and Engineering*, pp. 3-12, 1973

16. Chao, B. T. and Trigger, K. J., "Controlled Contact Cutting Tools," *Journal of Engineering for Industry*, pp. 139-151, May 1959.

17. Childs, T. H. C. and Mahdi, M. I., "On the Stress Distribution between the Chip and Tool during Metal Cutting," *Annals of the CIRP*, Vol. 38/1, pp. 55-58, 1989.

18. Cohen, P. H. and Black, J T., "Strain, Strain Rate and Shear Velocity Measurements in Metal Cutting," *High Energy Rate Fabrication*, Edited by Berman and Shroeder, ASME, pp. 271-278, 1978.

19. Coker, E., and Chakko, K., "Experiments on the Action of Cutting Tools" *Proceedings of The Institution of Mechanical Engineers*, London, England, p. 567, 1922.

20. Coker, E., "Report on the Action of Cutting Tools", *Proceedings of The Institution of Mechanical Engineers*, London, England, p. 357, 1925.

21. Cook, N.H., Shaw, M.C., "Visual Metal-Cutting Study," Mechanical Engineering, pp. 922-923, November 1951.

22. Cook, N. H., Finnie, L., and Shaw, M. C., "Discontinuous Chip Formation," *ASME Transactions*, Vol. 76, pp. 153-163, 1954.

23. Cocquilhat, M., "Experiences sur la Resistance Utile Produites dans le Forage", *Annales des Travaus Publics en Belgigque*, Vol 10, p. 199, 1851.

24. Cottrell, A.H., Theory of Crystal Dislocations, Gordon and Breach, London, England, 1964.

25. Dokanish, M. A., Elbestawi, M. A., Polat, U., and Tole, B., "Analysis of Stress during Exit in Interrupted Cutting with Chamfered Tools," *J. Mach. Tools Manufat.*, Vol. 29, pp. 519-534, 1989.

26. Dautzenbery, J. H., Veenstra, P. C., and Van der Wolf, A. C. H., "The Minimum Energy Principle for the Cutting Process in Theory and Experiment," *Annals of the CIRP*, Vol. 30/1, pp. 1-4., 1981.

27. DeGarmo E. P., Black, J T., and Kohser, R. A., Materials and Processes in Manufacturing, Seventh Edition, Macmillan Publishing Company, New York, 1988.

28. Dieter, George E., Mechanical Metallurgy, 3rd Edition, McGraw-Hill Publishing Company, New York, 1998.

29. Eggleston, D. M., Herzog, R., and Thomsen, E. G., "Observations on the Angle Relationships in Metal Cutting," *Journal of Engineering for Industry,* pp. 263-279, August, 1959.

30. Ernst, H., "The Physics of Metal Cutting," *ASM Symposium, Machining of Metals*, 1938.

31. Ernst, H., and Merchant, E., "Chip Formation, Friction, and High Quality Machined Surfaces", *ASM Symposium, The Surface Treatment of Metals*, p.299, 1941.

32. Friedel, J., Dislocations, Pergamon Press, London, UK, 1964.

33. Friedman, M. Y. and Lenz, E., "Investigation of the Tool-Chip Contact Length in Metal Cutting," *J. Mach. Tool Des. Res.* Vol. 10, pp. 401-416, 1969.

34. Gillis, P.P., and Gilman, J.J., "Dynamical Dislocation Theory of Crystal Plasticity," *Journal of Applied Physics*, pp. 3370-3380, November, 1965.

35. Haussner, A., "Das Holben von Metallen", *Mitteilungne des Technicshc Gewerbe Museums*, Wien, Nr. 2, p. 117, 1892.

36. Herbert, E.G., "Work-Hardening Properties of Metals", Transactions ASME, Vol 48, p. 705, 1926.

37. Hill, R., "The Mechanics of Machining: A New Approach," Journal of the Mechanics and Physics of Solids, Vol 3. pp. 47-58, 1954.

38. Holzer, A. J. and Wright, P. K., "Dynamic Plasticity: A Comparison Between Results from Mechanical Testing and Machining," *Materials Science and Engineering*, Vol. 51, pp. 81-92, 1981.

39. Huang, J., "Theoretical and Numerical Studies of Machining," PhD Dissertation, Auburn University, 1996.

40. Huang, J. M. and Black, J T., "An Evaluation of Chip Separation Criteria for the FEM Simulation of Machining," *Journal of Engineering for Industry,* 1996.

41. Hull, D. and Bacon, D.J., Introduction to Dislocations, Third Edition, Pergamon Press, Oxford, UK, 1984.

42. HSU, T. C, "A Study of the Normal and Shear Stresses on a Cutting Tool, *Journal of Engineering for Industry,* pp. 51-63, February 1966.

43. Hyzer, W.G. "High-Speed Video System Provides Instant Images," Industrial *Research and Development*, pp. 180-185, February 1981.

44. Ishi, S., "Macroscopic Kinematographs Applied to Research in Metal Cutting," *World Engineering Congress*, Tokyo, Japan, paper 478, 1929.

45. Iwata, K. and Ueda, K., "The Significance of Dynamic Crack Behavior in Chip Formation," *Annuals of the CIRP,* Vol. 25, pp. 65-70, 1976.

46. Iwata, K. and Ueda, K., "Chip Formation Mechanism in Single Crystal Cutting β Brass," *Annuals of the CIRP,* Vol. 29, pp. 41, 1980.

47. Joessel, H., "Experiments on the Most Favorable Form of Tool in Workshops from the Point of View of Economy of Power", *Annuaire de la Societe des Anciens Eleves des Ecoles Imperiales D'Arts et Meteiers*, 1865.

48. Klamecki, B. E. and Kim, S., "On the Plane Stress to Plane Strain Transition Across the Shear Zone in Metal Cutting," *Journal of Engineering for Industry,* Vol. 110, pp. 322-325, 1988.

49. Kobayashi, S., Herzog, R. P., Eggleston, D. M., and Thomsen, E. G., "A Critical Comparison of Metal-Cutting Theories with New Experimental Data," *Journal of Engineering for Industry,* pp. 333-347, August, 1960.

50. Kobayashi, S. and Thomsen, F. G., "Metal-Cutting Analysis—I: Re-Evaluation and New Method of Presentation of Theories," *Journal of Engineering for Industry,* pp. 63-70, February 1962.

51. Komanduri, R., Brown, R.H., "On the Mechanics of Chip Segmentation in Machining," *Journal of Engineering for Industry*, vol. 103, pp. 33-51, 1981.

52. Lee, E. H. and Shaffer, B. W., "The Theory of Plasticity Applied to a Problem of Machining, *Journal of Applied Mechanics*, Vol. 18, No. 4, pp. 405-413, 1951.

53. Lindner, G., Book Review of Taylor's "*On the Art of Cutting Metals*", Zietschrift VDI, Vol 51, 1907, p. 1070, 1907.

54. Liu, P. C. and Black, J T., "Shear Angle Model for Control Contact Machining of Aluminum and Brass, *Transactions of the North American Manufacturing Research Institution of SME,* pp. 167-174, 1990.

55. Mallock, A., "The Action of Cutting Tools" Proceedings of the Royal Society of London, London, England, Vol. 33, p.127, 1881.

56. Merchant, M. E., "Mechanics of the Metal Cutting Process—I. Orthogonal Cutting and a Type 2 Chip," *Journal of Applied Physics,* Vol. 16, pp. 267-317, 1945.

57. Merchant, M. E., "Mechanics of the Metal Cutting Process—II. Plasticity Conditions in Orthogonal Cutting," *Journal of Applied Physics,* Vol. 16, pp. 318-324, 1945.

58. Merchant, M. E., "Basic Mechanics of the Metal Cutting Process," *Journal of Applied Physics,* Vol. 16, pp. 168-175, 1944.

59. Moriwaki, T, Sugimura, N., and Luan, S, "Combined Stress, Material Flow and Heat Analysis of Orthogonal Micromachining of Copper," *Annals of the CIRP,* Vol. 42/1, pp. 75-78, 1993.

60. Okushima, K. and Hitomi, K., November, "An Analysis of the Mechanism of Orthogonal Cutting and Its Application to Discontinuous Chip Formation," *ASME Journal of Engineering for Industry,* pp. 545-556, 1961.

61. Oxley, P.L.B., "Shear Strain Solutions in Orthogonal Machining," *International Journal of Machine Tool Design and Research*, Vol 1, pp. 89-97, 1961.

62. Oxley, P. L. B., "Machinability: A Mechanics of Machining Approach," *On the Art of Cutting Metals – 75 Years Later,* ASME Publication PED, Vol. 7, pp. 31-84, 1982.

63. Oxley, P. L. B., Mechanics of Machining: An Analytical Approach to Assessing Machinability, John Wiley & Sons, New York, 1989.

64. Piispanen, V., "Lastuntnuodostumiesn Teoriaa", Teknillinen Aikakauslehti, Vol 27, p. 315, 1937.

65. Piispanen, V., "Theory of Formation of Metal Chips," *Journal of Applied Physics,* Vol 19, p. 876, 1948.

66. Ramalingham, S., Black J T., "On the Metal Physical Considerations in the Machining of Metals," Journal *of Engineering for Industry*, December, 1971.

67. Rowe, G. W. and Spick, P. T., "A New Approach to Determination of the Shear-Plane Angle in Machining," *Journal of Engineering for Industry,* pp. 531-538, 1967.

68. Shaw, M. C., Metal Cutting Principles, Clarendon Press, Oxford, 1984.

69. Shaw, M. C., "Forces and Power Requirements in Cutting and Grinding," *Proceedings of US- Taiwan Symposium on Advanced Manufacturing Processes,* Georgia Institute of Technology, pp. 1-15, 1993.

70. Shaw, M. C., Cook, N. H., and Finnie, I., "Shear Angle Relationship in Metal Cutting," *Transactions of the ASME, pp*. 273, 1953.

71. Schwerd, F. "Filmaufnahmen des Ablaufenden Spans bei Ueeblichen und bei Sher Hohen Schnittgeschwindigkeiten," *Zeitschrift VDI,* Vol 80, p233, 1935.

72. Oxley, P.L.B, and Stevenson, R., "

73. Taylor, F. W., "On the Art of Cutting Metals, *Transactions of the ASME,* Vol. 28, pp. 70-350, 1907.

74. The, J.H.L., "High-Speed Films of the Incipient Cutting Process in Machining at Conventional Speeds," *Journal of Engineering for Industry*, pp. 263-268, February, 1977.

75. Time, I., Memoire sur le Rabotage de Metaux, St. Petersburg, Russia 1877.

76. Tresca, H, "On Further Applications of the Flow of Solids," *Proceedings of the Institution of Mechanical Engineers, London, England,* p.301, 1878.

77. Trent, E. M., Metal Cutting, Second Edition, Butterworth's & Co Ltd, London, 1984.

78. Trent, E.M., and Wright, P.K., Metal Cutting, Fourth Edition, Butterworth's & Heinemann, London, 1984.

79. Ueda, K. and Iwata, K., "Chip Formation Mechanism in Single Crystal Cutting of /3-Brass," *Anna/s of the C/RP,* Vol. 29/1, pp. 41-46, 1980.

80. Usui, E., Kikuchi, K. and Hoshi, K., May 1 964, "The Theory of Plasticity Applied to Machining With Cut-Away Tools," *Journal of Engineering for Industry,* pp. 95-104.

81. Usui, E. and Shirakashi, T., " Mechanics of Machining—From 'Descriptive' to 'predictive Theory," *On the Art of Cutting Metals - 75 Years Later,* ASME Publication PED—Vol. 7, pp. 13-35, 1982.

82. Usui, F. and Shirakashi, T., "Mechanics of Machining—From 'Descriptive' to 'Predictive' Theory," *On the Art of Cutting Metals – 75 Years Later*, ASME Publication PED, Vol. 7, PP. 13-35, 1982.

83. Van Luttervelt, C. A., 1977, "The Split Shearzone – Mechanism of Chip Segmentation," *Annuals of the CIRP*, Vol. 25/1, pp. 33-38.

84. Von Turkovich, B. F., "Dislocation Theory of Shear Stress and Strain Rate in Metal Cutting," *Machine Tool Design and Research*, Proceedings of 8th International M.T.D.R. Conference, September 1967.

85. Von Turkovich, B. F, "Shear Stress in Metal Cutting," *Journal of Engineering for Industry,"* pp. 1 51-157, February 1970.

86. Von Turkovich, B. F., Black, J.T., "Micro-machining of Copper and Aluminum Crystals," Journal of Engineering for Industry, pp. 130-134, February 1970.

87. Von Turkovich, B.F., and Micheletti, G.F., "Flow Zone Models in Metal Cutting," *Advances in Machine Tool Design and Research Symposium, Birmingham, UK*, 1968.

88. Voort, V., Metallography Principles and Practices, McGraw-Hill Publishing Company, New York, 1984.

89. Warnecke, G., " A New Method of Visualizing the Cutting Process," 5th North American Metalworking Research Conference NAMRC, SME, pp. 229-236, 1977.

90. Weda, T. and Dean, T. A., "A New Energy Method Analysis of Plastic Distortion in Plane Strain Compression," *International Journal of Machine Tool Design and Research*, Vol 25, No. 3, pp. 199-207, 1985.

91. Weibach, H., Ingeniuer und Maschinenmechanik, Berlin, IG, 1896.

92. Wright, P. K, "Predicting the Shear Plane Angle in Machining From Work Material Strain-Hardening Characteristics," *Journal of Engineering for Industry,"* Vol. 104, pp. 285-292, 1982.

93. Wright, P. K. and Robinson, J. L., "Material Behavior in Deformation Zones of Machining Operation," *Metals Technology*, pp. 240-248, May 1977.

94. Zorev, N. N., Metal Cutting Mechanics, Pergamon Press, New York, 1966.

95. Zvorkin, K.A., Rabota I Usilie Neobkhodimyya dlya Oteleniya Metallicheskikh Struzhek, Moscow Russia, 1893.

96. Payton L.N., June 2000, "Orthogonal Machining of copper using a virtual quick stop device," Master's thesis, Auburn University, USA.

97. Payton, L. N., 2002, "Dislocation Theory of Orthogonal Metal Cutting of Cu-Zn Alloys," Doctoral Dissertation, Auburn University.

Appendix 1

Common Formula in Orthogonal Plate Machining Models

$$r_c \equiv \frac{t_o}{t_c} = \frac{t_1}{t_2} = \frac{V_c}{V}$$

$$\phi = \arctan\left(\frac{r_c \times \cos\alpha}{1 - r_c \sin\alpha}\right)$$

$$F = F_c \times \sin\alpha + F_t \cos\alpha$$

$$N = F_c \times \cos\alpha - F_t \times \sin\alpha$$

$$\mu = \frac{F}{N}$$

$$R = \sqrt{F_c^2 + F_t^2}$$

$$\beta = \arctan\left[\frac{F}{N}\right]$$

$$F_s = F_c \times \cos\phi - F_t \times \sin\phi$$

$$F_n = F_c \times \sin\phi - F_t \times \cos\phi$$

$$A_s = \frac{t_0 \times w}{\sin\phi} = \frac{t_1 \times w}{\sin\phi}$$

$$\tau_s = \frac{F_s}{A_s}$$

$$HP = \frac{F_c \times V/12}{33{,}000}$$

$$MRR = V \times w \times t_0 = V \times w \times t_1$$

$$HP_s = \frac{HP}{MRR}$$

$$V_c = \frac{V \times \sin\phi}{\cos(\phi - \alpha)}$$

$$V_s = \frac{V \times \cos\alpha}{\cos(\phi - \beta)}$$

$$U = U_s + U_f = \frac{F_c}{w \times V}$$

$$U_f = \frac{F \times V_c}{w \times V}$$

$$U_s = \frac{F_s \times V_s}{f_r \times t_0 \times V}$$

Black and Huang Model Predicts:

$$\varepsilon = \gamma = \frac{2 \times \cos\alpha}{1 + \sin\alpha}$$

$$\Psi = 45 - \phi + \frac{\alpha}{2}$$

Merchant Model Predicts:

$$\varepsilon = \gamma = \frac{\cos\alpha}{\sin\phi \times \cos(\phi - \alpha)}$$

$$\phi = 45 + \frac{\alpha}{2} - \frac{\beta}{2}$$

Appendix 2

Relevant Calibration and Specification Certificates

The calibration certificate for the Kistler 9257A dynamometer is given below.

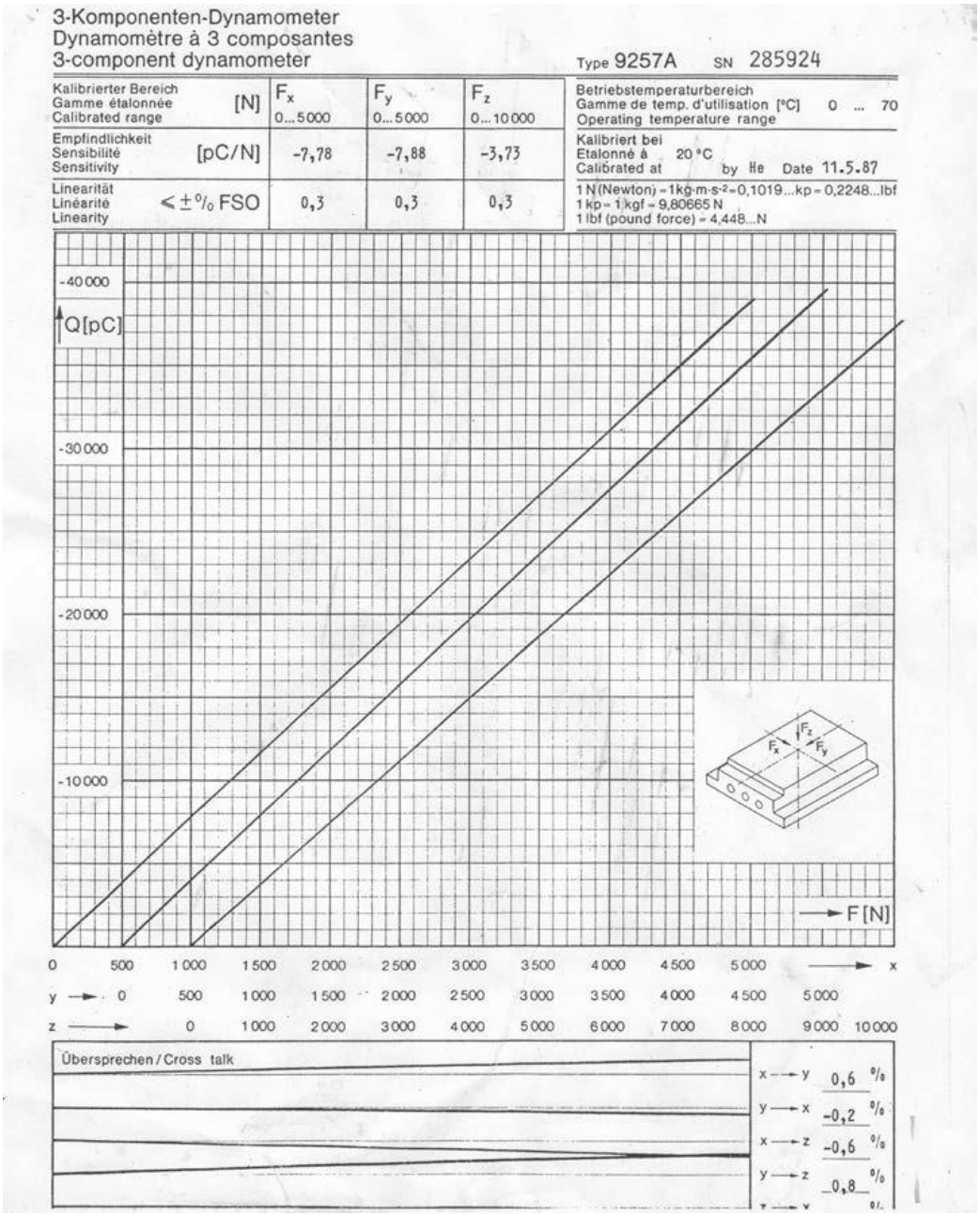

3-Komponenten-Dynamometer
Dynamomètre à 3 composantes
3-component dynamometer

Type 9257A SN 285924

		F_x	F_y	F_z
Kalibrierter Bereich / Gamme étalonnée / Calibrated range	[N]	0...5000	0...5000	0...10000
Empfindlichkeit / Sensibilité / Sensitivity	[pC/N]	-7,78	-7,88	-3,73
Linearität / Linéarité / Linearity	≤ ±% FSO	0,3	0,3	0,3

Betriebstemperaturbereich / Gamme de temp. d'utilisation [°C] / Operating temperature range: 0 ... 70

Kalibriert bei / Etalonné à / Calibrated at: 20 °C by He Date 11.5.87

1 N (Newton) = 1 kg·m·s⁻² = 0,1019...kp = 0,2248...lbf
1 kp = 1 kgf = 9,80665 N
1 lbf (pound force) = 4,448...N

-40000
Q[pC]
-30000
-20000
-10000

F_z F_x F_y

F [N]

0 500 1000 1500 2000 2500 3000 3500 4000 4500 5000 x

y 0 500 1000 1500 2000 2500 3000 3500 4000 4500 5000

z 0 1000 2000 3000 4000 5000 6000 7000 8000 9000 10000

Übersprechen / Cross talk

x → y	0,6	%
y → x	-0,2	%
x → z	-0,6	%
y → z	-0,8	%
z → x		%

The material composition certificate for the copper 10100 is given below.

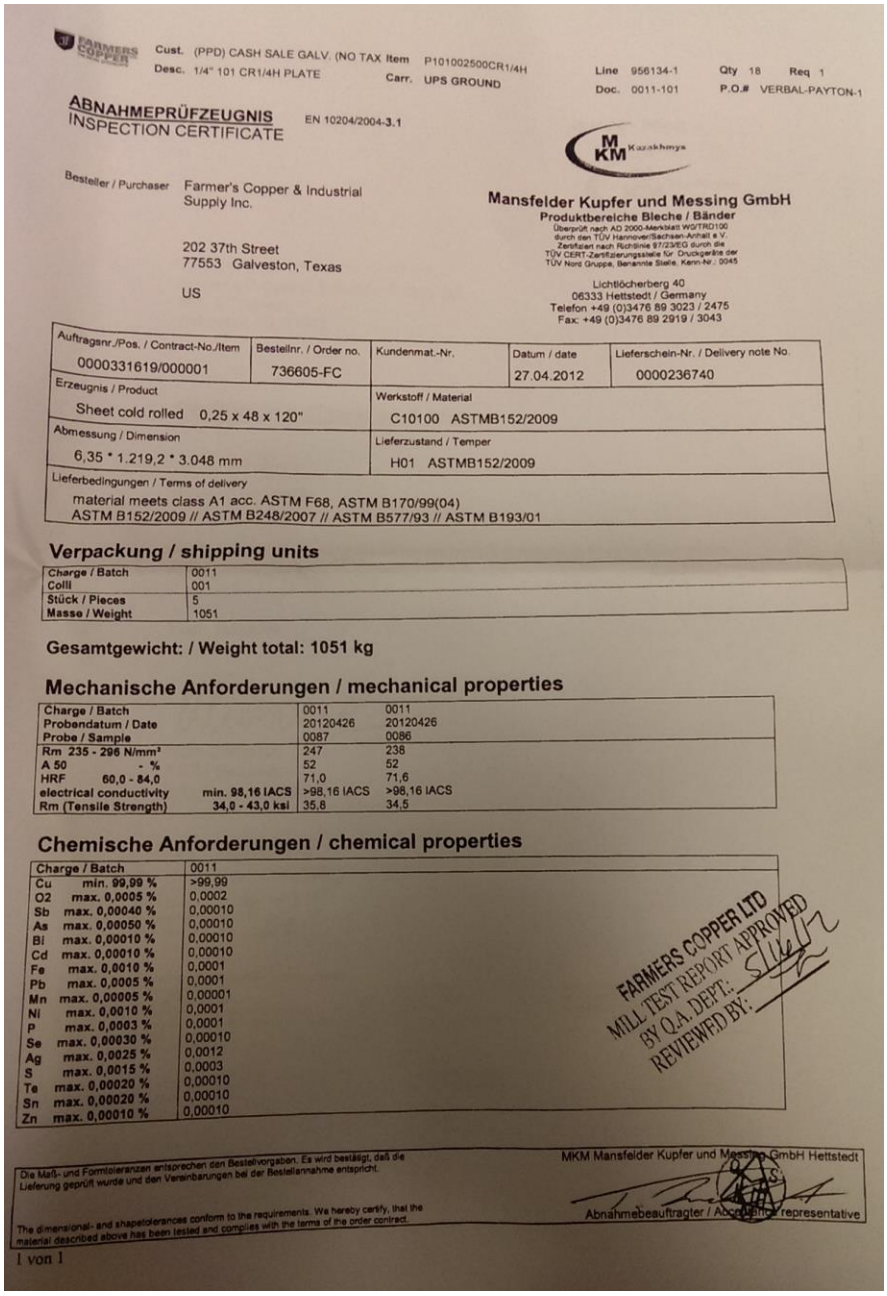

Cust. (PPD) CASH SALE GALV. (NO TAX Item P101002500CR1/4H Line 956134-1 Qty 18 Req 1
Desc. 1/4" 101 CR1/4H PLATE Carr. UPS GROUND Doc. 0011-101 P.O.# VERBAL-PAYTON-1

ABNAHMEPRÜFZEUGNIS
INSPECTION CERTIFICATE EN 10204/2004-3.1

Besteller / Purchaser: Farmer's Copper & Industrial Supply Inc.
202 37th Street
77553 Galveston, Texas
US

Mansfelder Kupfer und Messing GmbH
Produktbereiche Bleche / Bänder
Überprüft nach AD 2000-Merkblatt W0/TRO100 durch den TÜV Hannover/Sachsen-Anhalt e.V.
Zertifiziert nach Richtlinie 97/23/EG durch die TÜV CERT-Zertifizierungsstelle für Druckgeräte der TÜV Nord Gruppe, Benannte Stelle, Kenn-Nr.: 0045
Lichtlöcherberg 40
06333 Hettstedt / Germany
Telefon +49 (0)3476 89 3023 / 2475
Fax: +49 (0)3476 89 2919 / 3043

Auftragsnr./Pos. / Contract-No./Item	Bestellnr. / Order no.	Kundenmat.-Nr.	Datum / date	Lieferschein-Nr. / Delivery note No.
0000331619/000001	736605-FC		27.04.2012	0000236740

Erzeugnis / Product	Werkstoff / Material
Sheet cold rolled 0,25 x 48 x 120"	C10100 ASTMB152/2009
Abmessung / Dimension	**Lieferzustand / Temper**
6,35 * 1.219,2 * 3.048 mm	H01 ASTMB152/2009

Lieferbedingungen / Terms of delivery
material meets class A1 acc. ASTM F68, ASTM B170/99(04)
ASTM B152/2009 // ASTM B248/2007 // ASTM B577/93 // ASTM B193/01

Verpackung / shipping units

Charge / Batch	0011
Colli	001
Stück / Pieces	5
Masse / Weight	1051

Gesamtgewicht: / Weight total: 1051 kg

Mechanische Anforderungen / mechanical properties

Charge / Batch		0011	0011
Probendatum / Date		20120426	20120426
Probe / Sample		0087	0086
Rm 235 - 296 N/mm²		247	238
A 50	- %	52	52
HRF	60,0 - 84,0	71,0	71,6
electrical conductivity	min. 98,16 IACS	>98,16 IACS	>98,16 IACS
Rm (Tensile Strength)	34,0 - 43,0 ksi	35,8	34,5

Chemische Anforderungen / chemical properties

Charge / Batch		0011
Cu	min. 99,99 %	>99,99
O2	max. 0,0005 %	0,0002
Sb	max. 0,00040 %	0,00010
As	max. 0,00050 %	0,00010
Bi	max. 0,00010 %	0,00010
Cd	max. 0,00010 %	0,00010
Fe	max. 0,0010 %	0,0001
Pb	max. 0,0005 %	0,0001
Mn	max. 0,00005 %	0,00001
Ni	max. 0,0010 %	0,0001
P	max. 0,0003 %	0,0001
Se	max. 0,00030 %	0,00010
Ag	max. 0,0025 %	0,0012
S	max. 0,0015 %	0,0003
Te	max. 0,00020 %	0,00010
Sn	max. 0,00020 %	0,00010
Zn	max. 0,00010 %	0,00010

FARMERS COPPER LTD
MILL TEST REPORT APPROVED
BY Q.A. DEPT.:
REVIEWED BY:

Die Maß- und Formtoleranzen entsprechen den Bestellvorgaben. Es wird bestätigt, daß die Lieferung geprüft wurde und den Vereinbarungen bei der Bestellannahme entspricht.

The dimensional- and shapetolerances conform to the requirements. We hereby certify, that the material described above has been tested and complies with the terms of the order contract.

MKM Mansfelder Kupfer und Messing GmbH Hettstedt

Abnahmebeauftragter / Acceptance representative

1 von 1

Appendix 3

Measured Values

The first table below lists the specified runs parameters and the measured force, measured rake angle, and measured depth of cut collected by the high speed virtual quick stop device. The second table lists the measured chip thickness, chip thickness ratio, calculated and measured angles, and calculated forces.

Run	Material	Initial Thickness (in)	Material Hardness (BHN)	Rake Angle (degrees)	Feed Rate (in/min)	Depth of Cut (in)	Replicate	Measured Rake Angle (degrees)	Measured Depth of Cut (mil)	Fz Thrust Force (lbf)	Fy Cutting Force (lbf)
1	Al	0.125	32.3	35	7.5	0.008	1	35.8	7.5	19.98	75.80
2	Al	0.125	32.3	35	7.5	0.008	2	35.6	7.1	15.57	67.66
3	Al	0.125	32.3	35	7.5	0.008	3	36.6	8.8	21.75	84.12
4	Al	0.125	32.3	35	7.5	0.004	1	34.7	4.2	13.70	46.81
5	Al	0.125	32.3	35	7.5	0.004	2	35.3	4.1	10.22	35.00
6	Al	0.125	32.3	35	7.5	0.004	3	34.5	3.9	15.38	52.62
7	Al	0.125	32.3	35	3.75	0.008	1	36.4	10.4	18.49	87.42
8	Al	0.125	32.3	35	3.75	0.008	2	34.8	9.2	21.73	92.67
9	Al	0.125	32.3	35	3.75	0.008	3	35.9	8.1	19.98	86.94
10	Al	0.125	32.3	35	3.75	0.004	1	37.7	4.6	14.51	55.26
11	Al	0.125	32.3	35	3.75	0.004	2	35.6	4.0	8.25	38.78
12	Al	0.125	32.3	35	3.75	0.004	3	34.4	4.1	10.67	46.17
13	Al	0.125	32.3	45	7.5	0.008	1	45.0	7.8	15.67	64.12
14	Al	0.125	32.3	45	7.5	0.008	2	47.7	7.2	16.15	58.94
15	Al	0.125	32.3	45	7.5	0.008	3	45.9	6.4	15.74	58.23
16	Al	0.125	32.3	45	7.5	0.004	1	46.6	4.7	15.28	38.08
17	Al	0.125	32.3	45	7.5	0.004	2	44.7	3.5	14.85	37.84
18	Al	0.125	32.3	45	7.5	0.004	3	44.7	3.7	15.84	38.67
19	Al	0.125	32.3	45	3.75	0.008	1	47.2	8.5	15.91	57.62
20	Al	0.125	32.3	45	3.75	0.008	2	44.6	8.1	16.00	57.78
21	Al	0.125	32.3	45	3.75	0.008	3	44.4	8.2	15.68	56.64
22	Al	0.125	32.3	45	3.75	0.004	1	43.2	4.1	15.69	38.90
23	Al	0.125	32.3	45	3.75	0.004	2	46.6	4.1	16.67	39.35
24	Al	0.125	32.3	45	3.75	0.004	3	44.2	4.1	15.53	37.38

Run	Material	Initial Thickness (in)	Material Hardness (BHN)	Rake Angle (degrees)	Feed Rate (in/min)	Depth of Cut (in)	Replicate	Measured Rake Angle (degrees)	Measured Depth of Cut (mil)	Fz Thrust Force (lbf)	Fy Cutting Force (lbf)
25	Al	0.149	34.4	35	7.5	0.008	1	37.8	7.7	22.54	94.95
26	Al	0.149	34.4	35	7.5	0.008	2	38.1	6.9	22.30	89.44
27	Al	0.149	34.4	35	7.5	0.008	3	38.3	8.2	21.68	95.45
28	Al	0.149	34.4	35	7.5	0.004	1	35.8	5.3	14.71	57.28
29	Al	0.149	34.4	35	7.5	0.004	2	36.8	5.2	15.54	57.88
30	Al	0.149	34.4	35	7.5	0.004	3	36.0	5.0	13.31	55.78
31	Al	0.149	34.4	35	3.75	0.008	1	32.4	9.0	21.24	91.51
32	Al	0.149	34.4	35	3.75	0.008	2	33.1	10.6	22.75	93.14
33	Al	0.149	34.4	35	3.75	0.008	3	34.9	8.3	21.87	91.99
34	Al	0.149	34.4	35	3.75	0.004	1	34.2	4.4	12.43	51.32
35	Al	0.149	34.4	35	3.75	0.004	2	34.4	4.9	13.24	52.83
36	Al	0.149	34.4	35	3.75	0.004	3	34.5	5.0	12.16	50.90
37	Al	0.149	34.4	45	7.5	0.008	1	45.4	8.1	15.51	59.60
38	Al	0.149	34.4	45	7.5	0.008	2	44.4	8.2	16.08	56.41
39	Al	0.149	34.4	45	7.5	0.008	3	44.2	7.7	16.13	55.92
40	Al	0.149	34.4	45	7.5	0.004	1	42.6	4.6	15.05	39.95
41	Al	0.149	34.4	45	7.5	0.004	2	43.8	4.7	15.19	36.62
42	Al	0.149	34.4	45	7.5	0.004	3	45.1	4.1	15.07	37.56
43	Al	0.149	34.4	45	3.75	0.008	1	44.2	7.6	15.49	53.69
44	Al	0.149	34.4	45	3.75	0.008	2	44.8	8.2	15.34	55.34
45	Al	0.149	34.4	45	3.75	0.008	3	45.7	7.8	15.46	55.01
46	Al	0.149	34.4	45	3.75	0.004	1	44.6	4.3	15.33	35.84
47	Al	0.149	34.4	45	3.75	0.004	2	45.1	4.6	15.35	37.37
48	Al	0.149	34.4	45	3.75	0.004	3	43.7	4.4	15.34	36.97
49	Al	0.176	39.8	35	7.5	0.008	1	36.5	9.7	21.71	83.46
50	Al	0.176	39.8	35	7.5	0.008	2	34.9	9.7	22.00	83.19
51	Al	0.176	39.8	35	7.5	0.008	3	34.6	8.6	21.00	82.77
52	Al	0.176	39.8	35	7.5	0.004	1	33.8	4.1	10.93	42.25
53	Al	0.176	39.8	35	7.5	0.004	2	35.2	4.3	11.94	42.14
54	Al	0.176	39.8	35	7.5	0.004	3	34.4	4.3	13.03	42.42
55	Al	0.176	39.8	35	3.75	0.008	1	35.9	8.1	18.18	70.38
56	Al	0.176	39.8	35	3.75	0.008	2	35.3	7.8	18.35	76.59
57	Al	0.176	39.8	35	3.75	0.008	3	35.7	8.2	17.34	69.34
58	Al	0.176	39.8	35	3.75	0.004	1	35.1	5.9	12.04	45.74
59	Al	0.176	39.8	35	3.75	0.004	2	35.8	5.6	12.12	44.87
60	Al	0.176	39.8	35	3.75	0.004	3	36.8	5.7	11.73	43.65
61	Al	0.176	39.8	45	7.5	0.008	1	46.2	7.8	16.44	52.71
62	Al	0.176	39.8	45	7.5	0.008	2	44.4	7.3	16.77	53.38

Run	Material	Initial Thickness (in)	Material Hardness (BHN)	Rake Angle (degrees)	Feed Rate (in/min)	Depth of Cut (in)	Replicate	Measured Rake Angle (degrees)	Measured Depth of Cut (mil)	Fz Thrust Force (lbf)	Fy Cutting Force (lbf)
63	Al	0.176	39.8	45	7.5	0.008	3	46.5	7.7	17.10	53.63
64	Al	0.176	39.8	45	7.5	0.004	1	47.2	4.9	16.06	33.84
65	Al	0.176	39.8	45	7.5	0.004	2	48.6	4.5	15.91	35.06
66	Al	0.176	39.8	45	7.5	0.004	3	47.0	4.1	16.04	35.16
67	Al	0.176	39.8	45	3.75	0.008	1	44.2	7.6	16.09	49.73
68	Al	0.176	39.8	45	3.75	0.008	2	43.6	7.9	16.04	46.53
69	Al	0.176	39.8	45	3.75	0.008	3	44.5	7.8	15.98	50.84
70	Al	0.176	39.8	45	3.75	0.004	1	47.8	3.9	16.58	34.95
71	Al	0.176	39.8	45	3.75	0.004	2	48.1	4.2	16.75	35.94
72	Al	0.176	39.8	45	3.75	0.004	3	48.7	4.5	16.66	36.58
73	Cu	0.125	67	35	7.5	0.008	1	35.1	8.1	13.87	154.57
74	Cu	0.125	67	35	7.5	0.008	2	34.3	7.7	12.13	142.27
75	Cu	0.125	67	35	7.5	0.008	3	35.8	7.2	11.06	132.65
76	Cu	0.125	67	35	7.5	0.004	1	35.1	3.7	8.13	63.07
77	Cu	0.125	67	35	7.5	0.004	2	34.3	4.1	8.81	74.43
78	Cu	0.125	67	35	7.5	0.004	3	34.9	3.5	8.60	70.97
79	Cu	0.125	67	35	3.75	0.008	1	34.4	8.6	11.59	145.21
80	Cu	0.125	67	35	3.75	0.008	2	35.1	8.8	11.23	137.02
81	Cu	0.125	67	35	3.75	0.008	3	34.7	7.9	11.06	135.74
82	Cu	0.125	67	35	3.75	0.004	1	35.5	3.3	8.01	67.85
83	Cu	0.125	67	35	3.75	0.004	2	34.8	4.0	8.03	67.79
84	Cu	0.125	67	35	3.75	0.004	3	36.0	4.2	8.05	67.72
85	Cu	0.125	67	45	7.5	0.008	1	44.6	7.5	21.99	105.04
86	Cu	0.125	67	45	7.5	0.008	2	44.6	7.7	21.52	99.38
87	Cu	0.125	67	45	7.5	0.008	3	44.4	7.7	20.97	99.31
88	Cu	0.125	67	45	7.5	0.004	1	45.0	4.0	28.14	70.77
89	Cu	0.125	67	45	7.5	0.004	2	46.5	4.2	30.43	70.59
90	Cu	0.125	67	45	7.5	0.004	3	43.6	3.9	29.62	73.75
91	Cu	0.125	67	45	3.75	0.008	1	44.8	7.9	21.07	96.80
92	Cu	0.125	67	45	3.75	0.008	2	44.2	7.4	21.72	94.68
93	Cu	0.125	67	45	3.75	0.008	3	45.0	7.8	20.33	99.96
94	Cu	0.125	67	45	3.75	0.004	1	46.7	3.5	31.14	69.08
95	Cu	0.125	67	45	3.75	0.004	2	43.0	3.9	30.57	70.60
96	Cu	0.125	67	45	3.75	0.004	3	44.0	3.8	30.78	69.65
97	Cu	0.139	77	35	7.5	0.008	1	35.1	7.8	16.28	151.58
98	Cu	0.139	77	35	7.5	0.008	2	34.7	7.8	19.25	127.89
99	Cu	0.139	77	35	7.5	0.008	3	34.4	8.2	19.20	132.08
100	Cu	0.139	77	35	7.5	0.004	1	34.9	4.1	9.46	66.89

Run	Material	Initial Thickness (in)	Material Hardness (BHN)	Rake Angle (degrees)	Feed Rate (in/min)	Depth of Cut (in)	Replicate	Measured Rake Angle (degrees)	Measured Depth of Cut (mil)	Fz Thrust Force (lbf)	Fy Cutting Force (lbf)
101	Cu	0.139	77	35	7.5	0.004	2	35.5	3.5	10.09	75.91
102	Cu	0.139	77	35	7.5	0.004	3	34.4	3.9	9.23	67.12
103	Cu	0.139	77	35	3.75	0.008	1	35.8	8.2	15.15	149.18
104	Cu	0.139	77	35	3.75	0.008	2	34.5	8.5	14.05	146.72
105	Cu	0.139	77	35	3.75	0.008	3	34.8	7.5	12.16	134.77
106	Cu	0.139	77	35	3.75	0.004	1	34.4	4.1	7.73	68.77
107	Cu	0.139	77	35	3.75	0.004	2	35.0	4.1	7.84	69.23
108	Cu	0.139	77	35	3.75	0.004	3	34.9	3.8	7.80	63.04
109	Cu	0.139	77	45	7.5	0.008	1	44.1	8.7	2.15	88.55
110	Cu	0.139	77	45	7.5	0.008	2	44.3	7.3	4.74	77.64
111	Cu	0.139	77	45	7.5	0.008	3	43.8	8.0	3.58	85.47
112	Cu	0.139	77	45	7.5	0.004	1	44.6	3.9	8.53	49.86
113	Cu	0.139	77	45	7.5	0.004	2	44.4	3.6	8.75	47.12
114	Cu	0.139	77	45	7.5	0.004	3	43.6	3.7	11.61	54.91
115	Cu	0.139	77	45	3.75	0.008	1	43.8	7.4	3.57	76.28
116	Cu	0.139	77	45	3.75	0.008	2	44.0	7.6	3.43	76.68
117	Cu	0.139	77	45	3.75	0.008	3	44.4	8.0	3.50	82.93
118	Cu	0.139	77	45	3.75	0.004	1	45.5	4.0	29.55	70.48
119	Cu	0.139	77	45	3.75	0.004	2	44.6	3.9	32.16	70.17
120	Cu	0.139	77	45	3.75	0.004	3	43.9	3.7	31.67	69.91
121	Cu	0.169	81	35	7.5	0.008	1	35.4	8.6	22.18	115.40
122	Cu	0.169	81	35	7.5	0.008	2	35.1	8.0	21.71	106.61
123	Cu	0.169	81	35	7.5	0.008	3	36.3	7.8	21.67	107.24
124	Cu	0.169	81	35	7.5	0.004	1	35.2	4.2	23.29	64.45
125	Cu	0.169	81	35	7.5	0.004	2	35.1	3.9	23.31	65.01
126	Cu	0.169	81	35	7.5	0.004	3	35.1	4.2	23.44	66.27
127	Cu	0.169	81	35	3.75	0.008	1	36.0	6.9	22.64	110.62
128	Cu	0.169	81	35	3.75	0.008	2	34.9	8.4	21.97	105.82
129	Cu	0.169	81	35	3.75	0.008	3	34.6	8.2	21.49	108.34
130	Cu	0.169	81	35	3.75	0.004	1	34.9	3.8	23.97	63.63
131	Cu	0.169	81	35	3.75	0.004	2	34.5	4.5	24.01	66.38
132	Cu	0.169	81	35	3.75	0.004	3	35.0	4.2	24.12	66.18
133	Cu	0.169	81	45	7.5	0.008	1	45.8	7.9	29.82	99.39
134	Cu	0.169	81	45	7.5	0.008	2	44.7	8.1	29.27	98.75
135	Cu	0.169	81	45	7.5	0.008	3	46.2	7.7	29.47	97.41
136	Cu	0.169	81	45	7.5	0.004	1	46.4	3.7	37.37	71.56
137	Cu	0.169	81	45	7.5	0.004	2	45.8	4.0	37.02	72.24
138	Cu	0.169	81	45	7.5	0.004	3	47.7	3.4	37.39	69.06

Run	Material	Initial Thickness (in)	Material Hardness (BHN)	Rake Angle (degrees)	Feed Rate (in/min)	Depth of Cut (in)	Replicate	Measured Rake Angle (degrees)	Measured Depth of Cut (mil)	Fz Thrust Force (lbf)	Fy Cutting Force (lbf)
139	Cu	0.169	81	45	3.75	0.008	1	45.7	7.6	29.59	98.47
140	Cu	0.169	81	45	3.75	0.008	2	46.4	7.5	30.23	98.09
141	Cu	0.169	81	45	3.75	0.008	3	45.7	7.5	30.32	97.44
142	Cu	0.169	81	45	3.75	0.004	1	47.7	3.6	38.17	69.76
143	Cu	0.169	81	45	3.75	0.004	2	46.5	4.2	37.41	73.15
144	Cu	0.169	81	45	3.75	0.004	3	47.9	3.7	38.11	70.33
145	Cu	0.205	83	25	7.5	0.008	1	20.6	8.3	45.16	221.50
146	Cu	0.205	83	25	7.5	0.008	2	22.8	7.8	46.62	247.24
147	Cu	0.205	83	25	7.5	0.008	3	20.0	9.2	46.42	239.03
148	Cu	0.205	83	25	7.5	0.004	1	23.2	5.0	31.15	133.18
149	Cu	0.205	83	25	7.5	0.004	2	22.3	4.5	40.00	171.85
150	Cu	0.205	83	25	7.5	0.004	3	24.7	4.8	33.95	140.64
151	Cu	0.205	83	25	3.75	0.008	1	22.4	9.0	48.95	252.51
152	Cu	0.205	83	25	3.75	0.008	2	19.5	7.8	43.52	219.33
153	Cu	0.205	83	25	3.75	0.008	3	21.7	9.0	44.52	234.69
154	Cu	0.205	83	25	3.75	0.004	1	22.3	4.9	31.98	138.06
155	Cu	0.205	83	25	3.75	0.004	2	21.0	3.5	31.27	136.05
156	Cu	0.205	83	25	3.75	0.004	3	24.4	4.0	34.88	159.45
157	Cu	0.205	83	35	7.5	0.008	1	35.0	7.8	9.69	100.87
158	Cu	0.205	83	35	7.5	0.008	2	34.9	8.1	8.84	96.24
159	Cu	0.205	83	35	7.5	0.008	3	34.2	7.8	8.87	95.32
160	Cu	0.205	83	35	7.5	0.004	1	33.9	4.6	5.51	51.53
161	Cu	0.205	83	35	7.5	0.004	2	34.8	3.6	6.38	46.16
162	Cu	0.205	83	35	7.5	0.004	3	34.4	4.0	6.24	51.61
163	Cu	0.205	83	35	3.75	0.008	1	34.5	7.7	8.24	95.78
164	Cu	0.205	83	35	3.75	0.008	2	34.7	8.2	7.96	96.01
165	Cu	0.205	83	35	3.75	0.008	3	34.2	8.2	6.92	90.93
166	Cu	0.205	83	35	3.75	0.004	1	33.7	3.9	6.61	47.09
167	Cu	0.205	83	35	3.75	0.004	2	34.3	4.1	6.45	51.24
168	Cu	0.205	83	35	3.75	0.004	3	34.4	3.6	5.88	44.38
169	Cu	0.205	83	45	7.5	0.008	1	45.1	7.9	31.01	103.78
170	Cu	0.205	83	45	7.5	0.008	2	45.7	7.3	33.29	101.76
171	Cu	0.205	83	45	7.5	0.008	3	45.7	7.7	33.37	101.07
172	Cu	0.205	83	45	7.5	0.004	1	46.8	4.4	40.76	74.63
173	Cu	0.205	83	45	7.5	0.004	2	47.0	4.3	40.32	72.95
174	Cu	0.205	83	45	7.5	0.004	3	47.6	3.7	40.20	72.52
175	Cu	0.205	83	45	3.75	0.008	1	45.7	7.9	33.70	100.20
176	Cu	0.205	83	45	3.75	0.008	2	45.4	8.1	33.00	100.64

Run	Material	Initial Thickness (in)	Material Hardness (BHN)	Rake Angle (degrees)	Feed Rate (in/min)	Depth of Cut (in)	Replicate	Measured Rake Angle (degrees)	Measured Depth of Cut (mil)	Fz Thrust Force (lbf)	Fy Cutting Force (lbf)
177	Cu	0.205	83	45	3.75	0.008	3	45.6	7.5	34.27	96.72
178	Cu	0.205	83	45	3.75	0.004	1	47.0	3.2	40.57	70.85
179	Cu	0.205	83	45	3.75	0.004	2	45.5	3.7	40.35	72.69
180	Cu	0.205	83	45	3.75	0.004	3	48.4	3.8	40.70	70.84
181	Cu	0.245	84	25	7.5	0.008	1	21.5	8.4	42.78	207.55
182	Cu	0.245	84	25	7.5	0.008	2	21.4	8.4	45.39	220.28
183	Cu	0.245	84	25	7.5	0.008	3	24.2	8.3	46.71	224.34
184	Cu	0.245	84	25	7.5	0.004	1	20.5	4.8	30.50	136.75
185	Cu	0.245	84	25	7.5	0.004	2	21.8	4.1	32.92	141.26
186	Cu	0.245	84	25	7.5	0.004	3	21.3	6.4	41.76	191.31
187	Cu	0.245	84	25	3.75	0.008	1	20.0	7.8	41.26	200.70
188	Cu	0.245	84	25	3.75	0.008	2	20.6	8.2	41.96	208.83
189	Cu	0.245	84	25	3.75	0.008	3	20.1	8.7	40.30	199.03
190	Cu	0.245	84	25	3.75	0.004	1	20.1	6.0	27.42	111.20
191	Cu	0.245	84	25	3.75	0.004	2	21.3	4.2	34.48	149.46
192	Cu	0.245	84	25	3.75	0.004	3	20.7	3.7	28.40	114.42
193	Cu	0.245	84	35	7.5	0.008	1	34.3	8.0	8.87	91.59
194	Cu	0.245	84	35	7.5	0.008	2	34.9	8.1	7.72	89.99
195	Cu	0.245	84	35	7.5	0.008	3	34.6	8.0	7.56	91.30
196	Cu	0.245	84	35	7.5	0.004	1	36.3	4.5	7.47	50.01
197	Cu	0.245	84	35	7.5	0.004	2	36.4	4.1	7.65	50.17
198	Cu	0.245	84	35	7.5	0.004	3	36.0	3.9	7.75	48.69
199	Cu	0.245	84	35	3.75	0.008	1	34.6	7.8	9.10	91.23
200	Cu	0.245	84	35	3.75	0.008	2	34.1	7.8	7.42	85.99
201	Cu	0.245	84	35	3.75	0.008	3	34.7	7.8	6.77	83.26
202	Cu	0.245	84	35	3.75	0.004	1	38.2	4.2	7.80	47.71
203	Cu	0.245	84	35	3.75	0.004	2	37.1	4.1	8.09	49.00
204	Cu	0.245	84	35	3.75	0.004	3	36.9	4.1	7.62	48.55
205	Cu	0.245	84	45	7.5	0.008	1	45.7	7.6	36.14	102.08
206	Cu	0.245	84	45	7.5	0.008	2	46.0	7.8	35.59	103.21
207	Cu	0.245	84	45	7.5	0.008	3	45.5	7.8	35.42	102.91
208	Cu	0.245	84	45	7.5	0.004	1	46.7	3.9	42.90	75.46
209	Cu	0.245	84	45	7.5	0.004	2	47.0	3.8	42.78	75.13
210	Cu	0.245	84	45	7.5	0.004	3	48.6	3.5	42.99	73.36
211	Cu	0.245	84	45	3.75	0.008	1	45.6	7.8	35.67	100.69
212	Cu	0.245	84	45	3.75	0.008	2	46.1	7.5	36.83	97.63
213	Cu	0.245	84	45	3.75	0.008	3	45.9	7.3	36.21	98.33
214	Cu	0.245	84	45	3.75	0.004	1	48.7	3.7	42.94	71.16

Run	Material	Initial Thickness (in)	Material Hardness (BHN)	Rake Angle (degrees)	Feed Rate (in/min)	Depth of Cut (in)	Replicate	Measured Rake Angle (degrees)	Measured Depth of Cut (mil)	Fz Thrust Force (lbf)	Fy Cutting Force (lbf)
215	Cu	0.245	84	45	3.75	0.004	2	48.0	3.7	42.59	71.63
216	Cu	0.245	84	45	3.75	0.004	3	48.6	3.8	42.65	71.74
217	St	0.125	135	35	7.5	0.008	1	33.5	8.5	40.18	270.99
218	St	0.125	135	35	7.5	0.008	2	34.8	8.2	53.33	290.60
219	St	0.125	135	35	7.5	0.008	3	34.8	7.4	55.78	277.80
220	St	0.125	135	35	7.5	0.004	1	32.4	3.3	30.43	133.06
221	St	0.125	135	35	7.5	0.004	2	35.6	4.6	30.22	154.13
222	St	0.125	135	35	7.5	0.004	3	36.1	4.6	28.37	143.93
223	St	0.125	135	35	3.75	0.008	1	33.6	9.4	37.67	280.03
224	St	0.125	135	35	3.75	0.008	2	35.0	8.8	40.05	303.74
225	St	0.125	135	35	3.75	0.008	3	32.8	7.9	42.90	258.27
226	St	0.125	135	35	3.75	0.004	1	34.8	4.7	21.31	116.68
227	St	0.125	135	35	3.75	0.004	2	35.8	4.1	20.17	118.54
228	St	0.125	135	35	3.75	0.004	3	35.3	4.0	21.08	121.33
229	St	0.125	135	45	7.5	0.008	1	42.6	9.1	49.03	254.98
230	St	0.125	135	45	7.5	0.008	2	45.5	7.3	56.18	229.78
231	St	0.125	135	45	7.5	0.008	3	43.7	9.2	53.29	249.84
232	St	0.125	135	45	7.5	0.004	1	47.7	4.2	63.67	164.49
233	St	0.125	135	45	7.5	0.004	2	46.9	2.4	61.51	168.29
234	St	0.125	135	45	7.5	0.004	3	43.7	5.0	63.89	162.76
235	St	0.125	135	45	3.75	0.008	1	42.7	7.7	55.16	244.21
236	St	0.125	135	45	3.75	0.008	2	43.0	7.3	54.82	243.75
237	St	0.125	135	45	3.75	0.008	3	44.3	7.7	54.18	243.18
238	St	0.125	135	45	3.75	0.004	1	42.7	4.8	11.14	112.65
239	St	0.125	135	45	3.75	0.004	2	47.2	3.7	12.24	93.96
240	St	0.125	135	45	3.75	0.004	3	46.8	4.9	11.49	115.25
241	St	0.149	154	35	7.5	0.008	1	33.2	9.4	44.28	280.35
242	St	0.149	154	35	7.5	0.008	2	34.4	8.8	53.71	282.69
243	St	0.149	154	35	7.5	0.008	3	34.1	7.2	56.14	271.53
244	St	0.149	154	35	7.5	0.004	1	34.7	2.3	25.21	118.13
245	St	0.149	154	35	7.5	0.004	2	33.7	4.5	24.91	124.39
246	St	0.149	154	35	7.5	0.004	3	33.7	4.3	24.47	116.26
247	St	0.149	154	35	3.75	0.008	1	33.7	9.2	45.54	285.84
248	St	0.149	154	35	3.75	0.008	2	35.9	7.2	49.18	261.71
249	St	0.149	154	35	3.75	0.008	3	31.8	8.1	50.25	269.01
250	St	0.149	154	35	3.75	0.004	1	33.8	2.5	35.19	134.95
251	St	0.149	154	35	3.75	0.004	2	34.7	3.7	32.50	139.39
252	St	0.149	154	35	3.75	0.004	3	34.4	3.8	32.50	139.39

Run	Material	Initial Thickness (in)	Material Hardness (BHN)	Rake Angle (degrees)	Feed Rate (in/min)	Depth of Cut (in)	Replicate	Measured Rake Angle (degrees)	Measured Depth of Cut (mil)	Fz Thrust Force (lbf)	Fy Cutting Force (lbf)
253	St	0.149	154	45	7.5	0.008	1	46.7	9.6	59.22	267.34
254	St	0.149	154	45	7.5	0.008	2	43.7	7.8	62.19	239.90
255	St	0.149	154	45	7.5	0.008	3	44.5	3.3	61.39	246.20
256	St	0.149	154	45	7.5	0.004	1	45.9	6.0	68.00	177.50
257	St	0.149	154	45	7.5	0.004	2	46.9	4.0	71.23	165.16
258	St	0.149	154	45	7.5	0.004	3	46.7	3.0	70.08	166.45
259	St	0.149	154	45	3.75	0.008	1	45.0	5.2	64.85	246.81
260	St	0.149	154	45	3.75	0.008	2	47.3	6.9	65.49	235.02
261	St	0.149	154	45	3.75	0.008	3	45.9	5.0	63.41	252.95
262	St	0.149	154	45	3.75	0.004	1	45.2	4.1	72.10	177.66
263	St	0.149	154	45	3.75	0.004	2	45.3	4.3	72.36	171.55
264	St	0.149	154	45	3.75	0.004	3	42.9	4.2	71.27	171.45
265	St	0.176	171	35	7.5	0.008	1	33.2	8.8	45.83	263.77
266	St	0.176	171	35	7.5	0.008	2	33.6	8.7	52.52	252.48
267	St	0.176	171	35	7.5	0.008	3	33.3	8.3	56.37	265.73
268	St	0.176	171	35	7.5	0.004	1	35.0	4.4	28.00	125.81
269	St	0.176	171	35	7.5	0.004	2	33.3	4.2	26.61	116.78
270	St	0.176	171	35	7.5	0.004	3	34.1	3.9	25.90	118.88
271	St	0.176	171	35	3.75	0.008	1	33.9	8.7	43.73	261.54
272	St	0.176	171	35	3.75	0.008	2	33.6	7.8	48.86	254.71
273	St	0.176	171	35	3.75	0.008	3	33.3	7.6	46.70	244.59
274	St	0.176	171	35	3.75	0.004	1	34.1	3.3	33.10	121.65
275	St	0.176	171	35	3.75	0.004	2	34.7	4.5	33.81	143.09
276	St	0.176	171	35	3.75	0.004	3	34.7	3.8	32.84	130.27
277	St	0.176	171	45	7.5	0.008	1	45.0	9.0	65.90	262.80
278	St	0.176	171	45	7.5	0.008	2	46.9	7.1	69.14	235.31
279	St	0.176	171	45	7.5	0.008	3	46.9	7.6	68.09	235.05
280	St	0.176	171	45	7.5	0.004	1	43.5	4.6	68.39	159.66
281	St	0.176	171	45	7.5	0.004	2	47.1	3.5	71.12	157.26
282	St	0.176	171	45	7.5	0.004	3	47.3	3.8	70.29	159.61
283	St	0.176	171	45	3.75	0.008	1	45.2	8.2	69.10	239.92
284	St	0.176	171	45	3.75	0.008	2	44.8	7.7	67.37	237.51
285	St	0.176	171	45	3.75	0.008	3	43.8	7.4	67.59	233.14
286	St	0.176	171	45	3.75	0.004	1	47.1	4.0	72.59	164.93
287	St	0.176	171	45	3.75	0.004	2	45.6	3.9	75.35	168.28
288	St	0.176	171	45	3.75	0.004	3	48.2	3.4	75.96	163.92

Run	Cut Chip Thickness (in)	Chip thickness ratio	Phi (degrees)	Measured Phi (degrees)	Measured Psi (degrees)	Psi (degrees)	Friction Force, F (newtons)	Normal Force, N (newtons)	Fs Merchant (newtons)	Fn Merchant (newtons)	Fs Payton (newtons)	Fn Payton (newtons)
1	0.028	0.29	15.6	14.4	44.3	46.9	266.20	225.24	300.76	176.47	76.87	340.13
2	0.027	0.30	16.3	14.4	43.1	46.2	229.37	206.80	269.43	150.95	77.53	298.94
3	0.028	0.29	15.6	17.4	46.5	46.9	293.87	251.02	334.25	194.03	86.96	376.58
4	0.015	0.27	14.5	11.8	49.5	48.0	169.37	135.62	186.42	111.02	42.09	212.85
5	0.014	0.29	15.6	13.8	51.4	46.9	126.56	101.45	137.67	85.76	31.55	159.10
6	0.015	0.27	14.5	11.5	46.8	48.0	190.29	152.51	209.58	124.68	47.41	239.21
7	0.029	0.28	15.0	16.2	38.5	47.5	290.42	271.34	354.22	180.26	106.59	382.89
8	0.028	0.29	15.6	16.7	41.0	46.9	315.60	282.21	370.89	204.19	104.60	410.26
9	0.028	0.29	15.6	14.2	40.0	46.9	294.60	265.81	348.45	189.81	99.74	384.05
10	0.017	0.24	12.6	12.9	48.5	49.9	193.86	164.35	225.90	116.45	56.26	247.84
11	0.015	0.27	14.5	14.0	40.4	48.0	128.98	120.25	157.86	78.59	47.10	169.93
12	0.017	0.24	12.6	13.4	35.6	49.9	156.66	141.02	190.14	90.97	52.75	204.08
13	0.0185	0.43	23.8	17.8	34.3	43.7	250.98	152.38	232.91	178.77	44.73	290.19
14	0.018	0.44	24.6	21.4	37.0	42.9	236.18	134.61	208.43	174.52	33.98	269.71
15	0.018	0.44	24.6	16.5	39.0	42.9	232.66	133.64	206.30	171.56	34.43	266.10
16	0.0085	0.47	26.5	17.6	36.7	41.0	167.84	71.72	121.25	136.42	2.03	182.51
17	0.0085	0.47	26.5	14.4	38.4	41.0	165.75	72.32	121.16	134.25	3.38	180.81
18	0.008	0.50	28.7	15.4	36.4	38.8	171.44	71.81	117.11	144.35	0.74	185.87
19	0.018	0.44	24.6	23.3	38.2	42.9	231.29	131.20	203.53	171.13	32.70	263.90
20	0.018	0.44	24.6	23.3	37.5	42.9	232.09	131.42	204.01	171.80	32.60	264.71
21	0.018	0.44	24.6	23.2	35.8	42.9	227.46	128.84	199.99	168.36	31.99	259.45
22	0.0085	0.47	26.5	19.1	35.3	41.0	171.72	73.01	123.71	139.69	1.74	186.59
23	0.0085	0.47	26.5	20.0	28.6	41.0	176.19	71.33	123.54	144.47	-1.53	190.08
24	0.008	0.50	28.7	17.6	29.4	38.8	166.41	68.73	112.74	140.38	-0.18	180.05
25	0.027	0.30	16.3	12.3	40.9	46.2	324.38	288.46	377.23	214.77	106.08	420.92
26	0.028	0.29	15.6	11.3	43.2	46.9	309.45	269.02	356.40	202.76	95.73	398.70
27	0.027	0.30	16.3	13.4	41.7	46.2	322.53	292.49	380.46	211.73	110.51	421.15
28	0.017	0.24	12.6	10.5	43.0	49.9	199.75	171.16	234.45	119.29	59.59	256.21
29	0.0185	0.22	11.4	10.0	44.2	51.1	204.32	171.26	238.67	118.80	57.56	260.31
30	0.017	0.24	12.6	10.2	43.9	49.9	190.81	169.30	229.31	111.74	62.06	247.43
31	0.028	0.29	15.6	15.5	42.5	46.9	310.85	279.26	366.52	200.69	104.17	404.68
32	0.029	0.28	15.0	14.9	37.3	47.5	320.54	281.31	373.88	205.17	101.52	414.22
33	0.028	0.29	15.6	15.4	40.4	46.9	314.39	279.38	367.82	203.99	102.64	407.88
34	0.018	0.22	11.8	10.9	48.7	50.7	176.24	155.26	212.16	100.76	56.34	228.02
35	0.0175	0.23	12.2	11.7	42.8	50.3	183.04	158.73	217.33	107.08	56.27	235.65
36	0.018	0.22	11.8	12.3	42.7	50.7	174.19	154.46	210.61	99.20	56.57	225.83
37	0.017	0.47	26.5	24.4	29.9	41.0	236.28	138.68	206.47	180.08	37.71	271.36
38	0.0165	0.48	27.6	24.4	33.6	39.9	228.02	126.86	189.40	179.49	29.95	259.21

Run	Cut Chip Thickness (in)	Chip thickness ratio	Phi (degrees)	Measured Phi (degrees)	Measured Psi (degrees)	Psi (degrees)	Friction Force, F (newtons)	Normal Force, N (newtons)	Fs Merchant (newtons)	Fn Merchant (newtons)	Fs Payton (newtons)	Fn Payton (newtons)
39	0.016	0.50	28.7	25.0	27.6	38.8	226.62	125.16	183.81	182.30	28.91	257.26
40	0.009	0.44	24.6	18.9	28.4	42.9	173.00	78.31	133.65	134.90	6.15	189.80
41	0.0085	0.47	26.5	23.7	29.9	41.0	162.98	67.40	115.62	133.18	-0.10	176.37
42	0.0085	0.47	26.5	20.7	31.9	41.0	165.53	70.75	119.60	134.54	2.02	180.00
43	0.016	0.50	28.7	23.9	32.7	38.8	217.60	120.16	176.48	175.05	27.74	247.02
44	0.016	0.50	28.7	27.9	30.2	38.8	222.33	125.81	183.23	178.00	31.15	253.55
45	0.016	0.50	28.7	25.1	34.8	38.8	221.68	124.41	181.70	177.77	30.11	252.41
46	0.008	0.50	28.7	25.7	35.0	38.8	160.94	64.50	107.14	136.33	-2.00	173.38
47	0.008	0.50	28.7	23.8	30.9	38.8	165.83	69.27	113.09	139.68	0.53	179.72
48	0.0085	0.47	26.5	22.8	29.9	41.0	164.53	68.04	116.72	134.45	-0.11	178.05
49	0.027	0.30	16.3	17.6	42.8	46.2	292.05	248.72	329.23	196.88	85.77	373.90
50	0.028	0.29	15.6	16.0	47.5	46.9	292.43	247.00	329.98	194.00	84.06	373.44
51	0.027	0.30	16.3	16.7	47.6	46.2	287.70	248.04	327.19	192.99	87.16	369.73
52	0.015	0.27	14.5	11.8	51.0	48.0	147.63	126.04	169.83	94.02	43.63	189.15
53	0.016	0.25	13.4	12.1	55.1	49.1	151.04	123.07	169.95	95.26	39.42	190.80
54	0.0155	0.26	13.9	11.2	51.0	48.6	155.72	121.32	169.19	101.71	35.71	194.15
55	0.026	0.31	17.0	15.3	47.2	45.5	245.80	210.09	275.71	168.94	72.85	315.04
56	0.025	0.32	17.8	15.0	43.5	44.7	262.26	232.26	299.43	181.84	84.92	339.87
57	0.0255	0.31	17.4	15.7	47.2	45.1	240.07	208.41	271.24	165.82	74.01	309.18
58	0.016	0.25	13.4	17.2	50.6	49.1	160.59	135.94	185.43	99.41	46.43	205.21
59	0.016	0.25	13.4	14.7	52.9	49.1	158.65	132.57	181.59	98.85	44.34	201.94
60	0.0155	0.26	13.9	13.6	48.8	48.6	154.10	129.12	175.88	97.39	43.38	196.31
61	0.015	0.53	31.2	23.6	32.7	36.3	217.51	114.10	162.71	183.99	22.17	244.61
62	0.015	0.53	31.2	23.7	33.1	36.3	220.66	115.14	164.48	186.81	21.93	247.93
63	0.015	0.53	31.2	23.1	31.0	36.3	222.47	114.89	164.66	188.62	21.01	249.50
64	0.008	0.50	28.7	21.4	31.0	38.8	156.94	55.92	97.77	134.90	-8.40	166.39
65	0.008	0.50	28.7	23.9	33.8	38.8	160.33	60.24	102.88	136.93	-5.70	171.18
66	0.008	0.50	28.7	23.7	34.1	38.8	161.03	60.16	103.00	137.63	-6.05	171.80
67	0.015	0.53	31.2	23.0	31.6	36.3	207.03	105.83	152.18	175.79	18.55	231.77
68	0.015	0.53	31.2	24.2	34.3	36.3	196.81	95.90	140.10	168.24	13.29	218.53
69	0.015	0.53	31.2	21.5	32.8	36.3	210.18	109.64	156.63	177.94	20.86	236.14
70	0.006	0.67	41.7	18.9	32.9	25.8	162.09	57.80	66.96	158.53	-8.63	171.87
71	0.007	0.57	34.1	19.8	30.2	33.4	165.73	60.38	90.53	151.38	-7.63	176.22
72	0.007	0.57	34.1	21.4	32.8	33.4	167.48	62.65	93.08	152.67	-6.21	178.70
73	0.028	0.29	15.6	18.7	28.5	46.9	444.92	527.84	645.50	244.76	262.76	638.38
74	0.027	0.30	16.3	17.2	35.2	46.2	407.18	487.46	592.28	229.39	244.37	586.26
75	0.027	0.30	16.3	18.2	30.8	46.2	378.75	455.12	552.53	212.83	228.81	546.10
76	0.012	0.33	18.7	19.8	31.1	43.8	190.54	209.09	254.26	124.00	97.48	265.56

Run	Cut Chip Thickness (in)	Chip thickness ratio	Phi (degrees)	Measured Phi (degrees)	Measured Psi (degrees)	Psi (degrees)	Friction Force, F (newtons)	Normal Force, N (newtons)	Fs Merchant (newtons)	Fn Merchant (newtons)	Fs Payton (newtons)	Fn Payton (newtons)
77	0.0125	0.32	17.8	18.2	29.8	44.7	222.00	248.70	303.23	138.53	118.09	311.76
78	0.012	0.33	18.7	17.1	36.4	43.8	212.40	236.65	286.86	137.22	111.83	297.68
79	0.027	0.30	16.3	20.0	29.3	46.2	412.70	499.54	605.49	230.75	252.53	596.73
80	0.0265	0.30	16.7	19.4	34.0	45.8	390.50	470.61	569.61	222.49	237.13	563.68
81	0.026	0.31	17.0	19.9	30.0	45.5	386.63	466.36	562.95	223.77	235.14	558.29
82	0.0125	0.32	17.8	18.6	32.0	44.7	202.31	226.79	276.47	126.20	107.75	284.17
83	0.0125	0.32	17.8	19.3	32.2	44.7	202.21	226.51	276.17	126.18	107.54	283.95
84	0.0125	0.32	17.8	22.3	45.2	44.7	202.11	226.22	275.87	126.17	107.34	283.73
85	0.0135	0.59	35.8	29.7	30.5	31.7	399.57	261.23	321.74	352.67	88.43	469.12
86	0.013	0.62	37.6	31.4	20.9	29.9	380.29	244.88	291.77	345.63	80.71	445.05
87	0.013	0.62	37.6	27.0	24.0	29.9	378.31	246.43	293.04	343.47	82.89	443.82
88	0.005	0.80	52.5	25.0	28.3	15.0	311.12	134.07	92.41	325.93	4.81	338.74
89	0.005	0.80	52.5	25.8	21.7	15.0	317.75	126.31	83.84	331.50	-4.91	341.90
90	0.005	0.80	52.5	27.8	23.5	15.0	325.13	138.83	95.30	340.44	3.84	353.51
91	0.013	0.62	37.6	32.8	22.9	29.9	370.76	238.20	283.91	337.04	78.18	433.69
92	0.0125	0.64	39.6	32.0	21.2	27.9	366.13	229.48	263.04	342.81	71.90	426.08
93	0.013	0.62	37.6	28.4	24.7	29.9	378.34	250.47	297.06	342.98	86.62	445.40
94	0.005	0.80	52.5	24.9	23.1	15.0	315.24	119.32	77.25	328.10	-10.39	336.91
95	0.005	0.80	52.5	26.4	29.1	15.0	318.21	125.90	83.38	331.90	-5.45	342.17
96	0.005	0.80	52.5	29.0	24.4	15.0	315.86	122.26	80.08	329.10	-7.92	338.61
97	0.0275	0.29	16.0	18.0	23.0	46.5	446.06	510.82	628.38	255.03	247.13	631.52
98	0.027	0.30	16.3	20.8	19.4	46.2	396.44	416.91	522.01	241.84	186.75	544.15
99	0.0265	0.30	16.7	22.0	22.5	45.8	406.96	432.28	538.42	250.19	195.52	560.59
100	0.012	0.33	18.7	19.2	20.8	43.8	205.15	219.60	268.46	135.06	100.06	283.37
101	0.0125	0.32	17.8	17.3	26.1	44.7	230.44	250.86	307.78	145.95	116.11	320.24
102	0.012	0.33	18.7	19.1	21.0	43.8	204.88	221.01	269.74	134.40	101.44	283.78
103	0.0275	0.29	16.0	20.6	24.4	46.5	435.82	504.95	619.49	247.26	246.66	619.73
104	0.027	0.30	16.3	21.3	23.5	46.2	425.55	498.76	608.87	243.17	245.90	607.77
105	0.027	0.30	16.3	17.9	19.6	46.2	388.15	460.05	560.21	220.15	228.84	556.72
106	0.0125	0.32	17.8	20.6	34.2	44.7	203.61	230.86	280.75	126.24	110.76	287.21
107	0.012	0.33	18.7	18.9	27.2	43.8	205.19	232.26	280.62	131.53	111.27	289.25
108	0.012	0.33	18.7	16.5	29.4	43.8	189.26	209.78	254.57	122.57	98.69	264.74
109	0.0145	0.55	32.6	27.5	16.8	34.9	285.30	271.75	326.65	220.32	141.88	367.57
110	0.0135	0.59	35.8	25.8	13.9	31.7	259.12	229.28	267.75	219.14	112.66	327.14
111	0.014	0.57	34.1	26.1	18.5	33.4	280.10	257.55	305.71	226.55	130.75	357.34
112	0.005	0.80	52.5	21.7	17.2	15.0	183.66	129.99	104.96	199.03	49.81	219.43
113	0.005	0.80	52.5	22.6	21.1	15.0	175.72	120.69	96.77	189.94	44.26	208.53
114	0.005	0.80	52.5	22.0	22.5	15.0	209.23	136.20	107.78	225.19	45.76	245.42

Run	Cut Chip Thickness (in)	Chip thickness ratio	Phi (degrees)	Measured Phi (degrees)	Measured Psi (degrees)	Psi (degrees)	Friction Force, F (newtons)	Normal Force, N (newtons)	Fs Merchant (newtons)	Fn Merchant (newtons)	Fs Payton (newtons)	Fn Payton (newtons)
115	0.013	0.62	37.6	26.4	16.3	29.9	251.16	228.67	259.08	219.66	115.15	319.55
116	0.0125	0.64	39.6	28.1	20.0	27.9	251.99	230.38	253.16	229.10	116.41	320.97
117	0.0135	0.59	35.8	25.6	18.8	31.7	271.85	249.85	290.10	228.41	126.80	346.77
118	0.005	0.80	52.5	25.4	15.9	15.0	314.61	128.75	86.68	328.70	-1.45	339.94
119	0.005	0.80	52.5	23.4	25.5	15.0	321.86	119.55	76.60	334.69	-12.72	343.11
120	0.005	0.80	52.5	26.6	18.0	15.0	319.50	120.29	77.65	332.45	-11.13	341.22
121	0.02	0.40	23.0	22.1	18.8	39.5	375.27	363.90	433.79	291.69	149.50	500.90
122	0.019	0.42	24.5	24.0	19.5	38.0	351.11	333.08	391.73	284.21	133.32	465.24
123	0.019	0.42	24.5	22.5	23.1	38.0	352.58	335.48	394.35	285.21	134.77	467.65
124	0.0095	0.42	24.5	20.7	22.5	38.0	249.29	175.40	218.07	212.97	40.47	302.11
125	0.01	0.40	23.0	22.0	21.1	39.5	250.80	177.41	225.54	208.58	41.55	304.38
126	0.0095	0.42	24.5	21.6	22.2	38.0	254.48	181.66	225.18	216.93	43.63	309.61
127	0.02	0.40	23.0	20.4	15.9	39.5	364.72	345.33	413.43	285.22	137.90	482.97
128	0.019	0.42	24.5	27.7	17.7	38.0	350.04	329.53	388.03	283.80	130.66	462.64
129	0.019	0.42	24.5	25.5	19.7	38.0	354.75	339.95	399.14	286.52	137.73	471.63
130	0.009	0.44	26.0	22.3	23.8	36.5	249.67	170.69	207.48	220.04	36.12	300.27
131	0.0095	0.42	24.5	23.9	25.6	38.0	256.85	180.59	224.55	219.45	41.58	311.21
132	0.009	0.44	26.0	24.2	25.2	36.5	256.73	179.59	217.37	225.64	40.75	310.65
133	0.012	0.67	41.7	24.9	19.2	25.8	406.42	218.81	241.66	393.26	46.62	459.22
134	0.012	0.67	41.7	31.5	24.3	25.8	402.69	218.53	241.17	389.56	47.79	455.67
135	0.012	0.67	41.7	27.8	22.0	25.8	399.08	213.72	236.16	386.23	44.73	450.49
136	0.005	0.80	52.5	27.3	21.4	15.0	342.61	107.53	61.99	353.70	-31.77	357.68
137	0.005	0.80	52.5	26.4	19.1	15.0	343.67	110.80	65.09	355.17	-29.15	359.91
138	0.005	0.80	52.5	24.3	20.7	15.0	334.82	99.62	55.16	344.94	-36.09	347.46
139	0.0115	0.70	44.1	30.6	23.5	23.4	402.79	216.63	223.13	399.23	46.00	455.03
140	0.012	0.67	41.7	29.5	18.8	25.8	403.63	213.46	236.16	390.78	42.75	454.59
141	0.012	0.67	41.7	28.7	23.0	25.8	401.85	211.09	233.69	389.14	41.24	452.05
142	0.005	0.80	52.5	24.9	19.0	15.0	339.46	99.36	54.30	349.51	-38.11	351.65
143	0.005	0.80	52.5	25.8	18.7	15.0	347.73	112.41	66.16	359.41	-29.21	364.28
144	0.005	0.80	52.5	25.1	19.9	15.0	341.07	101.33	56.04	351.37	-36.91	353.89
145	0.039	0.21	11.5	15.3	28.0	46.0	598.46	808.09	925.43	393.37	359.99	938.92
146	0.041	0.20	10.9	13.9	27.3	46.6	652.73	909.09	1040.65	411.76	416.01	1038.96
147	0.041	0.20	10.9	16.3	25.6	46.6	636.50	876.37	1004.96	403.99	397.13	1007.69
148	0.021	0.19	10.6	13.8	27.6	46.9	375.94	478.37	556.69	245.48	201.46	574.09
149	0.023	0.17	9.7	9.4	27.2	47.8	484.32	617.62	723.77	303.61	260.67	740.32
150	0.023	0.17	9.7	12.6	29.1	47.8	401.26	503.16	591.41	253.80	208.76	608.77
151	0.0445	0.18	10.0	17.0	24.9	47.5	672.01	925.96	1068.34	409.46	419.88	1064.29
152	0.041	0.20	10.9	14.6	27.7	46.6	587.79	802.40	921.36	374.74	360.92	926.86

Run	Cut Chip Thickness (in)	Chip thickness ratio	Phi (degrees)	Measured Phi (degrees)	Measured Psi (degrees)	Psi (degrees)	Friction Force, F (newtons)	Normal Force, N (newtons)	Fs Merchant (newtons)	Fn Merchant (newtons)	Fs Payton (newtons)	Fn Payton (newtons)
153	0.0415	0.19	10.8	17.5	27.8	46.7	620.67	862.47	988.58	389.60	393.92	986.87
154	0.023	0.17	9.7	12.7	25.6	47.8	388.46	496.48	581.58	243.22	210.01	594.38
155	0.023	0.17	9.7	10.4	28.7	47.8	381.81	489.71	573.29	238.61	207.87	585.13
156	0.024	0.17	9.2	9.2	25.9	48.3	440.36	577.26	675.22	266.90	250.25	681.56
157	0.0185	0.43	25.2	23.1	28.2	37.3	292.67	342.80	387.52	230.21	168.93	417.89
158	0.0175	0.46	26.9	24.7	26.9	35.6	277.74	328.11	363.93	228.81	162.79	397.87
159	0.018	0.44	26.0	22.3	24.9	36.5	275.54	324.69	363.64	221.62	160.77	394.33
160	0.008	0.50	29.9	21.9	23.9	32.6	151.55	173.69	186.55	135.41	84.09	214.63
161	0.0075	0.53	32.2	19.0	28.0	30.3	141.04	151.93	158.67	133.41	69.64	195.26
162	0.008	0.50	29.9	18.4	29.0	32.6	154.43	172.14	185.26	138.41	81.38	216.47
163	0.018	0.44	26.0	24.3	23.1	36.5	274.39	327.99	366.72	219.97	164.23	394.84
164	0.018	0.44	26.0	25.9	24.3	36.5	273.96	329.51	368.15	219.30	165.78	395.15
165	0.018	0.44	26.0	24.6	27.3	36.5	257.20	313.69	349.91	205.21	159.49	372.98
166	0.0075	0.53	32.2	21.8	27.9	30.3	144.22	154.72	161.61	136.46	70.64	199.37
167	0.0075	0.53	32.2	17.9	23.0	30.3	154.25	170.26	177.62	145.71	79.80	215.44
168	0.007	0.57	34.8	18.6	26.8	27.7	134.64	146.70	147.06	134.25	67.96	187.16
169	0.011	0.73	46.6	29.2	22.7	20.9	423.96	228.89	216.71	430.31	49.23	479.28
170	0.011	0.73	46.6	30.3	20.7	20.9	424.77	215.35	203.15	430.74	36.40	474.85
171	0.011	0.73	46.6	28.0	18.8	20.9	422.88	212.93	200.79	428.78	34.89	472.17
172	0.005	0.80	52.5	26.0	15.7	15.0	362.95	106.52	58.34	373.73	-40.48	376.08
173	0.005	0.80	52.5	25.0	18.9	15.0	356.28	102.61	55.33	366.61	-41.55	368.42
174	0.005	0.80	52.5	24.4	18.0	15.0	354.53	101.65	54.60	364.75	-41.77	366.44
175	0.011	0.73	46.6	30.4	21.1	20.9	421.15	209.17	197.08	426.94	32.08	469.14
176	0.011	0.73	46.6	28.5	22.5	20.9	420.36	212.74	200.67	426.26	35.68	469.78
177	0.011	0.73	46.6	30.4	21.1	20.9	412.01	196.41	184.59	417.44	23.79	455.81
178	0.005	0.80	52.5	21.4	20.5	15.0	350.45	95.23	48.78	359.87	-46.13	360.22
179	0.005	0.80	52.5	25.8	17.7	15.0	355.54	101.72	54.54	365.76	-42.08	367.40
180	0.005	0.80	52.5	25.8	18.0	15.0	350.85	94.82	48.31	360.21	-46.66	360.42
181	0.035	0.23	12.9	16.8	27.7	44.6	562.65	756.32	857.36	391.84	335.56	880.91
182	0.035	0.23	12.9	15.9	28.4	44.6	597.10	802.73	909.95	415.80	356.19	934.89
183	0.035	0.23	12.9	15.8	27.6	44.6	610.04	816.59	926.22	425.55	360.94	953.26
184	0.023	0.17	9.7	14.9	37.7	47.8	380.04	493.98	576.94	235.76	212.43	585.94
185	0.0225	0.18	9.9	12.1	34.8	47.6	398.25	507.61	593.90	252.09	214.13	608.62
186	0.0235	0.17	9.4	13.8	28.4	48.1	528.00	692.75	809.01	322.78	300.57	817.52
187	0.035	0.23	12.9	15.9	30.8	44.6	543.62	731.55	829.15	378.42	324.89	851.55
188	0.035	0.23	12.9	17.3	35.7	44.6	561.72	763.00	863.69	389.52	341.70	883.71
189	0.035	0.23	12.9	18.6	31.7	44.6	536.61	726.64	822.88	372.59	324.52	842.99
190	0.0195	0.21	11.5	18.4	34.7	46.0	319.61	396.75	460.38	218.20	162.89	482.73

Run	Cut Chip Thickness (in)	Chip thickness ratio	Phi (degrees)	Measured Phi (degrees)	Measured Psi (degrees)	Psi (degrees)	Friction Force, F (newtons)	Normal Force, N (newtons)	Fs Merchant (newtons)	Fn Merchant (newtons)	Fs Payton (newtons)	Fn Payton (newtons)
191	0.0225	0.18	9.9	13.3	31.1	47.6	419.96	537.73	628.65	265.19	227.87	643.12
192	0.02	0.20	11.2	12.3	26.5	46.3	329.60	407.87	474.72	222.79	166.90	497.13
193	0.015	0.53	32.2	29.4	29.2	30.3	265.98	311.09	323.77	250.40	153.12	379.58
194	0.015	0.53	32.2	29.3	31.7	30.3	257.74	308.22	320.50	242.30	154.39	370.93
195	0.015	0.53	32.2	27.2	30.2	30.3	260.51	313.40	325.80	244.82	157.70	375.79
196	0.006	0.67	41.5	25.5	29.8	21.0	154.83	163.16	144.64	172.27	73.23	212.68
197	0.006	0.67	41.5	28.9	23.7	21.0	155.88	163.28	144.63	173.32	72.85	213.66
198	0.006	0.67	41.5	26.3	25.8	21.0	152.48	157.64	139.41	169.30	69.42	208.04
199	0.016	0.50	29.9	27.8	30.8	32.6	265.93	309.22	331.77	237.20	151.48	378.67
200	0.015	0.53	32.2	28.4	29.0	30.3	246.44	294.38	306.12	231.70	147.33	354.53
201	0.0155	0.52	31.0	28.0	31.3	31.5	237.10	286.12	302.01	216.50	144.31	342.43
202	0.006	0.67	41.5	27.6	26.9	21.0	150.15	153.94	136.00	166.57	67.21	204.26
203	0.006	0.67	41.5	30.7	32.3	21.0	154.50	157.89	139.43	171.34	68.71	209.95
204	0.0065	0.62	37.9	27.2	29.8	24.6	151.62	157.47	149.53	159.45	69.67	207.20
205	0.01	0.80	52.5	30.8	14.8	15.0	434.74	207.39	149.00	458.05	25.23	481.02
206	0.01	0.80	52.5	31.1	15.3	15.0	436.57	212.67	154.00	460.56	29.42	484.73
207	0.01	0.80	52.5	31.5	18.8	15.0	435.09	212.29	153.81	459.03	29.63	483.21
208	0.0045	0.89	59.4	26.2	11.9	8.1	372.29	102.39	6.47	386.06	-47.87	383.13
209	0.0045	0.89	59.4	24.9	14.8	8.1	370.86	101.75	6.21	384.52	-47.92	381.57
210	0.0045	0.89	59.4	24.4	15.5	8.1	365.94	95.53	1.41	378.20	-51.78	374.64
211	0.01	0.80	52.5	31.3	16.9	15.0	428.92	204.51	146.90	451.91	24.80	474.54
212	0.01	0.80	52.5	32.4	14.4	15.0	422.95	191.25	134.53	444.26	14.83	463.94
213	0.01	0.80	52.5	31.8	13.6	15.0	423.19	195.39	138.60	445.04	18.57	465.75
214	0.0045	0.89	59.4	27.6	14.2	8.1	358.89	88.78	-3.37	369.70	-55.32	365.55
215	0.0045	0.89	59.4	28.8	15.7	8.1	359.28	91.33	-1.00	370.71	-53.12	366.88
216	0.0045	0.89	59.4	25.0	12.9	8.1	359.78	91.50	-0.96	371.23	-53.14	367.41
217	0.02	0.40	23.0	18.8	34.1	39.5	837.81	884.90	1039.35	636.18	398.06	1151.75
218	0.02	0.40	23.0	18.1	30.5	39.5	935.74	922.82	1096.75	724.12	386.47	1256.12
219	0.019	0.42	24.5	16.1	33.8	38.0	912.02	869.93	1022.17	737.37	350.51	1210.66
220	0.006	0.67	41.5	23.7	25.7	21.0	450.37	407.20	353.74	493.47	153.23	587.51
221	0.0065	0.62	37.9	27.4	26.7	24.6	503.35	484.53	458.25	527.40	197.36	670.21
222	0.006	0.67	41.5	24.9	28.0	21.0	470.59	452.08	396.06	518.63	183.71	626.17
223	0.02	0.40	23.0	20.5	35.6	39.5	851.72	924.25	1080.73	641.63	426.54	1182.26
224	0.0215	0.37	21.2	18.7	32.6	41.3	920.91	1004.56	1195.44	654.32	465.83	1280.71
225	0.0195	0.41	23.7	17.3	33.2	38.8	815.24	831.62	974.97	636.90	361.22	1107.13
226	0.006	0.67	41.5	28.3	29.6	21.0	375.32	370.78	326.03	414.79	155.58	504.12
227	0.006	0.67	41.5	25.2	24.6	21.0	375.94	380.49	335.60	416.50	163.91	509.15

Run	Cut Chip Thickness (in)	Chip thickness ratio	Phi (degrees)	Measured Phi (degrees)	Measured Psi (degrees)	Psi (degrees)	Friction Force, F (newtons)	Normal Force, N (newtons)	Fs Merchant (newtons)	Fn Merchant (newtons)	Fs Payton (newtons)	Fn Payton (newtons)
228	0.006	0.67	41.5	25.3	21.7	21.0	386.37	388.34	342.23	427.75	166.06	522.03
229	0.016	0.50	28.7	22.5	37.5	38.8	956.20	647.79	890.45	735.56	232.56	1131.31
230	0.015	0.53	31.2	21.2	41.2	36.3	899.47	546.05	744.93	743.16	160.27	1039.96
231	0.016	0.50	28.7	23.7	37.8	38.8	953.45	618.22	861.29	741.23	206.29	1117.45
232	0.007	0.57	34.1	21.8	31.3	33.4	717.66	317.12	446.67	645.05	18.34	784.39
233	0.007	0.57	34.1	18.6	31.1	33.4	722.81	335.89	466.08	646.57	33.71	796.33
234	0.007	0.57	34.1	23.3	32.5	33.4	712.88	310.98	439.74	641.51	14.50	777.62
235	0.015	0.53	31.2	20.8	38.9	36.3	941.63	594.66	802.20	772.50	189.05	1097.52
236	0.0155	0.52	29.9	21.7	38.1	37.6	939.12	594.25	818.56	751.69	189.63	1095.04
237	0.015	0.53	31.2	20.2	36.7	36.3	935.28	594.47	800.50	766.39	191.30	1091.58
238	0.007	0.57	34.1	23.4	36.4	33.4	389.36	319.30	386.95	322.21	146.00	481.91
239	0.007	0.57	34.1	19.2	30.4	33.4	334.04	257.05	315.39	279.62	109.65	406.98
240	0.007	0.57	34.1	20.6	28.7	33.4	398.64	326.38	395.65	330.00	148.98	493.20
241	0.02	0.40	23.0	21.7	37.9	39.5	876.62	908.56	1070.55	669.24	401.13	1197.10
242	0.0195	0.41	23.7	20.0	43.1	38.8	916.96	893.01	1055.07	724.65	368.70	1225.70
243	0.019	0.42	24.5	17.0	41.4	38.0	897.33	846.18	996.14	727.27	336.23	1186.66
244	0.006	0.67	41.5	23.5	29.6	21.0	393.26	366.11	319.36	432.08	143.16	517.87
245	0.006	0.67	41.5	26.3	27.8	21.0	408.14	389.72	341.14	449.53	157.23	541.97
246	0.006	0.67	41.5	26.4	26.1	21.0	385.80	361.18	315.31	424.11	142.23	508.98
247	0.021	0.38	21.8	21.0	42.2	40.7	895.24	925.33	1105.69	659.65	407.40	1221.36
248	0.019	0.42	24.5	16.6	44.9	38.0	846.93	828.12	969.16	681.03	343.49	1133.62
249	0.02	0.40	23.0	18.5	40.6	39.5	869.44	852.02	1013.74	673.93	354.29	1164.62
250	0.006	0.67	41.5	22.3	24.9	21.0	472.52	401.94	346.02	514.89	138.34	604.73
251	0.006	0.67	41.5	23.7	29.1	21.0	474.08	425.00	368.75	519.03	158.07	616.75
252	0.006	0.67	41.5	26.2	23.8	21.0	474.08	425.00	368.75	519.03	158.07	616.75
253	0.015	0.53	31.2	21.6	34.6	36.3	1027.16	654.62	880.84	841.25	211.72	1199.48
254	0.015	0.53	31.2	21.7	37.3	36.3	950.16	558.97	769.57	789.31	152.81	1091.74
255	0.015	0.53	31.2	12.7	33.6	36.3	967.49	581.27	795.36	800.81	166.78	1116.28
256	0.0065	0.62	37.6	23.4	35.2	29.9	772.18	344.40	440.87	721.46	22.68	845.19
257	0.0065	0.62	37.6	21.3	37.9	29.9	743.52	295.44	388.63	699.34	-11.58	799.99
258	0.0065	0.62	37.6	19.3	34.3	29.9	743.97	303.11	396.29	698.80	-4.67	803.33
259	0.014	0.57	34.1	17.2	39.6	33.4	980.29	572.33	746.80	854.88	153.62	1124.69
260	0.014	0.57	34.1	21.0	39.2	33.4	945.19	533.23	701.79	827.77	130.94	1077.30
261	0.014	0.57	34.1	20.2	39.1	33.4	995.09	596.18	773.01	864.92	169.99	1147.49

Run	Cut Chip Thickness (in)	Chip thickness ratio	Phi (degrees)	Measured Phi (degrees)	Measured Psi (degrees)	Psi (degrees)	Friction Force, F (newtons)	Normal Force, N (newtons)	Fs Merchant (newtons)	Fn Merchant (newtons)	Fs Payton (newtons)	Fn Payton (newtons)
262	0.0065	0.62	37.6	22.4	37.8	29.9	785.58	332.04	430.34	736.34	6.14	852.85
263	0.006	0.67	41.7	20.6	39.9	25.8	767.18	311.98	355.27	748.12	-5.36	828.17
264	0.006	0.67	41.7	18.9	31.7	25.8	763.44	315.09	358.17	744.20	-1.05	825.90
265	0.019	0.42	24.5	21.4	41.8	38.0	839.96	844.19	983.68	671.24	360.96	1134.86
266	0.0185	0.43	25.2	21.5	43.3	37.3	835.53	785.98	916.44	689.93	311.37	1104.05
267	0.018	0.44	26.0	19.7	43.2	36.5	883.41	824.44	951.94	744.25	323.37	1164.28
268	0.0055	0.73	45.6	25.5	22.1	16.9	423.02	386.96	302.31	487.13	147.90	553.90
269	0.005	0.80	50.5	27.7	20.6	12.0	394.89	357.62	239.48	475.89	134.87	515.40
270	0.006	0.67	41.5	27.1	16.8	21.0	397.66	367.09	319.84	436.57	141.99	522.23
271	0.018	0.44	26.0	21.5	40.3	36.5	826.64	841.40	959.85	685.53	364.63	1121.75
272	0.017	0.47	27.8	19.0	43.2	34.7	827.91	803.43	900.43	721.22	330.36	1105.35
273	0.017	0.47	27.8	18.0	41.5	34.7	794.21	772.07	865.12	691.70	318.11	1060.98
274	0.005	0.80	50.5	25.2	20.2	12.0	430.99	358.79	231.00	511.00	119.25	547.96
275	0.006	0.67	41.5	25.9	21.2	21.0	488.28	435.12	377.20	534.28	160.49	634.02
276	0.0055	0.73	45.6	24.8	22.0	16.9	452.04	390.89	300.82	516.37	137.99	581.45
277	0.014	0.57	34.1	21.8	33.0	33.4	1033.90	619.32	803.05	898.67	176.52	1192.20
278	0.013	0.62	37.6	22.2	31.4	29.9	957.62	522.66	641.51	882.43	116.41	1084.74
279	0.013	0.62	37.6	24.0	31.6	29.9	953.50	525.16	643.45	878.03	120.30	1081.89
280	0.005	0.80	52.5	26.9	16.9	15.0	717.29	287.08	191.21	748.57	-9.27	772.55
281	0.005	0.80	52.5	23.5	16.7	15.0	718.33	270.93	175.06	747.50	-24.58	767.33
282	0.005	0.80	52.5	29.1	19.2	15.0	723.12	280.96	184.38	753.56	-17.15	775.60
283	0.013	0.62	37.6	24.4	39.2	29.9	971.98	537.29	657.85	894.79	124.43	1103.61
284	0.013	0.62	37.6	22.9	37.1	29.9	958.97	535.15	654.07	882.16	127.44	1090.77
285	0.013	0.62	37.6	24.7	31.3	29.9	945.90	520.69	638.04	871.06	119.07	1073.16
286	0.005	0.80	52.5	25.2	19.4	15.0	747.09	290.42	190.63	778.55	-17.59	801.36
287	0.005	0.80	52.5	27.1	21.6	15.0	766.31	292.28	189.98	797.86	-23.22	819.83
288	0.005	0.80	52.5	26.6	18.0	15.0	754.51	276.69	176.06	784.12	-33.11	802.96

Appendix 4

Calculated Values

The first table below lists calculated shear areas according to three different theories and calculated friction coefficients. The second table lists the calculated shear strains according to three theories and resultant calculated stresses as well the measured ultimate stresses from the tensile testing.

Run	Beta (degrees)	Shear Area, As Merchant (in^2)	Shear Area, As Payton (in^2)	Shear Area, As Adjusted (in^2)	Shear Stress, Ts Merchant (MPa)	Shear Stress, Ts Payton (MPa)	Shear Stress, Ts Adjusted (MPa)	Friction Co-efficient
1	49.8	0.0036	0.0036	0.0038	130.89	33.45	31.45	0.87
2	48.0	0.0034	0.0034	0.0037	122.09	35.13	32.90	0.84
3	49.5	0.0036	0.0036	0.0038	145.47	37.85	35.58	0.86
4	51.3	0.0019	0.0019	0.0020	150.32	33.94	32.15	0.90
5	51.3	0.0018	0.0018	0.0019	119.84	27.46	25.82	0.90
6	51.3	0.0019	0.0019	0.0020	169.00	38.23	36.21	0.90
7	46.9	0.0037	0.0037	0.0039	148.28	44.62	42.11	0.82
8	48.2	0.0036	0.0036	0.0038	161.42	45.52	42.80	0.84
9	47.9	0.0036	0.0036	0.0038	151.65	43.41	40.81	0.84
10	49.7	0.0022	0.0022	0.0023	158.64	39.51	37.92	0.87
11	47.0	0.0019	0.0019	0.0020	127.29	37.98	35.98	0.82
12	48.0	0.0022	0.0022	0.0023	133.53	37.05	35.55	0.84
13	58.7	0.0024	0.0024	0.0024	151.59	29.11	28.85	1.03
14	60.3	0.0023	0.0023	0.0023	140.20	22.86	22.53	1.05
15	60.1	0.0023	0.0023	0.0023	138.77	23.16	22.83	1.05
16	66.9	0.0011	0.0011	0.0011	174.74	2.92	2.85	1.17
17	66.4	0.0011	0.0011	0.0011	174.61	4.87	4.75	1.16
18	67.3	0.0010	0.0010	0.0010	181.46	1.14	1.10	1.17
19	60.4	0.0023	0.0023	0.0023	136.91	22.00	21.68	1.05
20	60.5	0.0023	0.0023	0.0023	137.23	21.93	21.61	1.06
21	60.5	0.0023	0.0023	0.0023	134.53	21.52	21.21	1.06
22	67.0	0.0011	0.0011	0.0011	178.29	2.51	2.44	1.17
23	68.0	0.0011	0.0011	0.0011	178.03	-2.20	-2.14	1.19
24	67.6	0.0010	0.0010	0.0010	174.69	-0.28	-0.27	1.18

Run	Beta (degrees)	Shear Area, As Merchant (in^2)	Shear Area, As Payton (in^2)	Shear Area, As Adjusted (in^2)	Shear Stress, Ts Merchant (MPa)	Shear Stress, Ts Payton (MPa)	Shear Stress, Ts Adjusted (MPa)	Friction Co-efficient
25	48.4	0.0034	0.0034	0.0037	170.94	48.07	45.01	0.84
26	49.0	0.0036	0.0036	0.0038	155.11	41.67	39.17	0.86
27	47.8	0.0034	0.0034	0.0037	172.40	50.08	46.89	0.83
28	49.4	0.0022	0.0022	0.0023	164.65	41.85	40.16	0.86
29	50.0	0.0024	0.0024	0.0025	152.74	36.84	35.65	0.87
30	48.4	0.0022	0.0022	0.0023	161.04	43.59	41.83	0.85
31	48.1	0.0036	0.0036	0.0038	159.52	45.34	42.62	0.84
32	48.7	0.0037	0.0037	0.0039	156.51	42.50	40.11	0.85
33	48.4	0.0036	0.0036	0.0038	160.08	44.67	42.00	0.84
34	48.6	0.0024	0.0024	0.0024	139.92	37.16	35.86	0.85
35	49.1	0.0023	0.0023	0.0024	147.83	38.28	36.84	0.86
36	48.4	0.0024	0.0024	0.0024	138.90	37.31	36.01	0.85
37	59.6	0.0022	0.0022	0.0022	148.77	27.17	26.47	1.04
38	60.9	0.0021	0.0021	0.0021	141.44	22.36	21.66	1.06
39	61.1	0.0020	0.0020	0.0021	142.41	22.40	21.56	1.07
40	65.6	0.0012	0.0012	0.0012	179.81	8.27	8.15	1.15
41	67.5	0.0011	0.0011	0.0011	166.62	-0.14	-0.14	1.18
42	66.9	0.0011	0.0011	0.0011	172.36	2.91	2.83	1.17
43	61.1	0.0020	0.0020	0.0021	136.73	21.49	20.69	1.07
44	60.5	0.0020	0.0020	0.0021	141.96	24.13	23.23	1.06
45	60.7	0.0020	0.0020	0.0021	140.77	23.33	22.45	1.06
46	68.2	0.0010	0.0010	0.0010	166.01	-3.10	-2.99	1.19
47	67.3	0.0010	0.0010	0.0010	175.23	0.83	0.80	1.18
48	67.5	0.0011	0.0011	0.0011	168.20	-0.15	-0.15	1.18
49	49.6	0.0034	0.0034	0.0037	149.19	38.86	36.39	0.87
50	49.8	0.0036	0.0036	0.0038	143.61	36.59	34.40	0.87
51	49.2	0.0034	0.0034	0.0037	148.26	39.50	36.99	0.86
52	49.5	0.0019	0.0019	0.0020	136.94	35.19	33.33	0.86
53	50.8	0.0021	0.0021	0.0022	127.61	29.60	28.23	0.89
54	52.1	0.0020	0.0020	0.0021	131.57	27.77	26.39	0.91
55	49.5	0.0033	0.0033	0.0035	130.28	34.42	32.10	0.86
56	48.5	0.0031	0.0031	0.0034	147.78	41.91	38.92	0.85
57	49.0	0.0032	0.0032	0.0034	130.96	35.73	33.25	0.86
58	49.8	0.0021	0.0021	0.0022	139.23	34.86	33.25	0.87
59	50.1	0.0021	0.0021	0.0022	136.34	33.29	31.75	0.87
60	50.0	0.0020	0.0020	0.0021	136.77	33.73	32.06	0.87
61	62.3	0.0019	0.0019	0.0019	136.06	18.54	17.64	1.09
62	62.4	0.0019	0.0019	0.0019	137.54	18.34	17.45	1.09

Run	Beta (degrees)	Shear Area, As Merchant (in^2)	Shear Area, As Payton (in^2)	Shear Area, As Adjusted (in^2)	Shear Stress, Ts Merchant (MPa)	Shear Stress, Ts Payton (MPa)	Shear Stress, Ts Adjusted (MPa)	Friction Co-efficient
63	62.7	0.0019	0.0019	0.0019	137.70	17.57	16.71	1.09
64	70.4	0.0010	0.0010	0.0010	151.50	-13.02	-12.53	1.23
65	69.4	0.0010	0.0010	0.0010	159.41	-8.83	-8.50	1.21
66	69.5	0.0010	0.0010	0.0010	159.59	-9.37	-9.02	1.21
67	62.9	0.0019	0.0019	0.0019	127.26	15.51	14.75	1.10
68	64.0	0.0019	0.0019	0.0019	117.16	11.11	10.57	1.12
69	62.5	0.0019	0.0019	0.0019	130.98	17.44	16.59	1.09
70	70.4	0.0007	0.0007	0.0008	143.92	-18.54	-17.16	1.23
71	70.0	0.0009	0.0009	0.0009	164.06	-13.83	-13.01	1.22
72	69.5	0.0009	0.0009	0.0009	168.68	-11.26	-10.59	1.21
73	40.1	0.0036	0.0036	0.0038	280.93	114.36	107.52	0.70
74	39.9	0.0034	0.0034	0.0037	268.38	110.73	103.70	0.70
75	39.8	0.0034	0.0034	0.0037	250.37	103.68	97.09	0.69
76	42.3	0.0015	0.0015	0.0016	262.63	100.69	93.07	0.74
77	41.8	0.0016	0.0016	0.0017	299.32	116.57	108.24	0.73
78	41.9	0.0015	0.0015	0.0016	296.29	115.51	106.78	0.73
79	39.6	0.0034	0.0034	0.0037	274.37	114.43	107.16	0.69
80	39.7	0.0034	0.0034	0.0036	263.53	109.70	102.52	0.69
81	39.7	0.0033	0.0033	0.0035	266.01	111.11	103.62	0.69
82	41.7	0.0016	0.0016	0.0017	272.91	106.36	98.76	0.73
83	41.8	0.0016	0.0016	0.0017	272.61	106.16	98.57	0.73
84	41.8	0.0016	0.0016	0.0017	272.32	105.96	98.39	0.73
85	56.8	0.0016	0.0016	0.0018	303.88	83.53	78.17	0.99
86	57.2	0.0016	0.0016	0.0017	287.49	79.53	74.09	1.00
87	56.9	0.0016	0.0016	0.0017	288.75	81.68	76.09	0.99
88	66.7	0.0006	0.0006	0.0006	236.69	12.32	11.48	1.16
89	68.3	0.0006	0.0006	0.0006	214.75	-12.57	-11.71	1.19
90	66.9	0.0006	0.0006	0.0006	244.09	9.83	9.16	1.17
91	57.3	0.0016	0.0016	0.0017	279.75	77.04	71.77	1.00
92	57.9	0.0015	0.0015	0.0016	270.60	73.96	68.64	1.01
93	56.5	0.0016	0.0016	0.0017	292.71	85.35	79.52	0.99
94	69.3	0.0006	0.0006	0.0006	197.86	-26.62	-24.81	1.21
95	68.4	0.0006	0.0006	0.0006	213.58	-13.96	-13.01	1.19
96	68.8	0.0006	0.0006	0.0006	205.11	-20.29	-18.90	1.20
97	41.1	0.0035	0.0035	0.0037	279.00	109.73	102.96	0.72
98	43.6	0.0034	0.0034	0.0037	236.54	84.62	79.25	0.76
99	43.3	0.0034	0.0034	0.0036	249.09	90.46	84.53	0.76
100	43.1	0.0015	0.0015	0.0016	277.29	103.35	95.53	0.75

Run	Beta (degrees)	Shear Area, As Merchant (in^2)	Shear Area, As Payton (in^2)	Shear Area, As Adjusted (in^2)	Shear Stress, Ts Merchant (MPa)	Shear Stress, Ts Payton (MPa)	Shear Stress, Ts Adjusted (MPa)	Friction Co-efficient
101	42.6	0.0016	0.0016	0.0017	303.82	114.61	106.42	0.74
102	42.8	0.0015	0.0015	0.0016	278.61	104.77	96.85	0.75
103	40.8	0.0035	0.0035	0.0037	275.06	109.52	102.77	0.71
104	40.5	0.0034	0.0034	0.0037	275.90	111.43	104.35	0.71
105	40.2	0.0034	0.0034	0.0037	253.86	103.70	97.11	0.70
106	41.4	0.0016	0.0016	0.0017	277.13	109.34	101.52	0.72
107	41.5	0.0015	0.0015	0.0016	289.85	114.93	106.24	0.72
108	42.1	0.0015	0.0015	0.0016	262.94	101.94	94.23	0.73
109	46.4	0.0018	0.0018	0.0019	284.20	123.45	116.77	0.81
110	48.5	0.0016	0.0016	0.0018	252.89	106.41	99.59	0.85
111	47.4	0.0017	0.0017	0.0018	277.01	118.47	111.45	0.83
112	54.7	0.0006	0.0006	0.0006	268.84	127.58	118.88	0.95
113	55.5	0.0006	0.0006	0.0006	247.86	113.35	105.63	0.97
114	56.9	0.0006	0.0006	0.0006	276.07	117.21	109.21	0.99
115	47.7	0.0016	0.0016	0.0017	255.28	113.46	105.71	0.83
116	47.6	0.0015	0.0015	0.0016	260.43	119.76	111.14	0.83
117	47.4	0.0016	0.0016	0.0018	273.99	119.76	112.09	0.83
118	67.7	0.0006	0.0006	0.0006	222.01	-3.70	-3.45	1.18
119	69.6	0.0006	0.0006	0.0006	196.21	-32.59	-30.37	1.22
120	69.4	0.0006	0.0006	0.0006	198.89	-28.51	-26.57	1.21
121	45.9	0.0025	0.0025	0.0027	274.07	94.46	85.64	0.80
122	46.5	0.0023	0.0023	0.0026	261.81	89.11	80.40	0.81
123	46.4	0.0023	0.0023	0.0026	263.56	90.07	81.27	0.81
124	54.9	0.0012	0.0012	0.0013	291.49	54.10	48.81	0.96
125	54.7	0.0012	0.0012	0.0014	285.00	52.51	47.61	0.96
126	54.5	0.0012	0.0012	0.0013	300.99	58.32	52.62	0.95
127	46.6	0.0025	0.0025	0.0027	261.21	87.13	79.00	0.81
128	46.7	0.0023	0.0023	0.0026	259.34	87.33	78.79	0.82
129	46.2	0.0023	0.0023	0.0026	266.76	92.05	83.05	0.81
130	55.6	0.0011	0.0011	0.0012	294.15	51.21	45.98	0.97
131	54.9	0.0012	0.0012	0.0013	300.16	55.59	50.15	0.96
132	55.0	0.0011	0.0011	0.0012	308.17	57.77	51.87	0.96
133	61.7	0.0014	0.0014	0.0016	259.70	50.10	46.37	1.08
134	61.5	0.0014	0.0014	0.0016	259.17	51.36	47.53	1.07
135	61.8	0.0014	0.0014	0.0016	253.79	48.07	44.49	1.08
136	72.6	0.0006	0.0006	0.0006	158.77	-81.37	-75.82	1.27
137	72.1	0.0006	0.0006	0.0006	166.71	-74.67	-69.58	1.26
138	73.4	0.0006	0.0006	0.0006	141.30	-92.43	-86.13	1.28

Run	Beta (degrees)	Shear Area, As Merchant (in^2)	Shear Area, As Payton (in^2)	Shear Area, As Adjusted (in^2)	Shear Stress, Ts Merchant (MPa)	Shear Stress, Ts Payton (MPa)	Shear Stress, Ts Adjusted (MPa)	Friction Co-efficient
139	61.7	0.0014	0.0014	0.0015	250.58	51.66	47.73	1.08
140	62.1	0.0014	0.0014	0.0016	253.78	45.94	42.51	1.08
141	62.3	0.0014	0.0014	0.0016	251.13	44.32	41.01	1.09
142	73.7	0.0006	0.0006	0.0006	139.09	-97.60	-90.95	1.29
143	72.1	0.0006	0.0006	0.0006	169.46	-74.83	-69.73	1.26
144	73.5	0.0006	0.0006	0.0006	143.54	-94.53	-88.08	1.28
145	36.5	0.0048	0.0048	0.0055	298.04	115.93	100.55	0.64
146	35.7	0.0051	0.0051	0.0058	317.98	127.12	110.54	0.62
147	36.0	0.0051	0.0051	0.0058	307.08	121.35	105.52	0.63
148	38.2	0.0026	0.0026	0.0030	331.70	120.04	104.51	0.67
149	38.1	0.0029	0.0029	0.0033	391.97	141.17	123.47	0.67
150	38.6	0.0029	0.0029	0.0033	320.29	113.06	98.88	0.67
151	36.0	0.0055	0.0055	0.0063	299.53	117.72	102.79	0.63
152	36.2	0.0051	0.0051	0.0058	281.53	110.28	95.90	0.63
153	35.7	0.0051	0.0051	0.0059	298.25	118.84	103.40	0.62
154	38.0	0.0029	0.0029	0.0033	314.97	113.74	99.47	0.66
155	37.9	0.0029	0.0029	0.0033	310.48	112.58	98.46	0.66
156	37.3	0.0030	0.0030	0.0034	349.72	129.62	113.59	0.65
157	40.5	0.0023	0.0023	0.0025	266.64	116.23	104.62	0.71
158	40.2	0.0021	0.0021	0.0024	265.95	118.96	106.58	0.70
159	40.3	0.0022	0.0022	0.0024	257.76	113.96	102.33	0.70
160	41.1	0.0010	0.0010	0.0011	300.00	135.22	120.42	0.72
161	42.9	0.0009	0.0009	0.0010	272.94	119.80	106.39	0.75
162	41.9	0.0010	0.0010	0.0011	297.93	130.87	116.55	0.73
163	39.9	0.0022	0.0022	0.0024	259.95	116.42	104.54	0.70
164	39.7	0.0022	0.0022	0.0024	260.96	117.51	105.52	0.69
165	39.3	0.0022	0.0022	0.0024	248.03	113.05	101.51	0.69
166	43.0	0.0009	0.0009	0.0010	277.99	121.51	107.91	0.75
167	42.2	0.0009	0.0009	0.0010	305.54	137.26	121.90	0.74
168	42.5	0.0008	0.0008	0.0009	271.35	125.40	111.23	0.74
169	61.6	0.0013	0.0013	0.0014	254.37	57.78	53.40	1.08
170	63.1	0.0013	0.0013	0.0014	238.45	42.73	39.49	1.10
171	63.3	0.0013	0.0013	0.0014	235.68	40.96	37.86	1.10
172	73.6	0.0006	0.0006	0.0006	149.42	-103.69	-96.62	1.29
173	73.9	0.0006	0.0006	0.0006	141.71	-106.41	-99.16	1.29
174	74.0	0.0006	0.0006	0.0006	139.85	-106.97	-99.68	1.29
175	63.6	0.0013	0.0013	0.0014	231.32	37.65	34.80	1.11
176	63.2	0.0013	0.0013	0.0014	235.54	41.88	38.71	1.10

Run	Beta (degrees)	Shear Area, As Merchant (in^2)	Shear Area, As Payton (in^2)	Shear Area, As Adjusted (in^2)	Shear Stress, Ts Merchant (MPa)	Shear Stress, Ts Payton (MPa)	Shear Stress, Ts Adjusted (MPa)	Friction Co-efficient
177	64.5	0.0013	0.0013	0.0014	216.66	27.92	25.81	1.13
178	74.8	0.0006	0.0006	0.0006	124.93	-118.15	-110.09	1.31
179	74.0	0.0006	0.0006	0.0006	139.71	-107.78	-100.43	1.29
180	74.9	0.0006	0.0006	0.0006	123.74	-119.52	-111.37	1.31
181	36.6	0.0043	0.0043	0.0050	309.39	121.09	104.44	0.64
182	36.6	0.0043	0.0043	0.0050	328.37	128.54	110.87	0.64
183	36.8	0.0043	0.0043	0.0050	334.24	130.25	112.34	0.64
184	37.6	0.0029	0.0029	0.0033	312.46	115.05	100.61	0.66
185	38.1	0.0028	0.0028	0.0032	329.15	118.67	103.68	0.67
186	37.3	0.0029	0.0029	0.0033	428.37	159.15	139.33	0.65
187	36.6	0.0043	0.0043	0.0050	299.21	117.24	101.12	0.64
188	36.4	0.0043	0.0043	0.0050	311.68	123.31	106.35	0.63
189	36.4	0.0043	0.0043	0.0050	296.95	117.11	101.01	0.64
190	38.9	0.0024	0.0024	0.0028	296.53	104.92	91.00	0.68
191	38.0	0.0028	0.0028	0.0032	348.40	126.29	110.33	0.66
192	38.9	0.0025	0.0025	0.0028	297.74	104.68	90.91	0.68
193	40.5	0.0018	0.0018	0.0020	278.46	131.70	116.96	0.71
194	39.9	0.0018	0.0018	0.0020	275.65	132.78	117.92	0.70
195	39.7	0.0018	0.0018	0.0020	280.22	135.63	120.45	0.69
196	43.5	0.0007	0.0007	0.0008	309.38	156.65	139.84	0.76
197	43.7	0.0007	0.0007	0.0008	309.36	155.82	139.10	0.76
198	44.0	0.0007	0.0007	0.0008	298.20	148.49	132.56	0.77
199	40.7	0.0019	0.0019	0.0022	266.76	121.80	108.47	0.71
200	39.9	0.0018	0.0018	0.0020	263.29	126.71	112.53	0.70
201	39.6	0.0019	0.0019	0.0021	251.06	119.97	106.67	0.69
202	44.3	0.0007	0.0007	0.0008	290.90	143.77	128.35	0.77
203	44.4	0.0007	0.0007	0.0008	298.24	146.96	131.20	0.77
204	43.9	0.0008	0.0008	0.0009	296.77	138.26	122.80	0.77
205	64.5	0.0012	0.0012	0.0013	190.82	32.32	30.11	1.13
206	64.0	0.0012	0.0012	0.0013	197.22	37.67	35.10	1.12
207	64.0	0.0012	0.0012	0.0013	196.98	37.94	35.35	1.12
208	74.6	0.0006	0.0006	0.0006	18.00	-133.08	-126.95	1.30
209	74.7	0.0006	0.0006	0.0006	17.25	-133.22	-127.08	1.30
210	75.4	0.0006	0.0006	0.0006	3.91	-143.96	-137.33	1.32
211	64.5	0.0012	0.0012	0.0013	188.13	31.76	29.60	1.13
212	65.7	0.0012	0.0012	0.0013	172.28	19.00	17.70	1.15
213	65.2	0.0012	0.0012	0.0013	177.51	23.78	22.16	1.14
214	76.1	0.0006	0.0006	0.0006	-9.37	-153.78	-146.69	1.33

Run	Beta (degrees)	Shear Area, As Merchant (in^2)	Shear Area, As Payton (in^2)	Shear Area, As Adjusted (in^2)	Shear Stress, Ts Merchant (MPa)	Shear Stress, Ts Payton (MPa)	Shear Stress, Ts Adjusted (MPa)	Friction Co-efficient
215	75.7	0.0006	0.0006	0.0006	-2.79	-147.66	-140.85	1.32
216	75.7	0.0006	0.0006	0.0006	-2.66	-147.74	-140.93	1.32
217	43.4	0.0025	0.0025	0.0027	656.67	251.50	228.03	0.76
218	45.4	0.0025	0.0025	0.0027	692.93	244.18	221.40	0.79
219	46.4	0.0023	0.0023	0.0026	683.16	234.26	211.36	0.81
220	47.9	0.0007	0.0007	0.0008	756.66	327.77	292.60	0.84
221	46.1	0.0008	0.0008	0.0009	909.43	391.69	347.88	0.80
222	46.1	0.0007	0.0007	0.0008	847.17	392.96	350.80	0.81
223	42.7	0.0025	0.0025	0.0027	682.81	269.49	244.35	0.74
224	42.5	0.0027	0.0027	0.0029	697.40	271.76	248.24	0.74
225	44.4	0.0024	0.0024	0.0026	633.35	234.65	212.24	0.78
226	45.3	0.0007	0.0007	0.0008	697.38	332.79	297.09	0.79
227	44.7	0.0007	0.0007	0.0008	717.86	350.60	312.98	0.78
228	44.9	0.0007	0.0007	0.0008	732.03	355.20	317.09	0.78
229	55.9	0.0020	0.0020	0.0021	689.87	180.18	173.45	0.98
230	58.7	0.0019	0.0019	0.0019	622.93	134.02	127.50	1.03
231	57.0	0.0020	0.0020	0.0021	667.28	159.82	153.86	1.00
232	66.2	0.0009	0.0009	0.0009	809.45	33.24	31.27	1.15
233	65.1	0.0009	0.0009	0.0009	844.62	61.09	57.47	1.14
234	66.4	0.0009	0.0009	0.0009	796.89	26.27	24.72	1.16
235	57.7	0.0019	0.0019	0.0019	670.83	158.09	150.40	1.01
236	57.7	0.0019	0.0019	0.0020	658.54	152.56	145.99	1.01
237	57.6	0.0019	0.0019	0.0019	669.40	159.97	152.19	1.00
238	50.6	0.0009	0.0009	0.0009	701.23	264.57	248.89	0.88
239	52.4	0.0009	0.0009	0.0009	571.55	198.71	186.94	0.91
240	50.7	0.0009	0.0009	0.0009	716.99	269.98	253.98	0.88
241	44.0	0.0025	0.0025	0.0027	676.38	253.44	229.79	0.77
242	45.8	0.0024	0.0024	0.0026	685.38	239.51	216.63	0.80
243	46.7	0.0023	0.0023	0.0026	665.76	224.71	202.75	0.81
244	47.0	0.0007	0.0007	0.0008	683.12	306.21	273.36	0.82
245	46.3	0.0007	0.0007	0.0008	729.71	336.31	300.23	0.81
246	46.9	0.0007	0.0007	0.0008	674.45	304.24	271.60	0.82
247	44.1	0.0026	0.0026	0.0028	662.03	243.93	222.27	0.77
248	45.6	0.0023	0.0023	0.0026	647.73	229.57	207.13	0.80
249	45.6	0.0025	0.0025	0.0027	640.49	223.84	202.96	0.80
250	49.6	0.0007	0.0007	0.0008	740.14	295.91	264.17	0.87
251	48.1	0.0007	0.0007	0.0008	788.76	338.12	301.85	0.84
252	48.1	0.0007	0.0007	0.0008	788.76	338.12	301.85	0.84

Run	Beta (degrees)	Shear Area, As Merchant (in^2)	Shear Area, As Payton (in^2)	Shear Area, As Adjusted (in^2)	Shear Stress, Ts Merchant (MPa)	Shear Stress, Ts Payton (MPa)	Shear Stress, Ts Adjusted (MPa)	Friction Co-efficient
253	57.5	0.0019	0.0019	0.0019	736.59	177.04	168.43	1.00
254	59.5	0.0019	0.0019	0.0019	643.54	127.78	121.57	1.04
255	59.0	0.0019	0.0019	0.0019	665.11	139.47	132.69	1.03
256	66.0	0.0008	0.0008	0.0008	868.81	44.70	41.65	1.15
257	68.3	0.0008	0.0008	0.0008	765.87	-22.82	-21.26	1.19
258	67.8	0.0008	0.0008	0.0008	780.96	-9.21	-8.58	1.18
259	59.7	0.0017	0.0017	0.0018	676.67	139.19	130.94	1.04
260	60.6	0.0017	0.0017	0.0018	635.89	118.64	111.61	1.06
261	59.1	0.0017	0.0017	0.0018	700.42	154.03	144.90	1.03
262	67.1	0.0008	0.0008	0.0008	848.06	12.10	11.27	1.17
263	67.9	0.0007	0.0007	0.0008	763.57	-11.52	-10.66	1.18
264	67.6	0.0007	0.0007	0.0008	769.80	-2.26	-2.09	1.18
265	44.9	0.0023	0.0023	0.0026	657.43	241.24	217.66	0.78
266	46.8	0.0023	0.0023	0.0025	630.57	214.24	192.83	0.82
267	47.0	0.0022	0.0022	0.0024	674.78	229.22	205.83	0.82
268	47.5	0.0007	0.0007	0.0007	697.80	341.40	308.11	0.83
269	47.8	0.0006	0.0006	0.0007	596.31	335.82	309.05	0.83
270	47.3	0.0007	0.0007	0.0008	684.14	303.72	271.14	0.83
271	44.5	0.0022	0.0022	0.0024	680.38	258.46	232.09	0.78
272	45.9	0.0021	0.0021	0.0023	678.81	249.05	222.65	0.80
273	45.8	0.0021	0.0021	0.0023	652.19	239.82	214.39	0.80
274	50.2	0.0006	0.0006	0.0007	575.19	296.92	273.25	0.88
275	48.3	0.0007	0.0007	0.0008	806.83	343.29	306.47	0.84
276	49.1	0.0007	0.0007	0.0007	694.36	318.52	287.46	0.86
277	59.1	0.0017	0.0017	0.0018	727.64	159.95	150.47	1.03
278	61.4	0.0016	0.0016	0.0017	632.10	114.71	106.86	1.07
279	61.2	0.0016	0.0016	0.0017	634.02	118.53	110.43	1.07
280	68.2	0.0006	0.0006	0.0006	489.75	-23.73	-22.11	1.19
281	69.3	0.0006	0.0006	0.0006	448.39	-62.97	-58.68	1.21
282	68.8	0.0006	0.0006	0.0006	472.26	-43.93	-40.94	1.20
283	61.1	0.0016	0.0016	0.0017	648.21	122.60	114.22	1.07
284	60.8	0.0016	0.0016	0.0017	644.48	125.57	116.98	1.06
285	61.2	0.0016	0.0016	0.0017	628.69	117.33	109.30	1.07
286	68.8	0.0006	0.0006	0.0006	488.27	-45.06	-41.98	1.20
287	69.1	0.0006	0.0006	0.0006	486.60	-59.48	-55.42	1.21
288	69.9	0.0006	0.0006	0.0006	450.94	-84.81	-79.03	1.22

Run	Shear Strain ϒ Merchant	Shear Strain ϒ Payton	Shear Strain ϒ Adjusted	Resultant Force (newtons)	Resultant Shear Stress Merchant (MPa)	Resultant Shear Stress Payton (MPa)	Resultant Shear Stress Adjusted (MPa)	Measured Ultimate Stress (MPa)
1	3.22	1.04	0.37	348.71	151.76	151.76	142.69	118.59
2	3.08	1.04	0.39	308.83	139.94	139.94	131.05	118.59
3	3.22	1.04	0.37	386.49	168.21	168.21	158.14	118.59
4	3.50	1.04	0.34	216.97	174.96	174.96	165.73	118.59
5	3.22	1.04	0.37	162.20	141.19	141.19	132.74	118.59
6	3.50	1.04	0.34	243.86	196.64	196.64	186.27	118.59
7	3.36	1.04	0.35	397.45	166.38	166.38	157.02	118.59
8	3.22	1.04	0.37	423.38	184.26	184.26	173.24	118.59
9	3.22	1.04	0.37	396.79	172.69	172.69	162.36	118.59
10	4.08	1.04	0.28	254.15	178.48	178.48	171.28	118.59
11	3.50	1.04	0.34	176.34	142.20	142.20	134.69	118.59
12	4.08	1.04	0.28	210.78	148.03	148.03	142.06	118.59
13	1.88	0.83	0.58	293.61	191.09	191.09	189.40	118.59
14	1.81	0.83	0.61	271.84	182.86	182.86	180.22	118.59
15	1.81	0.83	0.61	268.31	180.49	180.49	177.88	118.59
16	1.67	0.83	0.68	182.52	263.03	263.03	256.25	118.59
17	1.67	0.83	0.68	180.84	260.61	260.61	253.89	118.59
18	1.54	0.83	0.77	185.88	288.01	288.01	277.27	118.59
19	1.81	0.83	0.61	265.91	178.88	178.88	176.29	118.59
20	1.81	0.83	0.61	266.71	179.41	179.41	176.82	118.59
21	1.81	0.83	0.61	261.42	175.85	175.85	173.31	118.59
22	1.67	0.83	0.68	186.60	268.91	268.91	261.97	118.59
23	1.67	0.83	0.68	190.08	273.94	273.94	266.87	118.59
24	1.54	0.83	0.77	180.05	278.98	278.98	268.58	118.59
25	3.08	1.04	0.39	434.08	196.70	196.70	184.20	122.73
26	3.22	1.04	0.37	410.03	178.46	178.46	167.78	122.73
27	3.08	1.04	0.39	435.41	197.30	197.30	184.76	122.73
28	4.08	1.04	0.28	263.05	184.73	184.73	177.28	122.73
29	4.51	1.04	0.25	266.60	170.61	170.61	165.11	122.73
30	4.08	1.04	0.28	255.09	179.14	179.14	171.92	122.73
31	3.22	1.04	0.37	417.87	181.86	181.86	170.99	122.73
32	3.36	1.04	0.35	426.47	178.53	178.53	168.49	122.73
33	3.22	1.04	0.37	420.59	183.05	183.05	172.10	122.73
34	4.36	1.04	0.26	234.87	154.90	154.90	149.50	122.73
35	4.22	1.04	0.27	242.27	164.80	164.80	158.62	122.73
36	4.36	1.04	0.26	232.81	153.53	153.53	148.18	122.73
37	1.67	0.83	0.68	273.97	197.41	197.41	192.32	122.73
38	1.60	0.83	0.72	260.94	194.87	194.87	188.72	122.73

Run	Shear Strain ϒ Merchant	Shear Strain ϒ Payton	Shear Strain ϒ Adjusted	Resultant Force (newtons)	Resultant Shear Stress Merchant (MPa)	Resultant Shear Stress Payton (MPa)	Resultant Shear Stress Adjusted (MPa)	Measured Ultimate Stress (MPa)
39	1.54	0.83	0.77	258.88	200.57	200.57	193.09	122.73
40	1.81	0.83	0.61	189.90	255.49	255.49	251.80	122.73
41	1.67	0.83	0.68	176.37	254.17	254.17	247.61	122.73
42	1.67	0.83	0.68	180.01	259.42	259.42	252.73	122.73
43	1.54	0.83	0.77	248.57	192.58	192.58	185.40	122.73
44	1.54	0.83	0.77	255.46	197.92	197.92	190.53	122.73
45	1.54	0.83	0.77	254.20	196.94	196.94	189.59	122.73
46	1.54	0.83	0.77	173.39	268.66	268.66	258.64	122.73
47	1.54	0.83	0.77	179.72	278.48	278.48	268.09	122.73
48	1.67	0.83	0.68	178.05	256.59	256.59	249.96	122.73
49	3.08	1.04	0.39	383.61	173.83	173.83	162.78	135.14
50	3.22	1.04	0.37	382.78	166.59	166.59	156.63	135.14
51	3.08	1.04	0.39	379.86	172.13	172.13	161.19	135.14
52	3.50	1.04	0.34	194.11	156.53	156.53	148.27	135.14
53	3.79	1.04	0.31	194.83	146.28	146.28	139.51	135.14
54	3.65	1.04	0.32	197.40	153.51	153.51	145.92	135.14
55	2.94	1.04	0.41	323.35	152.79	152.79	142.49	135.14
56	2.81	1.04	0.43	350.32	172.90	172.90	160.55	135.14
57	2.87	1.04	0.42	317.91	153.50	153.50	142.84	135.14
58	3.79	1.04	0.31	210.40	157.97	157.97	150.66	135.14
59	3.79	1.04	0.31	206.75	155.24	155.24	148.05	135.14
60	3.65	1.04	0.32	201.04	156.34	156.34	148.61	135.14
61	1.41	0.83	0.87	245.62	205.39	205.39	195.40	135.14
62	1.41	0.83	0.87	248.90	208.13	208.13	198.01	135.14
63	1.41	0.83	0.87	250.39	209.38	209.38	199.20	135.14
64	1.54	0.83	0.77	166.60	258.15	258.15	248.52	135.14
65	1.54	0.83	0.77	171.27	265.39	265.39	255.49	135.14
66	1.54	0.83	0.77	171.90	266.36	266.36	256.43	135.14
67	1.41	0.83	0.87	232.51	194.43	194.43	184.98	135.14
68	1.41	0.83	0.87	218.94	183.08	183.08	174.18	135.14
69	1.41	0.83	0.87	237.06	198.23	198.23	188.59	135.14
70	1.06	0.83	1.53	172.09	369.86	369.86	342.27	135.14
71	1.28	0.83	1.02	176.39	319.65	319.65	300.71	135.14
72	1.28	0.83	1.02	178.81	324.04	324.04	304.83	135.14
73	3.22	1.04	0.37	690.34	300.45	300.45	282.48	248.21
74	3.08	1.04	0.39	635.15	287.81	287.81	269.52	248.21
75	3.08	1.04	0.39	592.10	268.31	268.31	251.25	248.21
76	2.67	1.04	0.46	282.89	292.19	292.19	270.09	248.21

Run	Shear Strain ϒ Merchant	Shear Strain ϒ Payton	Shear Strain ϒ Adjusted	Resultant Force (newtons)	Resultant Shear Stress Merchant (MPa)	Resultant Shear Stress Payton (MPa)	Resultant Shear Stress Adjusted (MPa)	Measured Ultimate Stress (MPa)
77	2.81	1.04	0.43	333.37	329.08	329.08	305.56	248.21
78	2.67	1.04	0.46	317.99	328.45	328.45	303.61	248.21
79	3.08	1.04	0.39	647.97	293.62	293.62	274.96	248.21
80	3.01	1.04	0.40	611.52	282.91	282.91	264.39	248.21
81	2.94	1.04	0.41	605.79	286.25	286.25	266.95	248.21
82	2.81	1.04	0.43	303.91	300.00	300.00	278.56	248.21
83	2.81	1.04	0.43	303.63	299.72	299.72	278.30	248.21
84	2.81	1.04	0.43	303.35	299.45	299.45	278.05	248.21
85	1.22	0.83	1.11	477.38	450.88	450.88	421.99	248.21
86	1.17	0.83	1.22	452.31	445.68	445.68	415.20	248.21
87	1.17	0.83	1.22	451.49	444.87	444.87	414.45	248.21
88	0.90	0.83	3.06	338.77	867.71	867.71	808.55	248.21
89	0.90	0.83	3.06	341.94	875.81	875.81	816.10	248.21
90	0.90	0.83	3.06	353.53	905.51	905.51	843.77	248.21
91	1.17	0.83	1.22	440.68	434.22	434.22	404.53	248.21
92	1.11	0.83	1.36	432.10	444.51	444.51	412.52	248.21
93	1.17	0.83	1.22	453.74	447.09	447.09	416.52	248.21
94	0.90	0.83	3.06	337.07	863.34	863.34	804.47	248.21
95	0.90	0.83	3.06	342.21	876.51	876.51	816.75	248.21
96	0.90	0.83	3.06	338.70	867.52	867.52	808.37	248.21
97	3.15	1.04	0.38	678.16	301.11	301.11	282.54	279.93
98	3.08	1.04	0.39	575.30	260.69	260.69	244.13	279.93
99	3.01	1.04	0.40	593.70	274.67	274.67	256.69	279.93
100	2.67	1.04	0.46	300.52	310.40	310.40	286.93	279.93
101	2.81	1.04	0.43	340.63	336.25	336.25	312.22	279.93
102	2.67	1.04	0.46	301.36	311.27	311.27	287.73	279.93
103	3.15	1.04	0.38	667.02	296.16	296.16	277.90	279.93
104	3.08	1.04	0.39	655.63	297.09	297.09	278.21	279.93
105	3.08	1.04	0.39	601.92	272.75	272.75	255.42	279.93
106	2.81	1.04	0.43	307.82	303.86	303.86	282.15	279.93
107	2.67	1.04	0.46	309.92	320.11	320.11	295.90	279.93
108	2.67	1.04	0.46	282.54	291.83	291.83	269.76	279.93
109	1.34	0.83	0.94	394.01	342.80	342.80	324.27	279.93
110	1.22	0.83	1.11	345.99	326.79	326.79	305.85	279.93
111	1.28	0.83	1.02	380.51	344.77	344.77	324.34	279.93
112	0.90	0.83	3.06	225.01	576.33	576.33	537.03	279.93
113	0.90	0.83	3.06	213.17	546.00	546.00	508.78	279.93
114	0.90	0.83	3.06	249.65	639.44	639.44	595.84	279.93

Run	Shear Strain ϒ Merchant	Shear Strain ϒ Payton	Shear Strain ϒ Adjusted	Resultant Force (newtons)	Resultant Shear Stress Merchant (MPa)	Resultant Shear Stress Payton (MPa)	Resultant Shear Stress Adjusted (MPa)	Measured Ultimate Stress (MPa)
115	1.17	0.83	1.22	339.67	334.69	334.69	311.80	279.93
116	1.11	0.83	1.36	341.43	351.24	351.24	325.96	279.93
117	1.22	0.83	1.11	369.23	348.73	348.73	326.38	279.93
118	0.90	0.83	3.06	339.94	870.70	870.70	811.33	279.93
119	0.90	0.83	3.06	343.34	879.42	879.42	819.46	279.93
120	0.90	0.83	3.06	341.40	874.44	874.44	814.81	279.93
121	2.14	1.04	0.62	522.73	330.27	330.27	299.45	321.30
122	2.01	1.04	0.67	483.97	323.45	323.45	291.84	321.30
123	2.01	1.04	0.67	486.68	325.27	325.27	293.47	321.30
124	2.01	1.04	0.67	304.81	407.44	407.44	367.61	321.30
125	2.14	1.04	0.62	307.20	388.19	388.19	351.97	321.30
126	2.01	1.04	0.67	312.67	417.94	417.94	377.09	321.30
127	2.14	1.04	0.62	502.27	317.34	317.34	287.73	321.30
128	2.01	1.04	0.67	480.74	321.30	321.30	289.89	321.30
129	2.01	1.04	0.67	491.33	328.38	328.38	296.28	321.30
130	1.89	1.04	0.74	302.44	428.76	428.76	385.01	321.30
131	2.01	1.04	0.67	313.98	419.69	419.69	378.67	321.30
132	1.89	1.04	0.74	313.31	444.17	444.17	398.85	321.30
133	1.06	0.83	1.53	461.58	496.03	496.03	459.02	321.30
134	1.06	0.83	1.53	458.17	492.36	492.36	455.63	321.30
135	1.06	0.83	1.53	452.71	486.50	486.50	450.20	321.30
136	0.90	0.83	3.06	359.09	919.75	919.75	857.04	321.30
137	0.90	0.83	3.06	361.09	924.86	924.86	861.80	321.30
138	0.90	0.83	3.06	349.32	894.74	894.74	833.73	321.30
139	1.02	0.83	1.75	457.35	513.62	513.62	474.59	321.30
140	1.06	0.83	1.53	456.60	490.67	490.67	454.07	321.30
141	1.06	0.83	1.53	453.92	487.80	487.80	451.41	321.30
142	0.90	0.83	3.06	353.71	905.96	905.96	844.19	321.30
143	0.90	0.83	3.06	365.45	936.03	936.03	872.21	321.30
144	0.90	0.83	3.06	355.81	911.34	911.34	849.20	321.30
145	4.67	1.27	0.28	1005.57	323.85	323.85	280.88	341.29
146	4.94	1.27	0.26	1119.15	341.97	341.97	297.36	341.29
147	4.94	1.27	0.26	1083.12	330.96	330.96	287.79	341.29
148	5.07	1.27	0.25	608.41	362.52	362.52	315.62	341.29
149	5.60	1.27	0.23	784.87	425.06	425.06	371.75	341.29
150	5.60	1.27	0.23	643.57	348.54	348.54	304.82	341.29
151	5.40	1.27	0.24	1144.12	320.78	320.78	280.09	341.29
152	4.94	1.27	0.26	994.66	303.93	303.93	264.28	341.29

Run	Shear Strain ϒ Merchant	Shear Strain ϒ Payton	Shear Strain ϒ Adjusted	Resultant Force (newtons)	Resultant Shear Stress Merchant (MPa)	Resultant Shear Stress Payton (MPa)	Resultant Shear Stress Adjusted (MPa)	Measured Ultimate Stress (MPa)
153	5.00	1.27	0.26	1062.58	320.58	320.58	278.93	341.29
154	5.60	1.27	0.23	630.39	341.40	341.40	298.58	341.29
155	5.60	1.27	0.23	620.96	336.30	336.30	294.11	341.29
156	5.87	1.27	0.21	726.05	376.05	376.05	329.56	341.29
157	1.95	1.04	0.70	450.74	310.14	310.14	279.15	341.29
158	1.83	1.04	0.78	429.88	314.14	314.14	281.45	341.29
159	1.89	1.04	0.74	425.85	301.86	301.86	271.06	341.29
160	1.65	1.04	0.92	230.51	370.69	370.69	330.13	341.29
161	1.54	1.04	1.06	207.30	356.59	356.59	316.68	341.29
162	1.65	1.04	0.92	231.26	371.89	371.89	331.20	341.29
163	1.89	1.04	0.74	427.63	303.12	303.12	272.20	341.29
164	1.89	1.04	0.74	428.52	303.75	303.75	272.76	341.29
165	1.89	1.04	0.74	405.65	287.54	287.54	258.20	341.29
166	1.54	1.04	1.06	211.51	363.83	363.83	323.11	341.29
167	1.54	1.04	1.06	229.74	395.19	395.19	350.96	341.29
168	1.43	1.04	1.23	199.12	367.42	367.42	325.91	341.29
169	0.97	0.83	2.04	481.80	565.52	565.52	522.68	341.29
170	0.97	0.83	2.04	476.24	558.99	558.99	516.65	341.29
171	0.97	0.83	2.04	473.46	555.73	555.73	513.64	341.29
172	0.90	0.83	3.06	378.26	968.84	968.84	902.78	341.29
173	0.90	0.83	3.06	370.76	949.64	949.64	884.89	341.29
174	0.90	0.83	3.06	368.82	944.66	944.66	880.25	341.29
175	0.97	0.83	2.04	470.23	551.94	551.94	510.14	341.29
176	0.97	0.83	2.04	471.13	553.00	553.00	511.11	341.29
177	0.97	0.83	2.04	456.43	535.75	535.75	495.17	341.29
178	0.90	0.83	3.06	363.16	930.17	930.17	866.75	341.29
179	0.90	0.83	3.06	369.80	947.18	947.18	882.60	341.29
180	0.90	0.83	3.06	363.43	930.87	930.87	867.40	341.29
181	4.15	1.27	0.32	942.65	340.18	340.18	293.40	343.36
182	4.15	1.27	0.32	1000.45	361.03	361.03	311.39	343.36
183	4.15	1.27	0.32	1019.30	367.83	367.83	317.26	343.36
184	5.60	1.27	0.23	623.25	337.54	337.54	295.20	343.36
185	5.47	1.27	0.23	645.19	357.57	357.57	312.38	343.36
186	5.74	1.27	0.22	871.03	461.20	461.20	403.78	343.36
187	4.15	1.27	0.32	911.42	328.90	328.90	283.68	343.36
188	4.15	1.27	0.32	947.47	341.91	341.91	294.90	343.36
189	4.15	1.27	0.32	903.30	325.97	325.97	281.15	343.36
190	4.67	1.27	0.28	509.47	328.15	328.15	284.62	343.36

Run	Shear Strain ϒ Merchant	Shear Strain ϒ Payton	Shear Strain ϒ Adjusted	Resultant Force (newtons)	Resultant Shear Stress Merchant (MPa)	Resultant Shear Stress Payton (MPa)	Resultant Shear Stress Adjusted (MPa)	Measured Ultimate Stress (MPa)
191	5.47	1.27	0.23	682.29	378.13	378.13	330.35	343.36
192	4.80	1.27	0.27	524.39	328.90	328.90	285.63	343.36
193	1.54	1.04	1.06	409.30	352.03	352.03	312.63	343.36
194	1.54	1.04	1.06	401.78	345.56	345.56	306.89	343.36
195	1.54	1.04	1.06	407.53	350.51	350.51	311.28	343.36
196	1.24	1.04	1.85	224.93	481.14	481.14	429.52	343.36
197	1.24	1.04	1.85	225.74	482.86	482.86	431.06	343.36
198	1.24	1.04	1.85	219.31	469.11	469.11	418.79	343.36
199	1.65	1.04	0.92	407.84	327.93	327.93	292.05	343.36
200	1.54	1.04	1.06	383.92	330.20	330.20	293.24	343.36
201	1.59	1.04	0.99	371.59	308.90	308.90	274.67	343.36
202	1.24	1.04	1.85	215.04	459.97	459.97	410.62	343.36
203	1.24	1.04	1.85	220.90	472.52	472.52	421.83	343.36
204	1.33	1.04	1.48	218.60	433.83	433.83	385.31	343.36
205	0.90	0.83	3.06	481.68	616.87	616.87	574.81	343.36
206	0.90	0.83	3.06	485.62	621.92	621.92	579.51	343.36
207	0.90	0.83	3.06	484.12	619.99	619.99	577.72	343.36
208	0.85	0.83	6.12	386.11	1073.38	1073.38	1023.92	343.36
209	0.85	0.83	6.12	384.57	1069.09	1069.09	1019.83	343.36
210	0.85	0.83	6.12	378.20	1051.39	1051.39	1002.94	343.36
211	0.90	0.83	3.06	475.18	608.55	608.55	567.06	343.36
212	0.90	0.83	3.06	464.18	594.46	594.46	553.92	343.36
213	0.90	0.83	3.06	466.12	596.94	596.94	556.24	343.36
214	0.85	0.83	6.12	369.71	1027.80	1027.80	980.44	343.36
215	0.85	0.83	6.12	370.71	1030.56	1030.56	983.07	343.36
216	0.85	0.83	6.12	371.23	1032.02	1032.02	984.47	343.36
217	2.14	1.04	0.62	1218.59	769.92	769.92	698.09	519.18
218	2.14	1.04	0.62	1314.23	830.34	830.34	752.87	519.18
219	2.01	1.04	0.67	1260.38	842.36	842.36	760.03	519.18
220	1.24	1.04	1.85	607.16	1298.73	1298.73	1159.40	519.18
221	1.33	1.04	1.48	698.67	1386.58	1386.58	1231.51	519.18
222	1.24	1.04	1.85	652.56	1395.84	1395.84	1246.09	519.18
223	2.14	1.04	0.62	1256.85	794.08	794.08	720.00	519.18
224	2.33	1.04	0.55	1362.79	795.04	795.04	726.23	519.18
225	2.08	1.04	0.64	1164.56	756.51	756.51	684.24	519.18
226	1.24	1.04	1.85	527.58	1128.51	1128.51	1007.44	519.18
227	1.24	1.04	1.85	534.88	1144.12	1144.12	1021.38	519.18
228	1.24	1.04	1.85	547.80	1171.76	1171.76	1046.05	519.18

Run	Shear Strain ϒ Merchant	Shear Strain ϒ Payton	Shear Strain ϒ Adjusted	Resultant Force (newtons)	Resultant Shear Stress Merchant (MPa)	Resultant Shear Stress Payton (MPa)	Resultant Shear Stress Adjusted (MPa)	Measured Ultimate Stress (MPa)
229	1.54	0.83	0.77	1154.97	894.81	894.81	861.43	519.18
230	1.41	0.83	0.87	1052.24	879.92	879.92	837.12	519.18
231	1.54	0.83	0.77	1136.33	880.37	880.37	847.52	519.18
232	1.28	0.83	1.02	784.60	1421.84	1421.84	1337.58	519.18
233	1.28	0.83	1.02	797.04	1444.39	1444.39	1358.78	519.18
234	1.28	0.83	1.02	777.76	1409.44	1409.44	1325.91	519.18
235	1.41	0.83	0.87	1113.68	931.30	931.30	886.01	519.18
236	1.47	0.83	0.82	1111.34	894.08	894.08	855.62	519.18
237	1.41	0.83	0.87	1108.22	926.73	926.73	881.66	519.18
238	1.28	0.83	1.02	503.54	912.51	912.51	858.43	519.18
239	1.28	0.83	1.02	421.50	763.83	763.83	718.56	519.18
240	1.28	0.83	1.02	515.21	933.65	933.65	878.31	519.18
241	2.14	1.04	0.62	1262.52	797.67	797.67	723.25	638.45
242	2.08	1.04	0.64	1279.96	831.47	831.47	752.04	638.45
243	2.01	1.04	0.67	1233.38	824.31	824.31	743.74	638.45
244	1.24	1.04	1.85	537.30	1149.28	1149.28	1025.99	638.45
245	1.24	1.04	1.85	564.32	1207.08	1207.08	1077.59	638.45
246	1.24	1.04	1.85	528.48	1130.43	1130.43	1009.16	638.45
247	2.27	1.04	0.57	1287.51	770.90	770.90	702.44	638.45
248	2.01	1.04	0.67	1184.51	791.66	791.66	714.28	638.45
249	2.14	1.04	0.62	1217.31	769.11	769.11	697.35	638.45
250	1.24	1.04	1.85	620.35	1326.94	1326.94	1184.59	638.45
251	1.24	1.04	1.85	636.69	1361.88	1361.88	1215.78	638.45
252	1.24	1.04	1.85	636.69	1361.88	1361.88	1215.78	638.45
253	1.41	0.83	0.87	1218.02	1018.55	1018.55	969.02	638.45
254	1.41	0.83	0.87	1102.38	921.85	921.85	877.02	638.45
255	1.41	0.83	0.87	1128.67	943.83	943.83	897.93	638.45
256	1.17	0.83	1.22	845.50	1666.20	1666.20	1552.27	638.45
257	1.17	0.83	1.22	800.07	1576.68	1576.68	1468.86	638.45
258	1.17	0.83	1.22	803.35	1583.13	1583.13	1474.88	638.45
259	1.28	0.83	1.02	1135.14	1028.54	1028.54	967.58	638.45
260	1.28	0.83	1.02	1085.23	983.32	983.32	925.04	638.45
261	1.28	0.83	1.02	1160.01	1051.08	1051.08	988.78	638.45
262	1.17	0.83	1.22	852.87	1680.73	1680.73	1565.80	638.45
263	1.06	0.83	1.53	828.19	1780.00	1780.00	1647.19	638.45
264	1.06	0.83	1.53	825.90	1775.09	1775.09	1642.65	638.45
265	2.01	1.04	0.67	1190.88	795.91	795.91	718.12	719.12
266	1.95	1.04	0.70	1147.12	789.28	789.28	710.42	719.12

Run	Shear Strain ϒ Merchant	Shear Strain ϒ Payton	Shear Strain ϒ Adjusted	Resultant Force (newtons)	Resultant Shear Stress Merchant (MPa)	Resultant Shear Stress Payton (MPa)	Resultant Shear Stress Adjusted (MPa)	Measured Ultimate Stress (MPa)
267	1.89	1.04	0.74	1208.35	856.53	856.53	769.13	719.12
268	1.17	1.04	2.46	573.31	1323.32	1323.32	1194.28	719.12
269	1.10	1.04	3.69	532.76	1326.54	1326.54	1220.78	719.12
270	1.24	1.04	1.85	541.19	1157.61	1157.61	1033.42	719.12
271	1.89	1.04	0.74	1179.52	836.09	836.09	750.78	719.12
272	1.77	1.04	0.82	1153.66	869.71	869.71	777.52	719.12
273	1.77	1.04	0.82	1107.64	835.02	835.02	746.50	719.12
274	1.10	1.04	3.69	560.79	1396.34	1396.34	1285.02	719.12
275	1.24	1.04	1.85	654.02	1398.95	1398.95	1248.87	719.12
276	1.17	1.04	2.46	597.60	1379.39	1379.39	1244.89	719.12
277	1.28	0.83	1.02	1205.20	1092.02	1092.02	1027.30	719.12
278	1.17	0.83	1.22	1090.97	1074.97	1074.97	1001.46	719.12
279	1.17	0.83	1.22	1088.56	1072.60	1072.60	999.25	719.12
280	0.90	0.83	3.06	772.60	1978.90	1978.90	1843.97	719.12
281	0.90	0.83	3.06	767.73	1966.40	1966.40	1832.33	719.12
282	0.90	0.83	3.06	775.79	1987.05	1987.05	1851.57	719.12
283	1.17	0.83	1.22	1110.60	1094.31	1094.31	1019.48	719.12
284	1.17	0.83	1.22	1098.18	1082.08	1082.08	1008.09	719.12
285	1.17	0.83	1.22	1079.74	1063.91	1063.91	991.16	719.12
286	0.90	0.83	3.06	801.55	2053.04	2053.04	1913.06	719.12
287	0.90	0.83	3.06	820.16	2100.71	2100.71	1957.48	719.12
288	0.90	0.83	3.06	803.65	2058.40	2058.40	1918.06	719.12

Appendix 5

Program Files

The figure below shows the LabVIEW file used to convert the force data from collection into an Excel file for further analysis.

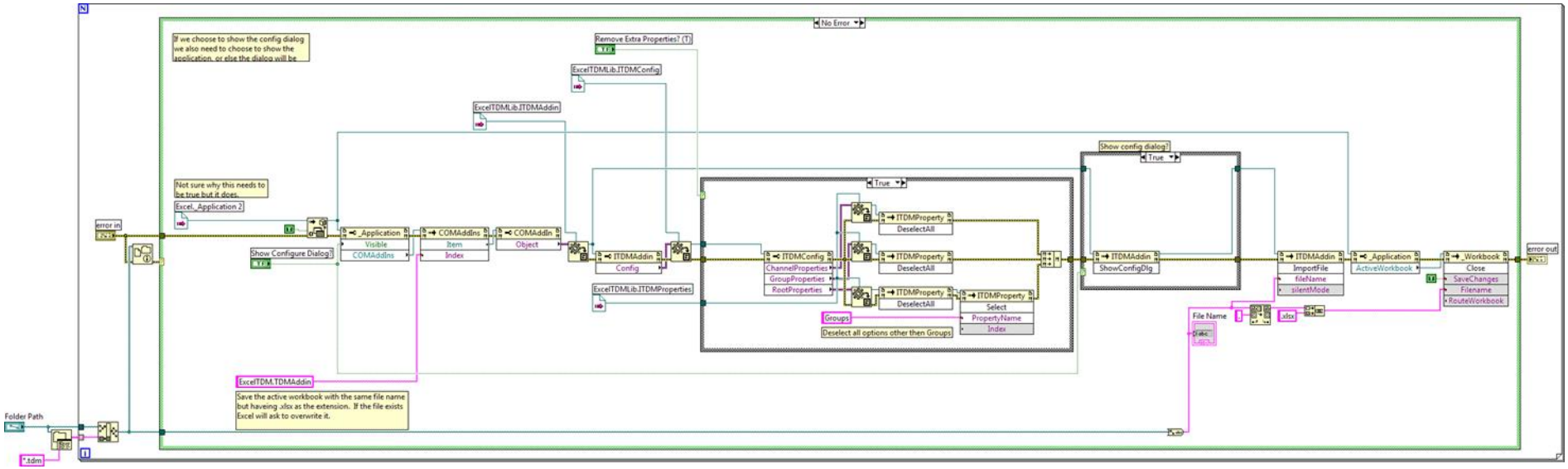

The following MATLAB code was used to generate the average force tables.

```
clear all
close all
clc

xlsfiles = dir('C:\Users\Chase\Desktop\Post Process Data\Thesis
Force Data\Saturday Files\*.xlsx');
ydatamean = zeros(length(xlsfiles),1);
zdatamean = zeros(length(xlsfiles),1);

for i = 1:length(xlsfiles)

    xlsname = xlsfiles(i).name;

    [num,txt,raw] = xlsread(fullfile('C:\Users\Chase\Desktop\Post
Process Data\Thesis Force Data\Saturday Files\',xlsname),2);

    ydata = num(:,2);
    zdata = num(:,3);

    plot(ydata,'LineWidth',2);
    hold on
    plot(zdata,'LineWidth',2,'color','red');
    hold off

    disp(sprintf(['File name: ',xlsname]));
    minpoint = input('Enter the min data point: ');
    maxpoint = input('Enter the max data point: ');
    %     minpoint = 250;
    %     maxpoint = 500;
    ydatamean(i) = mean(ydata(minpoint:maxpoint));
    zdatamean(i) = mean(zdata(minpoint:maxpoint));

    disp(sprintf([xlsname, ' mean: ',num2str(ydatamean(i))]));
    disp(sprintf([xlsname, ' mean:
',num2str(zdatamean(i)),'\n']));

end

xlsdata = {xlsfiles(:).name};
xlsdata = xlsdata';
xlsdata(:,2) = num2cell(ydatamean);
xlsdata(:,3) = num2cell(zdatamean);
headers = {'Sample Name','Cutting Force','Thrust Force'};

%%
xlswrite('C:\Users\Chase\Desktop\Post Process Data\Thesis Force
Data\Saturday Files\Mean Results\Mean
Results_Pick.xlsx',headers,'Sheet1','A1')
xlswrite('C:\Users\Chase\Desktop\Post Process Data\Thesis Force
Data\Saturday Files\Mean Results\Mean
Results_Pick.xlsx',xlsdata,'Sheet1','A2')
```

The following MATLAB code was used to calculate the angles of interest as well as the uncut chip thickness and tool angles using text files generated from GIMP.

```
clear all
close all
clc

milpercmm = 0.393700787;

scalefile = fopen('C:\Users\Chase\Desktop\Post Process Data\Scale
Data\Scale.txt');

scalefull = textscan(scalefile,'%q');
scalefull = [scalefull{:}];

scaleremain = scalefull{20};

i = 1;
while true
    [scale{i}, scaleremain] = strtok(scaleremain);
    if isempty(scaleremain),  break;  end
    i = i+1;
end

[scalex1,scaley1] = strtok(scale{4},',');
scaley1 = strtok(scaley1,',');

scalex1 = str2double(scalex1);
scaley1 = str2double(scaley1);

[scalex2,scaley2] = strtok(scale{5},',');
scaley2 = strtok(scaley2,',');

scalex2 = str2double(scalex2);
scaley2 = str2double(scaley2);

pixpermil = abs(scaley2 - scaley1)/milpercmm;

%%
anglefiles = dir('C:\Users\Chase\Desktop\Post Process Data\Angle
Data\*.txt');

for i = 1:length(anglefiles)

    anglefile = anglefiles(i).name;

    anglefilenum = fopen(['C:\Users\Chase\Desktop\Post Process
Data\Angle Data\',anglefile]);

    anglefull = textscan(anglefilenum,'%q');
    anglefull = [anglefull{:}];

    angleremain = anglefull{20};
```

```
j = 1;
while true
    [angle{j}, angleremain] = strtok(angleremain);
    if isempty(angleremain),  break;  end
    j = j+1;
end

[planex1,planey1] = strtok(angle{4},',');
planey1 = strtok(planey1,',');

planex1 = str2double(planex1);
planey1 = str2double(planey1);

[planex2,planey2] = strtok(angle{5},',');
planey2 = strtok(planey2,',');

planex2 = str2double(planex2);
planey2 = str2double(planey2);

[toolx1,tooly1] = strtok(angle{9},',');
tooly1 = strtok(tooly1,',');

toolx1 = str2double(toolx1);
tooly1 = str2double(tooly1);

[toolx2,tooly2] = strtok(angle{10},',');
tooly2 = strtok(tooly2,',');

toolx2 = str2double(toolx2);
tooly2 = str2double(tooly2);

[onsetx1,onsety1] = strtok(angle{14},',');
onsety1 = strtok(onsety1,',');

onsetx1 = str2double(onsetx1);
onsety1 = str2double(onsety1);

[onsetx2,onsety2] = strtok(angle{15},',');
onsety2 = strtok(onsety2,',');

onsetx2 = str2double(onsetx2);
onsety2 = str2double(onsety2);

[shearx1,sheary1] = strtok(angle{19},',');
sheary1 = strtok(sheary1,',');

shearx1 = str2double(shearx1);
sheary1 = str2double(sheary1);

[shearx2,sheary2] = strtok(angle{20},',');
sheary2 = strtok(sheary2,',');
```

```
    shearx2 = str2double(shearx2);
    sheary2 = str2double(sheary2);

    %     [chipx1,chipy1] = strtok(angle{24},',');
    %     chipy1 = strtok(chipy1,',');
    %
    %     chipx1 = str2double(chipx1);
    %     chipy1 = str2double(chipy1);
    %
    %     [chipx2,chipy2] = strtok(angle{25},',');
    %     chipy2 = strtok(chipy2,',');
    %
    %     chipx2 = str2double(chipx2);
    %     chipy2 = str2double(chipy2);

    planeangle(i) = atand((planey1-planey2)/(planex2-planex1));

    toolangle(i) = atand((toolx2-toolx1)/(tooly1-tooly2)) +
planeangle(i);

    phi(i) = atand((onsety2-onsety1)/(onsetx2-onsetx1)) +
planeangle(i);

    if shearx1 < shearx2
        psi(i) = 90 + atand((shearx2-shearx1)/(sheary1-sheary2))
+ planeangle(i) - phi(i);
    else
        psi(i) = 90 - atand((shearx1-shearx2)/(sheary1-sheary2))
+ planeangle(i) - phi(i);
    end

    uncut(i) = (planey1 - onsety1)/pixpermil;

    %     cut(i) = sqrt((chipx2-chipx1)^2 + (chipy2-
chipy1)^2)/pixpermil;
end

xlsdata = {anglefiles(:).name};
xlsdata = xlsdata';
xlsdata(:,2) = num2cell(toolangle');
xlsdata(:,3) = num2cell(phi');
xlsdata(:,4) = num2cell(psi');
xlsdata(:,5) = num2cell(uncut');
% xlsdata(:,6) = num2cell(cut');

headers = {'Sample Name','Tool Angle','Phi','Psi','Uncut Chip
Thickness'};

xlswrite('C:\Users\Chase\Desktop\Post Process Data\Angle
Data\Results\Results.xlsx',headers,'Sheet1','A1')
xlswrite('C:\Users\Chase\Desktop\Post Process Data\Angle
Data\Results\Results.xlsx',xlsdata,'Sheet1','A2')

fclose('all');
```